

RICE UNIVERSITY

**Foam for Mobility Control in Alkaline/Surfactant
Enhanced Oil Recovery Process**

by

Wei Yan

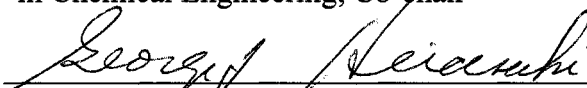
A THESIS SUBMITTED
IN PARTIAL FULFILLMENT OF THE
REQUIREMENTS FOR THE DEGREE

Doctor of Philosophy

APPROVED, THESIS COMMITTEE:



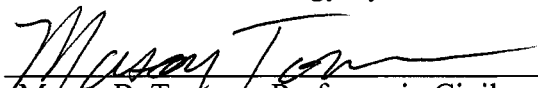
Clarence A. Miller, Louis Calder Professor
in Chemical Engineering, Co-chair



George J. Hirasaki, A. J. Hartsook Professor
in Chemical Engineering, Co-chair



Walter G. Chapman, William W. Akers
Chair in Chemical Engineering, Professor in
Chemical Engineering, Director of
Environmental & Energy Systems Institute



Mason B. Tomson, Professor in Civil and
Environmental Engineering

HOUSTON, TEXAS

MAY 2006

UMI Number: 3216802

INFORMATION TO USERS

The quality of this reproduction is dependent upon the quality of the copy submitted. Broken or indistinct print, colored or poor quality illustrations and photographs, print bleed-through, substandard margins, and improper alignment can adversely affect reproduction.

In the unlikely event that the author did not send a complete manuscript and there are missing pages, these will be noted. Also, if unauthorized copyright material had to be removed, a note will indicate the deletion.

UMI[®]

UMI Microform 3216802

Copyright 2006 by ProQuest Information and Learning Company.

All rights reserved. This microform edition is protected against unauthorized copying under Title 17, United States Code.

ProQuest Information and Learning Company
300 North Zeeb Road
P.O. Box 1346
Ann Arbor, MI 48106-1346

ABSTRACT

Foam for Mobility Control in Alkaline/Surfactant

Enhanced Oil Recovery Process

by

Wei Yan

This thesis addresses several key issues in the design of foam for mobility control in alkaline-surfactant enhanced oil recovery processes. First, foam flow in fracture systems was studied. A theory for foam flow in a uniform fracture was developed and verified by experiment. The apparent viscosity was found to be the sum of contributions arising from liquid between bubbles and the resistance to deformation of the interfaces of bubbles passing through the fracture. Apparent viscosity increases with gas fractional flow and is greater for thicker fractures (for a given bubble size), indicating that foam can divert flow from thicker to thinner fractures. The diversion effect was confirmed experimentally and modeled using the above theory for individual fractures. The amount of surfactant solution required to sweep a heterogeneous fracture system decreases greatly with increasing gas fractional flow owing to the diversion effect and to the need for less liquid to occupy a given volume when foam is

used. The sweep efficiency's sensitivity to bubble size was investigated theoretically in a heterogeneous fracture system with log-normal distributed apertures.

Second, the foam application in forced convection of alkaline-surfactant enhanced oil recovery processes was studied. From sand pack experiments for the alkaline-surfactant-polymer process, a 0.3 PV slug of the surfactant blend studied can recover almost all the waterflood residual crude oil when followed by a polymer solution as mobility control agent. But this blend is a weak foamer near its optimum salinity while one of its components, IOS, is a good foamer. Two types of processes were tested in sand packs to study possible process improvements and cost savings from replacing some polymer by foam for mobility control. The first used IOS foam as drive after the surfactant slug, while the second, which is preferred, involved injecting gas with the surfactant slug containing polymer followed by IOS foam. It was found that foam has higher apparent viscosity in high than in low permeability region. Thus, use of foam should be more attractive in heterogeneous system to get better sweep efficiency.

ACKNOWLEDGEMENTS

I have been very fortunate to study under the direction of Professors George Hirasaki and Clarence Miller. Their wisdom and authoritative knowledge on foam, interfacial phenomena, and flow in porous media have guided me throughout my thesis work. I deeply appreciate their help, trust and support.

I thank Professors Mason Tomson and Walter Chapman for serving in my thesis committee. I am also grateful to the many individuals who helped me in my research. Professor Shi-Yow Lin, Dr. Maura Puerto and Mr. Dick Chronister provided guidance and assistance for setting up my experimental device. Dr. Frank Zhao helped me with the image analysis software.

I thank the United States Department of Energy for financial support.

Many fellow students in Dr. Hirasaki's and Dr. Miller's laboratories have offered me help, support, and most important of all, their friendships. I am grateful to this awesome group of people.

I thank my wife Yan for her constant support, love and understanding.

Last but certainly not least, I am grateful and eternally indebted to my parents Hongzhi Yan and Zhi Ling. Their love and spirit of dedication to their society, friends, and the humanity as a whole has been a constant source of inspiration.

TABLE OF CONTENTS

Table of Contents.....	IX
List of Tables.....	X
List of Figures.....	XIX
Chapter 1 Introduction.....	1
1.1 Enhanced oil recovery.....	1
1.2 Foam.....	6
1.3 Thesis scope and organization.....	9
Chapter 2 Technical background.....	13
2.1 Fundamentals of flow in porous media.....	13
2.2 Surfactants.....	15
2.3 Fundamentals of Foam Flow in porous Media.....	19
2.4 Mechanisms of Foam Formation and Decay.....	24
2.4.1 Foam formation.....	25
2.4.2 Foam destruction.....	30
2.5 Foam stability to crude oil in porous media.....	35
2.6 Foam flow in capillary tubes.....	46
2.7 Effect of heterogeneity on foam flow.....	51
2.8 Alkaline surfactant enhanced oil recovery process.....	60

2.9	Enhanced oil recovery in fractured carbonate reservoir.....	63
Chapter 3	Foam flow in homogeneous fracture.....	66
3.1	Foam apparent viscosity in homogeneous fracture.....	66
3.2	Experimental methods.....	71
3.3	Foam bubble size measurement in fractures.....	74
3.4	Foam apparent viscosity in homogeneous fracture experiment results.....	75
3.5	Bulk foam apparent viscosity.....	80
3.6	Contrary diversion effect.....	84
Chapter 4	Foam diversion in heterogeneous fractures.....	87
4.1	Foam apparent viscosity in heterogeneous fractures	87
4.2	Prediction of sweep efficiency in heterogeneous fractures.....	89
4.3	Fractures with log-normal distribution fractures.....	91
4.4	Experimental methods.....	93
4.5	Experimental results for apparent viscosity and sweep in heterogeneous fractures.....	94
4.5.1	Apparent viscosity.....	95
4.5.2	Sweep efficiency.....	97
4.6	Sensitivity of foam bubble size to sweep efficiency in heterogeneous fractures.....	102

4.6.1	Foam bubble size with some constant ratio (>1) to aperture.....	105
4.6.2	Foam bubbles at constant size ($>$ aperture) in different layers.....	109
4.6.3	Foam bubbles at constant size ($<$ aperture) in different layers.....	112
4.6.4	Foam bubbles at constant size ($>$ some apertures and $<$ some apertures) in different layers.....	114
Chapter 5	Surfactant evaluation for foam-aided alkaline/surfactant enhanced oil recovery process.....	119
5.1	Selection of surfactants.....	119
5.2	Foam strength with different surfactants.....	124
5.3	Foam stability with the presence of residual oil.....	128
Chapter 6	Alkaline/surfactant/polymer/foam enhanced oil recovery process.....	133
6.1	Alkaline/surfactant/polymer EOR process.....	134
6.2	Foam drive possibility in alkaline/surfactant/polymer process.....	139
6.3	Foam drive in alkaline/surfactant/polymer process.....	143
6.4	Alkaline/surfactant/polymer/foam process.....	151

6.4.1	40 darcy sand pack.....	153
6.4.2	200 darcy sand pack.....	156
6.4.3	Comparison between the flooding in 40 darcy and 200 darcy sand packs.....	159
6.5	Calculations for ASPF in heterogeneous systems.....	165
Chapter 7	Conclusions and recommendations.....	177
7.1	Conclusions.....	177
7.1.1	Foam flow in homogeneous fracture.....	177
7.1.2	Foam diversion in heterogeneous fractures.....	179
7.1.3	Surfactant evaluation.....	180
7.1.4	Foam in alkaline/surfactant/polymer/foam EOR process	181
7.2	Recommendations for future work.....	182
7.2.1	Foam flow in fractures.....	182
7.2.2	Surfactant.....	184
7.2.3	ASPF process.....	184
	References.....	186
	Appendices.....	197
	Appendix A.....	197
	Appendix B.....	199

Appendix C.....	202
-----------------	-----

LIST OF TABLES

Table 5.1 Surfactants used in the experiments for alkaline-surfactant EOR process.....	121
Table 6.1 Revenue and expense calculation for ASPF process.....	175
Table 6.2 Revenue and expense calculation for ASP process.....	176

LIST OF FIGURES

Fig. 2.1 Classification of surfactants.....	17
Fig. 2.2 Schematic of surfactant behavior above the CMC.....	18
Fig. 2.3 Cross-sectional view of cornered pores.....	20
Fig. 2.4 Pore level schematic of foam in porous media.....	22
Fig. 2.5 Schematic of capillary snap-off mechanism.....	26
Fig. 2.6 Schematic of lamella division mechanism.....	28
Fig. 2.7 Schematic of leave-behind mechanism.....	29
Fig. 2.8 Disjoining pressure π curve governs the stability of a thin Film.....	31
Fig. 2.9 Foam lamella translating from left to right in a periodically constricted tube.....	33
Fig. 2.10 Foam lamella translating from left to right in a periodically constricted tube.....	35
Fig. 2.11 Photomicrograph of two-dimensional foam containing emulsified oil drops that have drained from the foam films into the Plateau borders.....	36
Fig. 2.12 Aqueous foam, pseudoemulsion and emulsion films and Plateau borders containing oil drops.....	39

Fig. 2.13 Configurations of oil at the gas-aqueous solution interface.....	40
Fig. 2.14 Oil lens, definition of $\theta^*(\theta_{ow})$ and unstable bridge configurations.....	44
Fig. 2.15 Schematic profile of several defoaming mechanisms.....	45
Fig. 2.16 Mechanisms affecting apparent viscosity in smooth capillaries.....	49
Fig. 2.17 Bubble configurations when the bubbles are separated and when they are touching.....	49
Fig. 2.18 Sketches of capillary-pressure and fractional-flow curves operating during a two-phase displacement.....	53
Fig. 2.19 Relationship between capillary-entry pressure, limiting capillary pressure, and permeability.....	55
Fig. 2.20 Schematic of the correlation between foam mobility and permeability.....	56
Fig. 3.1 Mechanisms affecting apparent viscosity in smooth capillaries...	67
Fig. 3.2 Detailed diagram of homogeneous fracture model.....	72
Fig. 3.3 Set -up diagram for foam mobility control experiment in fracture model.....	73

Fig. 3.4 Bubble size measurement results from image processing method and capillary tube method match each other.....	75
Fig. 3.5 Effect of flow rate and fractional flow on apparent viscosity.....	77
Fig. 3.6 Effect of flow rate and fractional flow on apparent viscosity.....	77
Fig. 3.7 Effect of flow rate and fractional flow on apparent viscosity.....	78
Fig. 3.8 Effect of flow rate and fractional flow on apparent viscosity.....	78
Fig. 3.9 Effect of ratio of aperture/bubble size on apparent viscosity....	79
Fig. 3.10 Bulk foam apparent viscosity in fractures measurement and prediction.....	83
Fig. 3.11 Apparent viscosity at different ratio of foam bubble diameter to aperture and different gas fractional flow.....	86
Fig. 4.1 Detailed diagram of heterogeneous fracture model.....	94
Fig. 4.2 Apparent viscosity for aperture ratio of 0.1 mm/0.2 mm, bubble size = 0.4 mm and $Re = 0.22$	96
Fig. 4.3 Apparent viscosity for aperture ratio of 0.05 mm/0.15 mm, bubble size = 0.4 mm and $Re = 0.22$	97
Fig. 4.4 Surfactant solution sweeping heterogeneous fracture, $Re = 0.22$, fracture aperture ratio = 0.05 mm(top)/0.15 mm(bottom)....	100

Fig. 4.5 Foam/surfactant solution sweeping heterogeneous fracture, $Re = 0.22$, $f_g = 0.9$, fracture aperture ratio = $0.05 \text{ mm}(\text{top})/0.15 \text{ mm}(\text{bottom})$, $D_b = 0.4 \text{ mm}$	100
Fig. 4.6 Surfactant solution sweeping heterogeneous fracture at different fracture aperture ratio (for thinner region only).....	101
Fig. 4.7 Comparison between the calculation and the experiment results for foam/surfactant sweep in heterogeneous fractures with 1:3 aperture ratio.....	101
Fig. 4.8 Sweep efficiency by foam with bubble size 2 times aperture in each layer.....	106
Fig. 4.9 Sweep efficiency by foam with bubble size 5 times of aperture in each layer.....	106
Fig. 4.10 Apparent viscosity in a heterogeneous fracture system with $V=0.8$ when the bubble diameter in a fixed ratio to the aperture of each layer.	108
Fig. 4.11 Sweep efficiency by foam with bubble size 6.4 times of the log-mean aperture which is equal to the largest aperture in the heterogeneous fracture system.....	109

Fig 4.12 Apparent viscosity in a heterogeneous fracture system with $V=0.8$ when the bubble diameter is equal to the largest aperture in the heterogeneous system.....	111
Fig. 4.13 sweep efficiency by foam with bubble size 125 times of aperture.....	111
Fig. 4.14 sweep efficiency by bulk foam.....	113
Fig. 4.15 Apparent viscosity in a heterogeneous fracture system with $V=0.8$ when the bubble diameter is smaller than any aperture.....	113
Fig 4.16 sweep efficiency by foam with bubble size equal to log-mean aperture.....	115
Fig 4.17 Apparent viscosity in a heterogeneous fracture system with $V=0.8$ when the bubble diameter is equal to the log-mean aperture.....	115
Fig 4.18 sweep efficiency by foam with bubble size 5 times log-mean aperture.....	116
Fig. 4.19 Apparent viscosity in a heterogeneous fracture system with $V=0.8$ when the bubble diameter is equal to 5 times log-mean aperture.....	116
Fig. 4.20 Comparison of sweep efficiency at different bubble size.....	118

Fig. 5.1 Aqueous phase behavior of N67-7PO&IOS blends, 1% Na ₂ CO ₃ + various NaCl.....	123
Fig. 5.2 Aqueous phase behavior of N67-7PO&IOS blends, 1% Na ₂ CO ₃ + various CaCl ₂	124
Fig. 5.3 Foam strength at different surfactant composition.....	125
Fig. 5.4 Foam strength at different salinity.....	126
Fig. 5.5 Short sand pack setup.....	130
Fig. 5.6 Comparison of foam strength with or without residual oil by different surfactant or surfactant blends.....	132
Fig. 6.1 Photos showing behavior during ASP flood of silica sand pack.....	135
Fig. 6.2 Effluents for different pore volume for ASP experiment.....	135
Fig. 6.3 Measured cumulative oil recovery for ASP flood in silica sand pack.....	136
Fig. 6.4 Time-dependence of pressure drop during ASP flood in silica sand pack.....	136
Fig. 6.5 Photos of unsuccessful ASP flood at 4% NaCl.....	138
Fig. 6.6 Photo of phase separation with polymer at 4% NaCl.....	138
Fig. 6.7 Time-dependence of pressure drop during unsuccessful ASP flood.....	139

Fig. 6.8 Foam sweep the sand pack presaturated with polymer/surfactant.....	141
Fig. 6.9 Apparent viscosity during the sweeping the sand pack presaturated with polymer/surfactant.....	142
Fig. 6.10 Photos showing behavior during ASPF flood of silica sand pack.....	145
Fig. 6.11 Recovery history for ASPF experiment.....	146
Fig. 6.12 Effluents for different pore volume for ASPF experiment.....	146
Fig. 6.13 Pressure history for ASPF experiment.....	147
Fig. 6.14 Photos showing behavior during ASPF flood of silica sand pack at optimized condition.....	149
Fig. 6.15 Recovery history for ASPF experiment at optimized condition.....	149
Fig. 6.16 Effluents for different pore volume for ASPF experiment at optimized condition.....	150
Fig. 6.17 Pressure history for ASPF experiment at optimized condition.....	150
Fig. 6.18 Pictures for the displacement of residual crude oil by polymer/foam in 40 darcy sand pack.....	153

Fig. 6.19 Pictures for effluents for polymer/foam flooding in 40 darcy sand pack.....	154
Fig. 6.20 Recovery efficiency for polymer/foam flooding in 40 darcy sand pack.....	154
Fig. 6.21 Pressure history for polymer/foam flooding in 40 darcy sand pack.....	155
Fig. 6.22 Pictures for the displacement of residual crude oil by polymer/foam in 200 darcy sand pack.....	157
Fig. 6.23 Pictures for effluents for polymer/foam flooding in 200 darcy sand pack.....	158
Fig. 6.24 Recovery efficiency for polymer/foam flooding in 200 darcy sand pack.....	158
Fig. 6.25 Pressure history for polymer/foam flooding in 200 darcy sand pack.....	159
Fig. 6.26 Apparent viscosity during the foam displacing oil for both 40 darcy and 200 darcy sand packs.....	160
Fig. 6.27 Schematic description of the different regions during the ASPF process in sand pack.....	164
Fig. 6.28 Schematic of a reservoir with 2 layers at different permeability.....	166

Fig. 6.29 schematic illustration of ASPF flooding.....	168
Fig. 6.30 Sweep efficiency of foam or polymer sweep in a heterogeneous system with 5:1 permeability ratio and 1:4 thickness ratio.....	172
Fig. C.1 Schematic illustration of heterogeneous reservoirs.....	202

Chapter 1

INTRODUCTION

1.1 Enhanced oil recovery

Crude oil development and production in U.S. oil reservoirs can include up to three distinct phases: primary, secondary, and tertiary (or enhanced) recovery.

During primary recovery, the natural pressure of the reservoir or gravity drives oil into the wellbore, and combined with artificial lift techniques (such as pumps), brings the oil to the surface. But only about 10 percent of a reservoir's original oil in place is typically produced during primary recovery. Shortly after World War II, producers began to employ secondary recovery techniques to extend the productive life of U.S. oil fields, often increasing ultimate recovery to 20 to 40 percent of the original oil in place. For the most part, these techniques have involved injecting water to displace oil and drive it to a production wellbore. In some cases, the reinjection of natural gas has been employed to maintain

reservoir pressure (natural gas is often produced simultaneously with the oil from a reservoir).

According to Green and Willhite [1998], conventional oil recovery (including primary and secondary recovery) typically recovers only 35-50% of the original oil-in-place. However, with much of the easy-to-produce oil already recovered from U.S. oil fields, producers have attempted several tertiary, or enhanced oil recovery (EOR), techniques that offer prospects for producing more of the reservoir's original oil in place. An estimated 377 billion barrels of oil in place represent the "stranded" resource that could be the target for EOR applications.

Enhanced oil recovery (EOR) is oil recovery by the injection of fluids other than water, such as steam, gas, surfactant solution, or carbon dioxide. It is important that the injected fluid contacts as much of the reservoir as possible. EOR includes a number of thermal, gas-injection, and chemical processes that can substantially increase reservoir recovery beyond that of conventional oil production. Normally, EOR processes fall into one of three categories [Lake, 1990]: thermal, chemical or solvent methods.

Thermal methods involve the introduction of heat such as the injection of steam to lower the viscosity, or thin, the heavy viscous oil, and improve its ability to flow through the reservoir. Because of steam's much lower density in comparison with the resident liquids in the reservoir, it tends to rise and accumulate at the top of the formation. Therefore, steam flood works best only when gravity can be made favorable to the process. This occurs when steam is injected updip and when there is large gravity flux that drives the heated oil to the producer downdip in the reservoir. In other words, steam works best in a reservoir with large dip angles and/or high permeability [Hirasaki, 1989]. But in other situations, gravity sometimes works against steam drive and diminishes its efficiency. In such case, gravity override occurs as steam rises to the top of the reservoir. Together with reservoir heterogeneity, gravity override results in early steam production and reduced volumetric sweep efficiency.

Foam has been shown to enhance the effectiveness of steam flooding. With foam, steam mobility is reduced and the process results in less override and more piston-like steam drive. This approach is called "steam foam flooding". A very efficient lower mobility drive fluid is created by foaming the steam [Hirasaki, 1989].

Chemical methods involve the use of long-chained molecules called polymers to increase the effectiveness of waterfloods, or the use of detergent-like surfactants to help lower the interfacial tension that often prevents oil droplets from moving through a reservoir. The most common chemical flooding method is polymer flooding, which consists of adding polymer to the water of a waterflood to decrease its mobility. The resulting increase in viscosity, as well as decrease in aqueous phase permeability that occurs with some polymers, causes a lower mobility ratio. This lowering increases the efficiency of the waterflood through greater volumetric sweep efficiency and lower swept zone oil saturation. The greater recovery efficiency constitutes the economic incentive for polymer flooding when applicable [Lake, 1990].

Also, it was found that capillary forces caused large quantities of oil to be left behind in well-swept zones of waterflooded oil reservoirs. Capillary forces are the consequence of the interfacial tension (IFT) between the oil and water phases. The predominant EOR technique for achieving low IFT is micellar-polymer (MP) flooding. Lowering interfacial tension recovers additional oil by reducing the capillary forces that leave oil behind during immiscible displacement. This trapping is best expressed as a competition

between viscous forces, which mobilize the oil, and capillary forces, which trap the oil [Lake, 1990].

A major disadvantage of MP flooding is the high cost of the polymer. If foam generated with the surfactant can be substituted for polymer as a mobility control agent in MP processes, the cost would be lower. The same is true for alkaline/surfactant processes in which much of the surfactant is soap formed in alkaline solutions from organic acids present in the crude oil.

Solvent methods use solvent to extract oil from the permeable media. The oil extraction can be brought about by many fluids: organic alcohols, ketones, refined hydrocarbons, condensed petroleum gas (LPG), natural gas and liquefied natural gas (LNG), carbon dioxide, air, nitrogen, exhaust gas, flue gas, and others. In the early 1960's, LPG was used as the main solvent. With the increase of LPG price, carbon dioxide became the leading solvent from 1980's although other fluids were used also [Stalkup, 1985].

Foam can be used in solvent method EOR processes involving gas injection: natural gas, carbon dioxide, or nitrogen. Like steam flooding, these gas displacement processes face the same problem of poor sweep efficiency, which can be improved by the use of foam.

1.2 Foam

Foam is a two-phase system in which gas bubbles are enclosed by liquid. Foam may contain more or less liquid, according to circumstances. Dry foam has little liquid: it consists of thin films, which may be idealized as single surface. The bubbles take the form of polyhedral cells, with these surfaces as their faces, whose thickness are not uniform during drainage because the thinning rate at the center of the film is much lower than the thinning rate at the periphery [Frankel and Mysels, 1962]. The films meet in lines (the edges of the polyhedra) and the lines meet at vertices. In two dimensions, the dry foam consists of polygonal cells. See Fig. 1.1.

Most foam owes its existence to the presence of surfactants, that is, materials which are surface active. They are concentrated on the surface. They reduce the surface energy or tension associated with surfaces. More importantly, they stabilize the thin film against rupture. In aqueous foam,

surfactant molecules are amphiphilic; their two parts are hydrophobic and hydrophilic so that they can stay on the water surface. See Fig. 1.2.

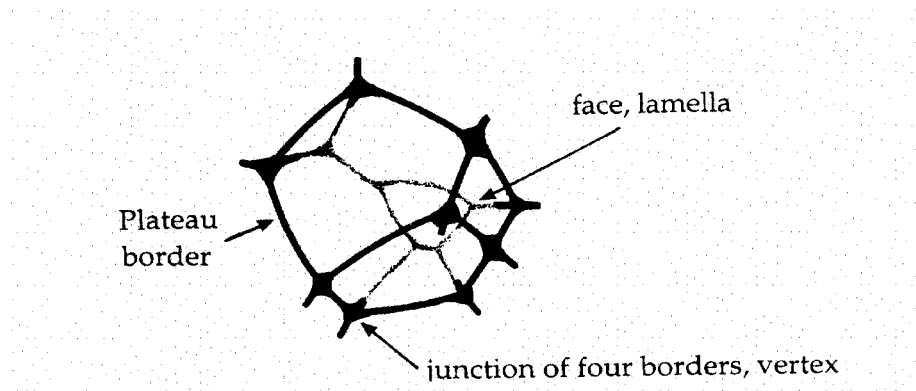


Fig.1.1 Three-dimensional foam consists of cells whose faces are thin films, meeting in Plateau borders (Weaire, 1999)

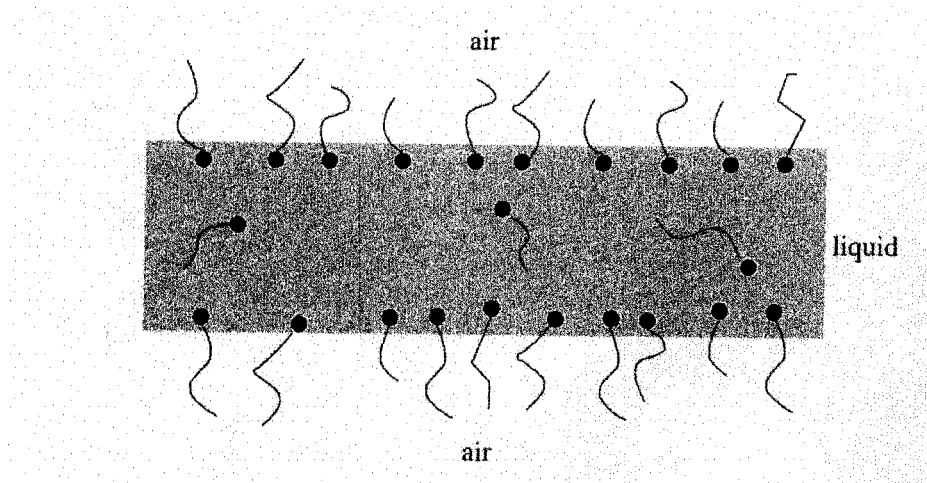


Fig.1.2 Surfactant molecules stabilize thin films (Weaire, 1999)

Foam which contains more than one percent of liquid does not conform to the geometrical description above. The liquid is mainly to be found in Plateau borders, which are channels of finite width, replacing the lines in the dry foam (see Fig. 1.3). An individual polyhedral cell has its sharp edges and corners rounded off. As the fraction of liquid increases, the swelling of the Plateau borders eventually leads to the extreme limit of wet foam. From Fig. 1.4, we can see the bubbles have recovered a nearly spherical shape, and any further increase of liquid will allow them to come apart.

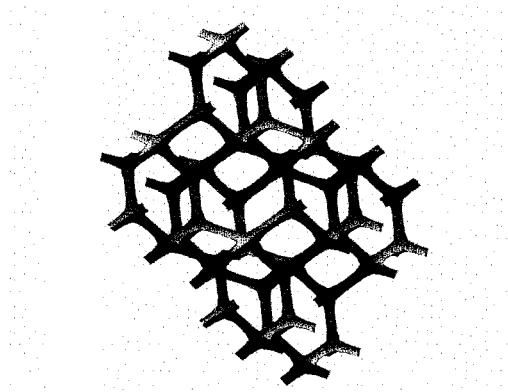


Fig.1.3 In a foam the Plateau borders form a continuous network (Weaire, 1999)

In porous media, foam exists as gas bubbles whose shapes conform to the solid matrix. Hirasaki (1989) defined foam in porous media as “a

dispersion of a gas in a liquid such that the liquid phase is continuous (i.e. connected) and at least some part of the gas phase is made discontinuous by thin liquid films called lamellae.”

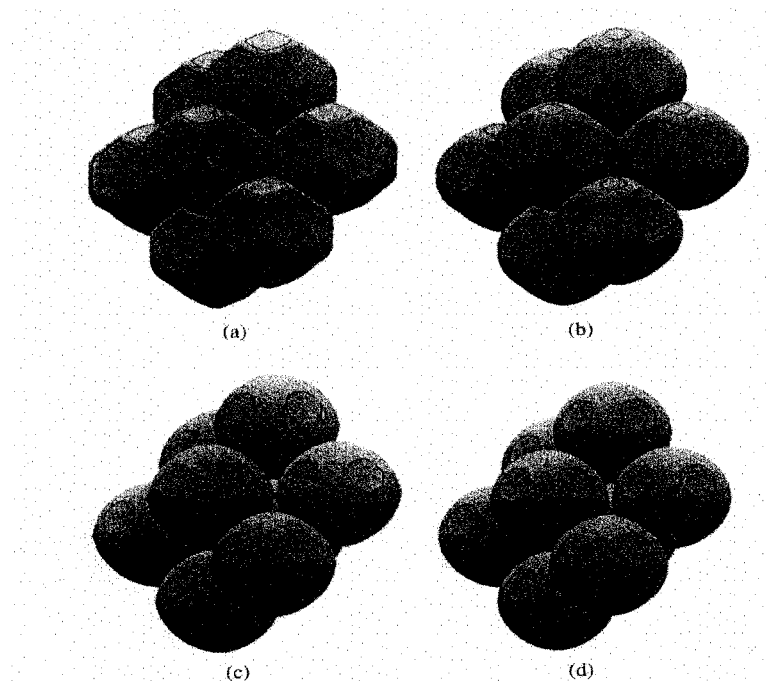


Fig.1.4 Examples of simulations of wet foam (Weaire, 1999). From (a) to (d), with the increase of fraction of liquid, the shape of the bubbles is more and more spherical.

1.3 Thesis scope and organization

This thesis’s goal is to develop an improved understanding of foam flow in both fractured and unfractured porous media to facilitate the application

of foam for mobility control, especially for surfactant and alkaline surfactant processes.

Chapter 2 provides the technical background for the thesis. Foam flow in porous media, mechanism of foam formation and foam decay, foam stability to crude oil in porous media, foam flow in capillary tubes, the effect of heterogeneity on foam flow and alkaline surfactant enhanced oil recovery in fractured carbonate reservoir are reviewed.

Chapter 3 describes the mechanism for foam apparent viscosity when foam flows in homogeneous fractures. Two contributions – liquid slug and foam bubble deformation are found to be responsible for the foam apparent viscosity with bubble diameter larger than aperture. The apparent viscosity for bulk foam can be predicted by semi-empirical model. The contrary diversion effect is also described.

Chapter 4 studies the foam flow in heterogeneous fractures with different apertures. The apparent viscosity for foam with bubble diameter larger than aperture can be calculated by the sum of the liquid slug and bubble deformation contributions in heterogeneous fractures. The experimental

results for foam flow in two layer heterogeneous fractures fit the prediction from theory. Calculation for foam sweep in heterogeneous fractures is expanded to multi-layer fractures with apertures in log-normal distribution. The sweep efficiency sensitivity to bubble size is discussed.

Chapter 5 investigates the surfactant work for alkaline-surfactant EOR process, including the foaming and calcium tolerance ability of new surfactants used in alkaline-polymer-surfactant process, surfactant stability to residual crude oil and foam strength with different surfactants.

Chapter 6 focuses on alkaline/surfactant/polymer/foam (ASPF) enhanced oil recovery process. Two different ASPF processes are developed – one is the foam drive after surfactant slug and the other is foam injection from the beginning. Higher apparent viscosity is found in sand packs with larger permeability. The advantage of ASPF in heterogeneous reservoir is discussed.

Chapter 7 gives the conclusions for this study and recommendations for future work.

In appendices, the derivations for the equivalent lamellae per unit length, calculation for sweep efficiency in 2 layer fracture system and the calculation for Dykstra-Parson's model are given.

Chapter 2

TECHNICAL BACKGROUND

2.1 Fundamentals of flow in porous media

A porous medium is a solid matrix with interconnected holes or pores, such as packed columns of sand, rocks, and soils. Macroscopically, Darcy's law can describe flow in a porous medium at a low Reynolds number:

$$\vec{u} = -\frac{k}{\mu}(\nabla p - \rho \vec{g}) \quad (2.1)$$

The above equation of Darcy's law is for a single-phase flow. It relates flow in porous media to the pressure gradient. The term k/μ (also represented by the symbol λ) is the mobility of the fluid in the porous medium. It includes a macroscopic property of the porous medium -- the permeability k and a fluid-dependent property -- the viscosity μ . The superficial velocity u , also known as the Darcy velocity, is the volumetric flow rate divided by the entire cross-sectional area of the porous medium, $u = q/A$. The actual flow, however, is limited only to the pore spaces in

the porous medium. Therefore, the actual mean velocity within the pores, or the interstitial velocity v , is related to the superficial velocity by $v = u/\phi$, where ϕ is the porosity – another macroscopic property of the porous medium.

For multiphase flow, Darcy's law can be written for each phase i as:

$$\vec{u}_i = \vec{v}_i \phi = -\frac{k \cdot k_{ri}(S_i)}{\mu_i} (\nabla p_i - \rho \vec{g}) \quad (2.2)$$

The term $k \cdot k_{ri}(S_i)$ is the effective permeability of the porous medium and is a product of the intrinsic permeability k and the relative permeability k_{ri} that is a function of the fluid saturation S_i . The mobility of phase i is expressed as $\lambda_i = \frac{k \cdot k_{ri}(S_i)}{\mu_i}$.

Another important concept for foam flow in porous media is capillary pressure. For foam, capillary pressure is the difference between gas and liquid phase pressure. From Young-Laplace equation, the capillary pressure is:

$$P_c = 2\sigma C_m + \Pi(h) \quad (2.3)$$

Where P_c is the capillary pressure, C_m is the mean interfacial curvature of the film, and σ is the bulk surface tension. Π is first introduced by Derjaguin and co-workers [1936], which is the film disjoining pressure. Π is a function of film thickness, h . Positive values of Π reflect net repulsive film forces, and negative values of Π indicate net attractive forces. The capillary pressure depends on the liquid saturation.

2.2 Surfactants

The term “surfactants” is a contraction of “surface active agents.” As the name implies, a surfactant is a substance that is active or highly enriched at the surface or interface between phases [Miller and Neogi, 1985]. A typical surfactant monomer is composed of a polar (hydrophilic) moiety, and a nonpolar (hydrophobic) moiety; the entire monomer is sometimes called an amphiphile because of this dual nature. The monomer is represented by a “tadpole” symbol, with the nonpolar moiety being the tail and the polar moiety being the head.

Surfactants can be divided into four categories by their polar moieties: anionic, cationic, nonionic and amphoteric.

- **Anionic.** The anionic (negatively charged) surfactant ion is balanced with a cation (usually sodium) associated with the monomer. In an aqueous solution, the neutral molecules ionize to free cations from the anionic monomers.
- **Cationic.** The surfactants are cationic if the polar moiety is positively charged. The surfactant molecule contains an inorganic anion to balance the charge.
- **Nonionic.** Nonionic surfactants do not form ionic bonds. When they are dissolved in aqueous solution, however, nonionic surfactants exhibit surfactant properties. The most frequently used nonionic surfactants are prepared by adding ethylene oxide to long-chain hydrocarbons with terminal polar groups, e.g., -OH, -COOH. The procedure introduces ethoxy groups, which are polar in nature and form hydrogen bonds with water.
- **Amphoteric.** This class of surfactants contains aspects of two or more of the other classes. The ionic character or the polar group depends on the pH of the solution.

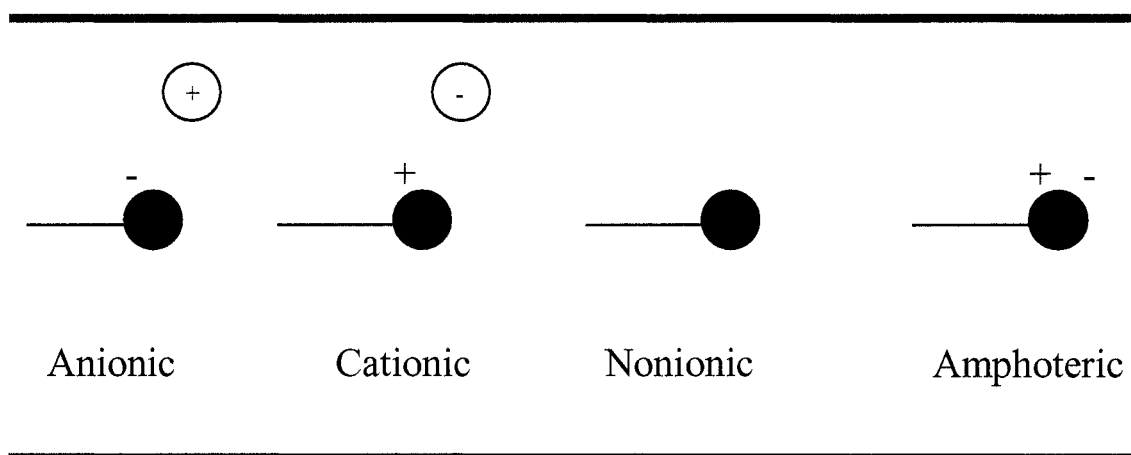


Fig. 2.1 Classification of surfactants (Lake, 1989)

Surfactants have a “head” and a “tail”, the “head” prefers polar media such as water while the “tail” has an affinity with non-polar media like oil or air. Consequently, surfactant molecules tend to adsorb at the interface between the polar and non-polar phases, which results in the reduction of the interfacial tension.

As shown in Fig. 2.2, some surfactant molecules are adsorbed on the air/water or oil/water interface and form a monolayer. At low concentration, all the rest of the surfactant molecules are dissolved in the solution as individual surfactant monomers. Above a particular concentration, however, some surfactant molecules form aggregates that

are called micelles [Miller and Neogi, 1985]. The critical concentration for micelles to be formed is called the critical micelle concentration, or CMC. Above CMC, virtually all further increases in surfactant concentration cause growth only in the micelle concentration.

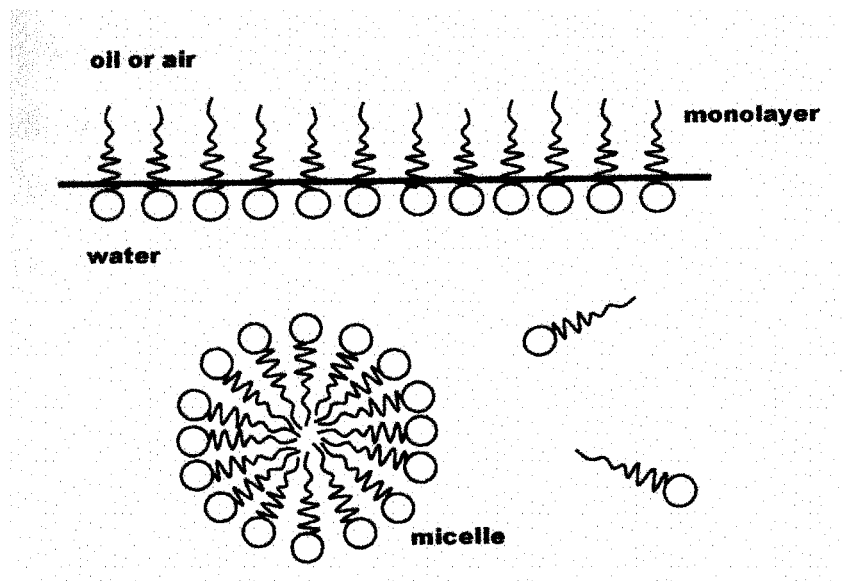


Fig. 2.2 Schematic of surfactant behavior above the CMC (Tanzil, 2001)

Surfactants have two important functions in EOR processes. One is to lower the interfacial tension (IFT) between oil and water phase. Below CMC, IFT decreases significantly with the increase of surfactant concentration. Above CMC, the addition of pure surfactant does not change IFT much. The other function of a surfactant is to stabilize foams used for mobility control. This occurs because it can stabilize the lamellae

of foams owing to repulsive (electrostatic obstructive) between head groups of surfactant molecules adsorbed on the film surfaces.

2.3 Fundamentals of Foam Flow in porous Media

The behavior of foam in porous media is intimately related to media connectivity and geometry. Porous media have several attributes that are important to foam flow. First, they are characterized by the size distribution of the pore bodies interconnected through the pore-throats of another size distribution. Foam generation and destruction mechanisms depend strongly on the body to throat size aspect ratio. Second, pores are not cylindrical but exhibit corners. For large pores, the wetting fluid resides in the corners of gas-occupied pores and in thin wetting films coating the pore walls (see Fig. 2.3). The non-wetting phase resides in the central portion of the large pores. Small pores are completely filled with wetting fluid. Hence, the wetting phase remains continuous. Third, when flow rates are very low and capillary forces dominate, the capillary pressure is set by the local saturation of the wetting phase and the value of the interfacial tension. Local imbalances in capillary pressure tend to equalize through the interlinked, continuous wetting phase. During biphasic flow, the nonwetting fluid flows in interconnected large pore

channels. Wetting fluid flows in interconnected small channels and in the corners of the nonwetting -phase occupied pores because of pressure gradients in the aqueous phase.

When the characteristic length scale of the pore space is much greater than the size of individual foam bubbles, the foam is called bulk foam. When the gas fraction is low, the bulk foam is “spherical foam” which consists of well-separated, spherical bubbles. When the gas fraction is high, the bulk foam is called “polyhedral foam” which consists of polyhedral bubbles separated by surfactant-stabilized thin liquid films called lamellae.

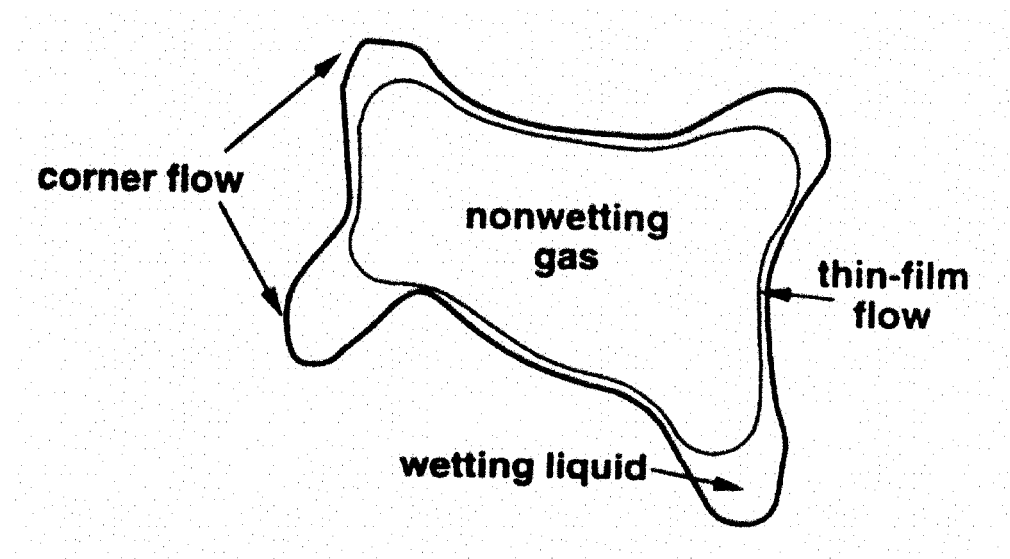


Fig. 2.3 Cross-sectional view of cornered pores. The wetting fluid is held in the pore corners. (Kovscek and Radke, 1994)

On the other hand, when the characteristic pore size is comparable to or less than the characteristic size of the dispersed gas bubbles, the bubbles and lamellae span pores completely. At low gas fractional flow, the pore-spanning bubbles are widely spaced, separated by thick wetting liquid lenses or bridges. At high gas fractional flow, the pore-spanning bubbles are in direct contact, separated by lamellae. Hirasaki and Lawson [1985] denote this direct-contact morphology as the individual-lamellae regime.

Although both bulk foam and individual-lamellae foam can exist in principle, effluent bubble sizes equal to or larger than pore dimensions are usually reported. It is now generally accepted that single bubbles and lamellae span the pore space of most porous media undergoing foam flow in the absence of fractures.

Fig. 2.4 shows the schematic of foam flow in porous media. The gas can be trapped or flowing as a continuous or discontinuous phase. In discontinuous gas foam, the entire gas phase is made discontinuous by lamellae, and no gas channels are continuous over sample-spanning dimensions. Gas is encapsulated in small packets or bubbles by surfactant-stabilized aqueous films. In continuous gas foam, the media

contain some interconnected gas channels that are uninterrupted by lamellae over macroscopic distances.

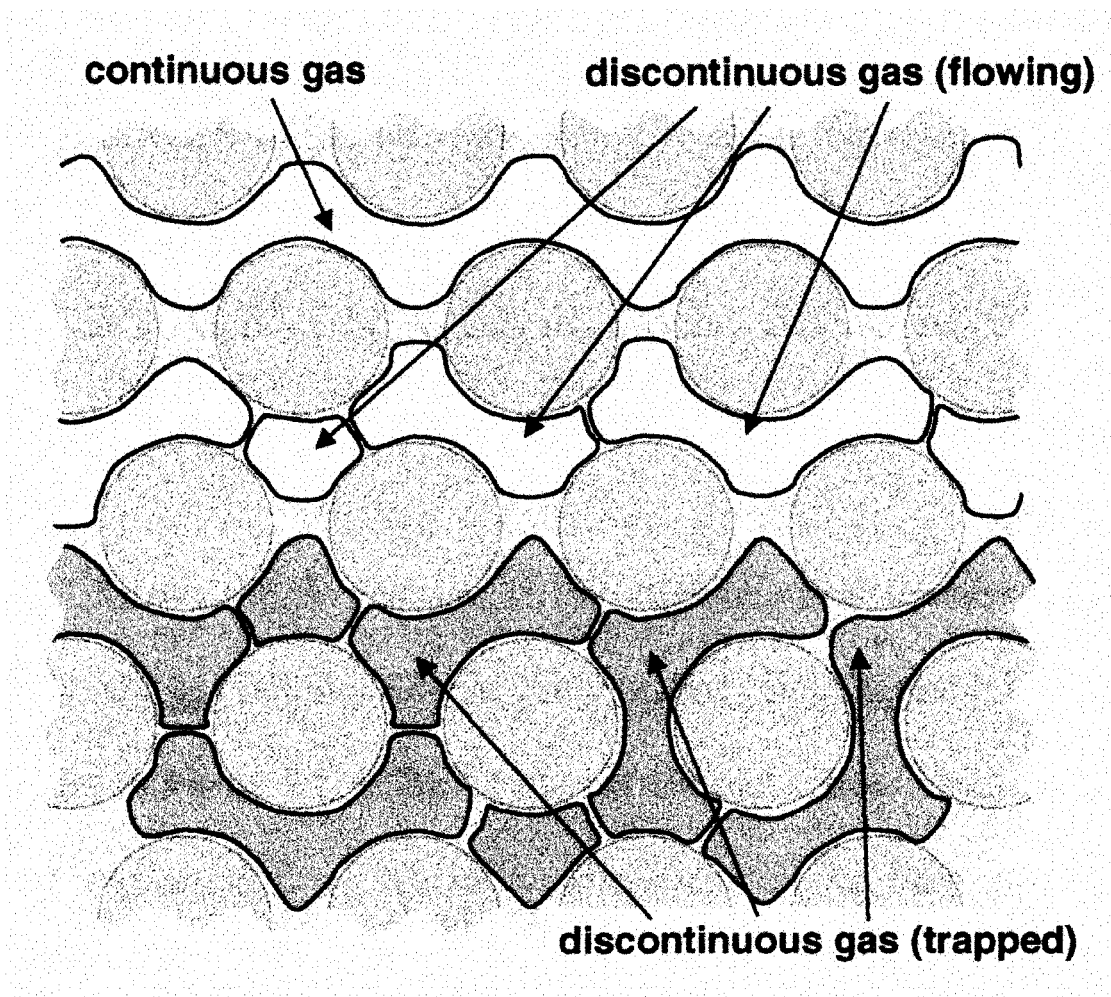


Fig. 2.4 Pore level schematic of foam in porous media (Tanzil, 2001)

Generally speaking, discontinuous foam forms under coinjection of gas and surfactant solution, provided that the wetting phase saturation and flow rate is high enough for foam generation. When the wetting phase

saturation is low enough, the lamella generation rate may become lower than that of rupture, and paths of continuous gas flow may result.

Fig. 2.4 is also a summary of the pore-level microstructure of foam during flow through porous media. Because of the dominance of capillary forces, wetting surfactant solution flows as a separate phase in the small pore spaces. Minimal wetting liquid transports as lamellae. So the wetting-phase relative permeability is unchanged when foam is present. When both flowing and trapped gas exist, flowing foam transports in large pores because the resistance there is less than in the smaller pores. Then bubble trapping can happen only in intermediate-sized pores. The relative permeability of flowing-foam is solely a function of the gas saturation of flowing bubbles and is much reduced by the trapped foam saturation. The foam bubbles, which move in the largest backbone channels, parade in series as trains. They are usually destroyed and recreated. Bubble-trains usually exist in a time-averaged sense.

Thus, we can divide foam into “weak” foam and “strong” foam. For “weak foam” with no moving lamellae, the increase in trapped gas saturation is crucial to the behavior of foam flow as it results in the blockage of gas

pathways, which reduces the relative permeability of gas. The trapped gas reduces mobility, but the rest of the gas flows as continuous gas.

“Strong” foam flows by a different mechanism. The lamellae make the flowing gas discontinuous. Then the bubble trains face much higher resistance than in continuous flow. The apparent viscosity of the discontinuous foam is usually much greater than in continuous flow. The combined effect of the reduction of gas relative permeability and the increase of apparent gas viscosity greatly increases the mobility reduction effect of the foam.

Generally speaking, the most important factors that affect foam trapping and mobilization are pressure gradient, gas velocity, pore geometry, bubble size, and bubble-train length. Increasing the pressure gradient can open up new channels, which were occupied by trapped gas.

2.4 Mechanisms of Foam Formation and Decay

As described above, the identity of a single bubble or train is not conserved over large distances. Bubble trains usually exist in a time-averaged sense. The bubbles comprising these trains are usually

destroyed and recreated. So obviously it is necessary to discuss the mechanism of foam formation and decay.

2.4.1 Foam Formation

Until now, three fundamental pore-level foam generation mechanisms are generally accepted: capillary snap-off, lamella-division and leave-behind. Generally, capillary snap-off and lamella-division generate strong foam (discontinuous gas) while leave-behind generates weak foam (continuous gas).

Capillary snap-off

Capillary snap-off can repeatedly occur during multiphase flow in porous media regardless of the presence or absence of surfactant. It is recognized as a mechanical process.

As in Fig. 2.5a, a gas finger first enters a liquid filled pore-throat. At that time, the interface curvature and capillary pressure rise to the equilibrium entry value. As the bubble passes through the pore throat, the curvature and the capillary pressure at the bubble front fall with the expansion of the interface (see figure 2.5b). A pressure gradient develops which drives

liquid from the pore body toward the pore throat, where it accumulates as a collar. As the collar grows, snap-off occurs. The generated foam bubble has a similar size to that of the pore bodies (see figure 2.5c).

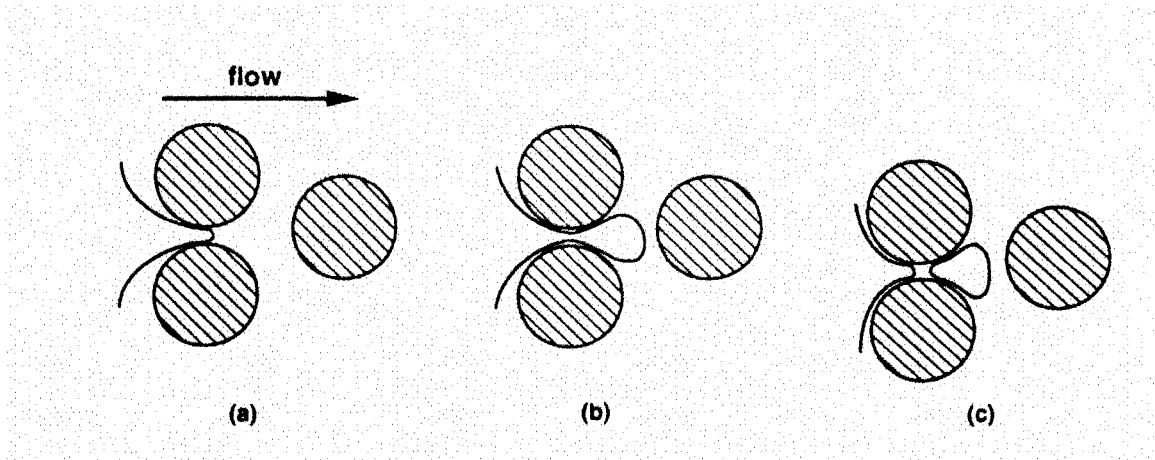


Fig. 2.5 Schematic of capillary snap-off mechanism showing (a) gas entry into liquid filled pore-throat (b) gas finger and wetting collar formation prior to breakup (c) liquid lens after snap-off (Kovscek and Radke, 1994)

There are some conditions for the snap-off to happen. First, a sufficient amount of wetting phase is needed. Second, the pressure difference across the interface in the throat must be greater than that at the leading surface. Or, in other words, the liquid pressure in the throat must be smaller than that at the leading surface. Indeed, the capillary pressure at the leading surface must be smaller than the critical value p_c^{sn} . From Kovscek and Radke [1994], this critical value p_c^{sn} is about half of the

capillary entry pressure, that is $p_c^{sn} \approx \frac{1}{2} p_c^e$. From hydrodynamic analysis, the pore body radius must be at least two times of that of pore throat to create sufficient capillary pressure reduction for snap off [Kovscek and Radke, 1994].

From the above description, it is evident that snap-off depends on liquid saturation or, equivalently, on the medium capillary pressure. Except for alteration of solution properties such as surface tension, it is essentially independent of surfactant formulation.

Lamella division

The preconditions for lamella division are that the foam lamellae must preexist and the pressure gradient must be large enough to mobilize the lamellae. As indicated in Fig. 2.6, a moving lamella train encounters a point where flow branches in two directions. Then the lamella may split into two and enter both flow paths.

The most important factors that govern lamella division are the pressure gradient, pore geometry and bubble size. The bubble size must be larger

than that of the pore body for the lamella to span the pore space. Otherwise the bubble just flows through one of the two paths from the branch point. When the flowing lamella train is surrounded by stationary lamellae, lamella division does not happen because the stationary lamellae or bubbles can act as pore walls to prevent branching of the flow. Falls *et al.* [1988], Rossen [2002] and Tanzil [2002] pointed out that lamella division should also depend on the pressure gradient and be proportional to gas velocity. Lamella division can generate discontinuous gas foam, which is strong foam.

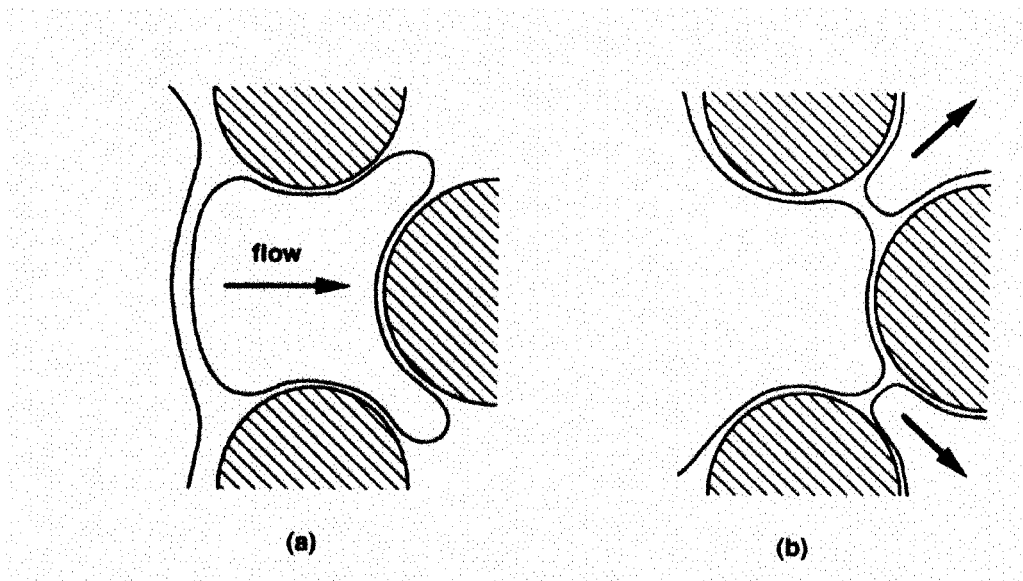


Fig. 2.6 Schematic of lamella division mechanism. A lamella is flowing from the left to the right. (a) Lamellae approaching branch point (b) Divided lamellae (Kovscek and Radke, 1994)

Leave-behind

Snap-off and lamella division can generate strong foam. Here we discuss the mechanism for weak foam generation, leave-behind.

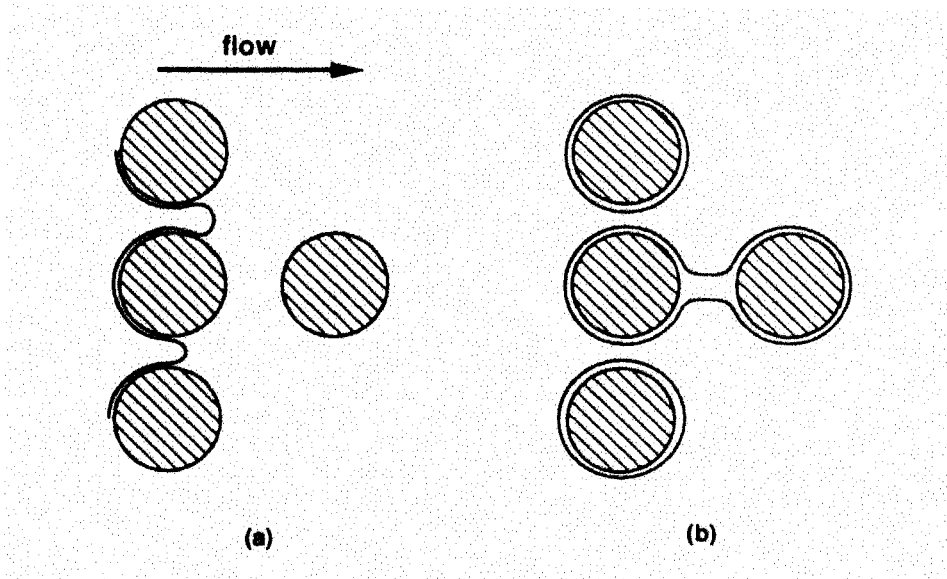


Fig. 2.7 Schematic of leave-behind mechanism. (a) Gas invasion (b) Stable lens (Kovscek and Radke, 1994)

When two gas fingers invade adjacent liquid-filled pore bodies, a lamella is left behind (see Fig. 2.7). A stationary stable lamella emerges as long as the capillary pressure is not too high and the pressure gradient is not too large.

The lamella from leave-behind is generally oriented to the direction of flow and can generate only continuous gas foam, which is weak foam.

2.4.2 Foam Destruction

The foam generation is often accompanied by foam destruction. Two mechanisms of foam destruction or coalescence have been found. They are capillary suction and gas diffusion. Because capillary suction coalescence is the primary mechanism for lamellae breakage, the discussion is focused on it, and only briefly touch upon foam coarsening by gas diffusion.

Capillary suction coalescence

Coalescence due to capillary suction is strongly affected by surfactant formulation. Thin lamellae are not thermodynamically stable and their existence is under the excess normal capillary pressure within the films, which are mainly intermolecular interactions. This can be described as the disjoining pressure π , which is the combined effect of repulsive and attractive forces within a lamella [Miller and Neogi, 1985]. Here π is a function of film thickness. When π is positive, repulsive forces dominate. When it is negative, attractive forces are indicated. When surfactant is absent, the disjoining pressure π is negative, which shows attractive van der Waals forces dominate. Then the lamella will collapse immediately. On the contrary, when a surfactant is adsorbed at the gas/liquid interface,

the lamella can be stabilized. The disjoining pressure π may be positive from the repulsive forces of the electrical double-layer caused by the adsorption of ionic surfactants. The main factors determining the stabilizing effects are the surfactant concentration, surfactant structure, and the ionic content of the aqueous solution.

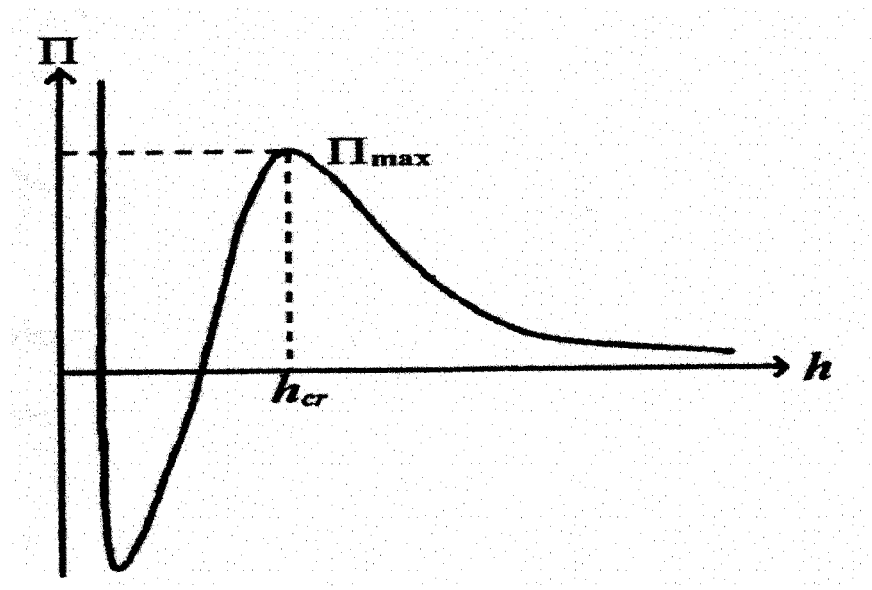


Fig. 2.8 Disjoining pressure π curve governs the stability of a thin film, h_{cr} is the critical film thickness corresponding to the maximum disjoining pressure π_{max} (Kovscek and Radke, 1994)

As shown in Fig. 2.8, from experiments, the isotherm of disjoining pressure to the thickness of the lamella film is “S” shaped just as a pressure-volume isotherm for real gas and liquid. When a static trapped film is in equilibrium at a flat interface, the disjoining pressure is equal to

the capillary pressure. The capillary pressure in a foam depends on the wetting-liquid saturation. During drainage or gas injection, the liquid saturation decreasing causes an increase of capillary pressure. In turn, the thickness of the lamella film decreases until π_{\max} is reached. When the capillary pressure increases further over π_{\max} , the film ruptures.

Coalescence behavior of flowing foam bubbles is more complicated than that of static lamella. In Fig. 2.9, a moving thin film undergoes squeezing and stretching as it translates from a pore body to a throat to another pore body. It causes film thickness to oscillate about the equilibrium film thickness established for the static film. A thin film with mobile surface will rupture during stretching if its thickness falls below the critical film thickness h_{cr} [Jimenez and Radke, 1996; Singh *et al.*, 1997]. Therefore, a moving thin film could rupture at a limiting capillary pressure p_c^* , which is less than the maximum disjoining pressure π_{\max} . In other words, moving lamellae can be even less stable than static ones.

Besides the disjoining pressure π , Marangoni effect is also a restoring and stabilizing force in a lamella [Alvarez, 1998]. When the lamella film is

stretched in the pore space, the stretching can cause a reduction in surfactant concentration and an increase in the local surface tension if the surfactant transports slowly to the lamella surface. Then the liquid can be dragged from the low surface tension region to the high surface tension region by surface flow. So the increased surface tension works against lamella thinning.

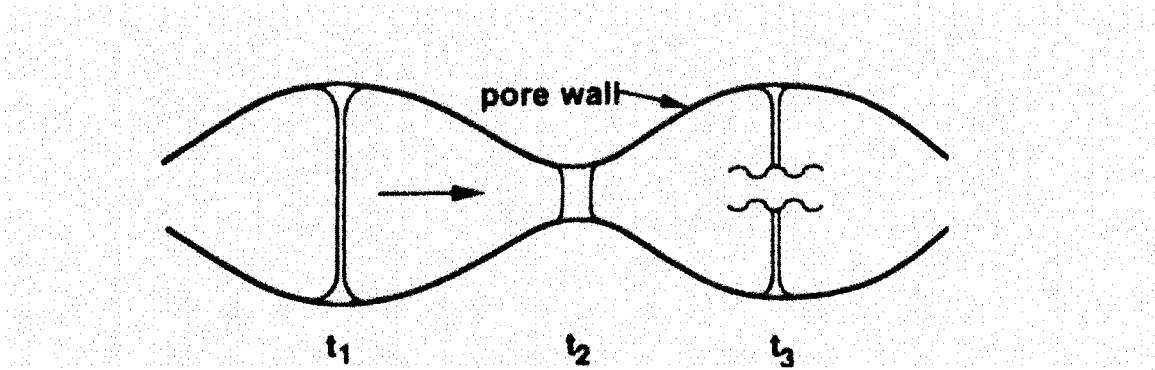


Fig. 2.9 Foam lamella translating from left to right in a periodically constricted tube (Kovscek and Radke, 1994)

Singh, Hirasaki and Miller [1997] found that Jimenez and Radke's previous theory could be applied only to a limited regime. They found that when the film surface is immobilized by surfactants, moving lamellae may be more stable than stationary lamellae. For this case, moving lamella trains will switch paths as stationary lamellae rupture and new paths of least

resistance appear. This may be the preferred mode of foam flow when it is desired to contact as much of the porous medium as possible with flowing continuous gas foam. When the film is mobile, the stationary lamellae will be more stable than the moving lamellae. This case is in qualitative agreement with Jimenez and Radke's theory. So the choice of a suitable surfactant is important for the stability of foam in porous media.

Gas diffusion

For trapped foam bubbles, the gas on the concave side of the bubble has a higher capillary pressure than that on the convex side. The pressure difference drives the gas to diffuse from the concave side to the convex side through the liquid film. The film moves to the pore throat and the lamella curvature diminishes. In porous media, coalescence by gas diffusion can take place only when two lamellae happen to reach the same pore throat. It is mainly governed by pore dimensions and the location in the pore space. Gas diffusion mechanism is less important than capillary suction mechanism in foam coalescence in porous media.

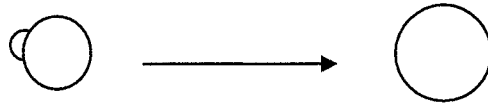


Fig. 2.10 Gas diffusion mechanism for bubble coalescence

2.5 Foam Sensitivity to Crude Oil in Porous Media

Most experiments about foam flow in porous media were done by injecting gas and aqueous surfactant solution or gas only. In true EOR field use, crude oil is present. It is necessary to understand the oil's effect on the foam stability.

When a surfactant solution comes in contact with oil during flow in a porous medium, oil can be emulsified. Fig. 2.11 shows the presence of emulsified oil droplets inside a capillary network. The oil has drained from the thinning foam film and is trapped inside the Gibbs-Plateau borders. Under the capillary pressure inside the Gibbs-Plateau border, the three phases (gas, water, and oil) come in contact and three types of aqueous films are formed (Fig. 2.12): foam film between the bubbles; emulsion

film between the oil drops; and pseudoemulsion film between the oil drops and the gas phase (bubbles), which is an asymmetrical, oil-water-gas film.

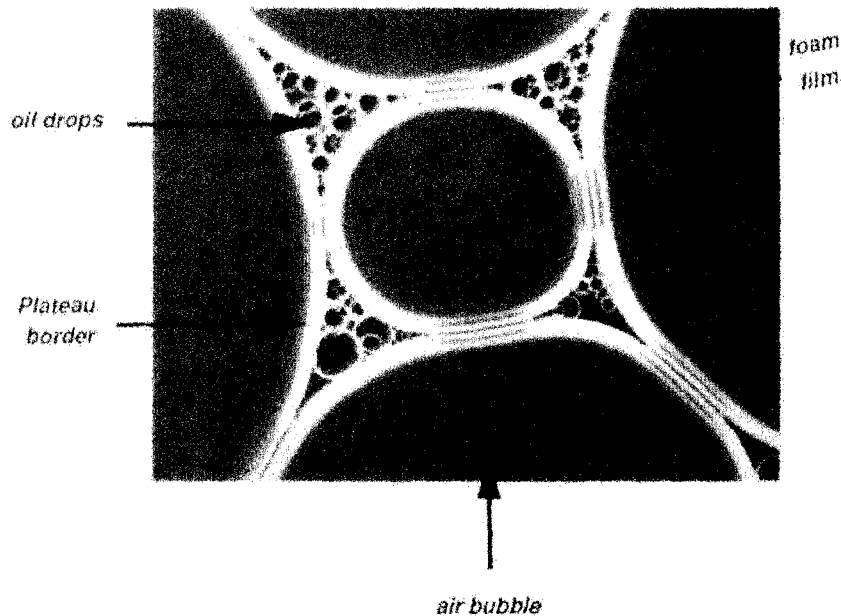


Fig. 2.11 Photomicrograph of two-dimensional foam containing emulsified oil drops that have drained from the foam films into the Plateau borders (Wasan, Koczó, and Nikolov, 1994)

For the oil to break the foam, the drops have to enter the aqueous surface. A strong indicator of whether the drop will enter is given by the so-called classical entering coefficient, which was defined by Robinson and Woods [1948] as:

$$E = \gamma_{AW} + \gamma_{OW} - \gamma_{AO} \quad (2.3)$$

where $\gamma_{AW}, \gamma_{OW}, \gamma_{AO}$ are the air-water, oil-water, and air-oil interfacial tensions respectively.

When E is positive, entry is expected. E may have different values for the initial un-equilibrated fluids and the final situation after equilibrium is reached.

If the drop can enter the interface, the spreading coefficient S of oil on water, which was defined by Harkins [1941], should be considered:

$$S = \gamma_{AW} - \gamma_{OW} - \gamma_{AO} \quad (2.4)$$

If $S > 0$, the oil can spread, the interface can expand and this expansion can result in a thinning of the film. It produces local thinning of the foam film, which can lead to rupture.

Besides the spreading coefficient S , the bridging coefficient B is also important. It is defined as:

$$B = \gamma_{AW}^2 + \gamma_{OW}^2 - \gamma_{AO}^2 \quad (2.5)$$

Even when $S < 0$, so that the oil drop forms a lens at the air-water surface instead of spreading, the foam can become unstable once the drop has entered its other surface so that it spans the film, provided that $B > 0$.

The effect of emulsified oil on foams is closely connected with the configuration of oil relative to the aqueous and gas phase. From Wasan, Koczko and Nikolov [1994], the configuration can be one of the following (figure 2.12):

- a. An oil drop without interaction with the gas-liquid surface is generally the initial oil configuration inside the foam. The entry coefficient is less than zero ($E < 0$). So the oil drop can retain its configuration.
- b. If the oil drop interacts with the gas-liquid surface, the drop gets deformed and separated by a pseudoemulsion film from the gas

phase. The entry coefficient can be less than zero if this is a steady state. It can also be greater than zero if this is a meta-stable state.

- c. If the pseudoemulsion film ruptures, the oil drop enters the surface, and an oil lens is formed at the solution surface. For this state, the entry coefficient is greater than zero but spreading coefficient is less than zero.
- d. A spread oil layer or film can form from the lens on the solution surface. At that time, the spreading coefficient is equal to zero.

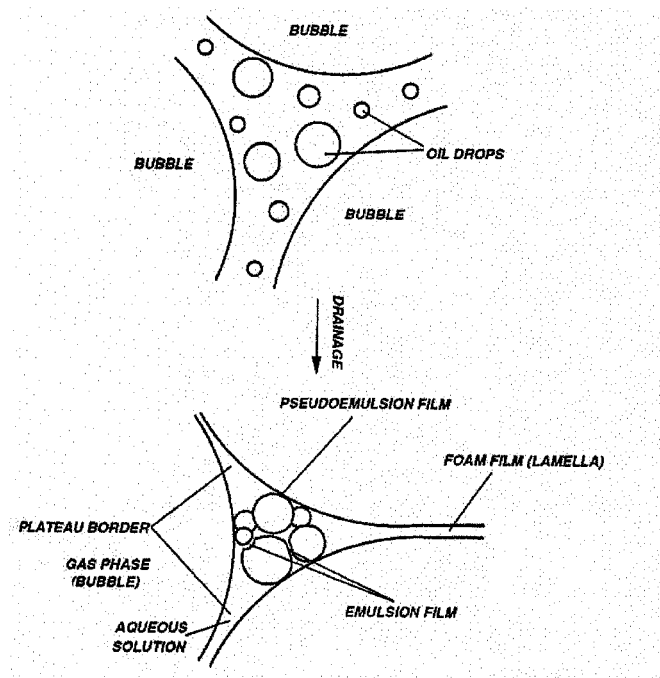


Fig. 2.12 Aqueous foam, pseudoemulsion and emulsion films and Plateau borders containing oil drops (Wasan, Koczó, and Nikolov, 1994)

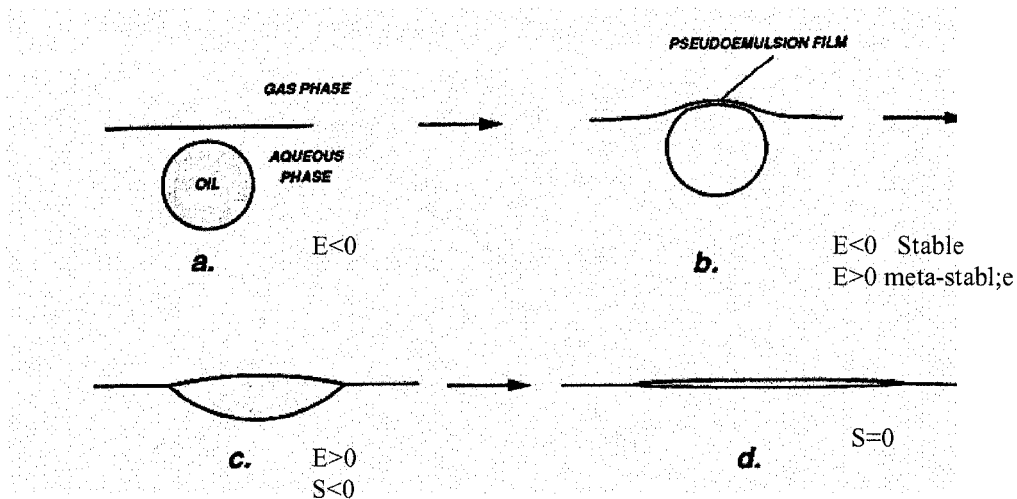


Fig. 2.13 Configurations of oil at the gas-aqueous solution interface.

a. oil drop inside the solution; b. oil drop at the surface separated by a pseudoemulsion film from the gas phase; c. oil lens; d. spread oil layer at the solution surface. (Wasan, Koczko, and Nikolov, 1994)

Entry barrier

The formation of oil bridges from pre-emulsified oil drops requires the rupture of the pseudoemulsion film. The film may be stabilized by various surface forces, which suppress the drop entry and impede the antifoam action of oil.

The entry coefficient E is a thermodynamic property. It determines whether the particular configuration of the oil drop is energetically favorable or not, but can not predict the fate of the oil drops under

dynamic conditions which exist within the draining foam film. So its application to the physical processes in porous media is limited.

Some different parameters have been suggested to quantify the entry barriers for oil drops, such as the modified entry coefficient E_g by Bergeron et al [1993], which is described as:

$$E_g = - \int_0^{\pi_{AS}(h_E)} h d\pi_{AS} \quad (2.6)$$

where the lower limit of the integral corresponds to $\Pi_{AS}(h \rightarrow \infty) = 0$, h_E is the equilibrium thickness of the thin film at a particular disjoining pressure. The classical entry coefficient E can be obtained when $h_E \rightarrow 0$ [Bergeron et al., 1993].

Another possible quantity as a measure of the pseudoemulsion film is the capillary pressure. The critical capillary pressure is the most adequate measure of the film stability because the capillary pressure is the actual external variable that forces the film surfaces toward each other against the repulsive forces (disjoining pressure) stabilizing the film. Hadjiiski et al

[1996] developed the film trapping technique (FTT) to measure the critical capillary pressure.

Oil antifoam mechanism

1. Spreading-fluid entrainment

When $E > 0$ and $S > 0$, oil droplets emerge into the air-foaming liquid surface and spread as a duplex film. If an oil droplet simultaneously emerges into both surfaces of a film, a duplex film of oil simultaneously spreads over both surfaces of the foam film. Then the film is expanded, which increases the area of film but decreases its thickness. A region composed entirely of oil is produced and rupture may happen. The process is shown in Fig. 2.14A.

2. Bridging-Dewetting mechanism

Many examples were found for which $E > 0$ and $S < 0$ but where the foam film is unstable. The bridging-dewetting mechanism was proposed by Garrett [1980] to explain the phenomenon.

As shown in Fig. 2.14, if an oil lens bridges a plane-parallel foam film by emerging into both air-water surfaces, no configuration of mechanical

stability is available to the lens if the angle θ^* , formed by the tangents to the air-water and oil-water surfaces so denoted as θ_{OW} later on, is $> 90^\circ$. By a vector force balance at the three-phase contact point, θ_{OW} can be related to the three interfacial tensions by

$$\cos\theta_{OW} = \frac{\gamma_{AO}^2 - \gamma_{AW}^2 - \gamma_{OW}^2}{2\gamma_{AW}\gamma_{OW}} \quad (2.7)$$

The critical condition for rupture ($\theta_{OW} > 90^\circ, \cos\theta_{OW} < 0$) can be expressed as $\gamma_{AO}^2 - \gamma_{AW}^2 - \gamma_{OW}^2 < 0$, that is actually $B > 0$.

The precondition for this antifoam mechanism is that the oil drop is sufficiently hydrophobic. If not, when the oil drop is more hydrophilic, the curvature of the air-water interfaces is concave or $\theta_{OW} < 90^\circ$, the resulting pressure difference pulls liquid toward the drop to increase the film thickness, tending to stabilize the film.

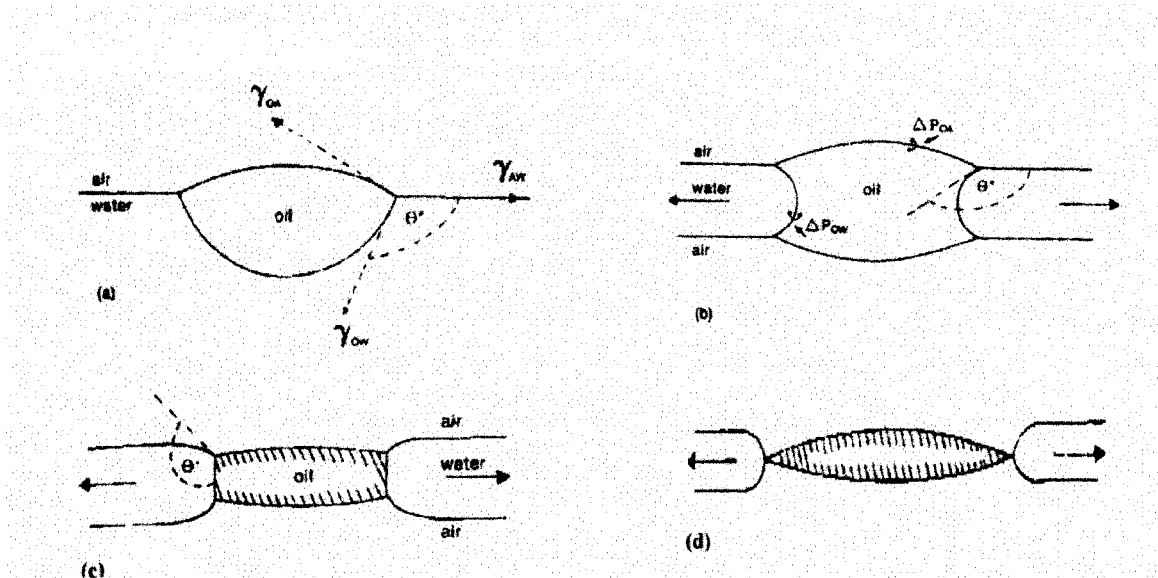


Fig 2.14 Oil lens, definition of $\theta^*(\theta_{ow})$ and unstable bridge configurations (Garrett, 1993)

3. Oil-bridging stretching mechanism

In the bridging-dewetting mechanism of Fig. 2.13, the film surfaces were assumed to be perfectly flat. But in reality, foam film surfaces have deformability. Taking the deformability into account, Denkov [1999] presented the oil-bridging stretching mechanism to explain the unstable foam film. The oil bridges might be in equilibrium with the meniscus surrounding them even if the bridging coefficient B is positive. When B is positive, the relative size of the bridge to the film thickness determines if the equilibrium is stable or not. When the bridges are large, the

equilibrium is always unstable. The critical value depends on the three-phase contact angle (i.e. on the value of B). Once shifted from the equilibrium state, the unstable bridges spontaneously expand and eventually rupture the foam film. At negative value of B , the bridges are in stable equilibrium with the contiguous meniscus.

Below figure 2.15 is a schematic illustration of the above three defoaming mechanisms. For all of these mechanisms, the first step is drop entry, for which the entry coefficient E is positive and the entry barrier is small.

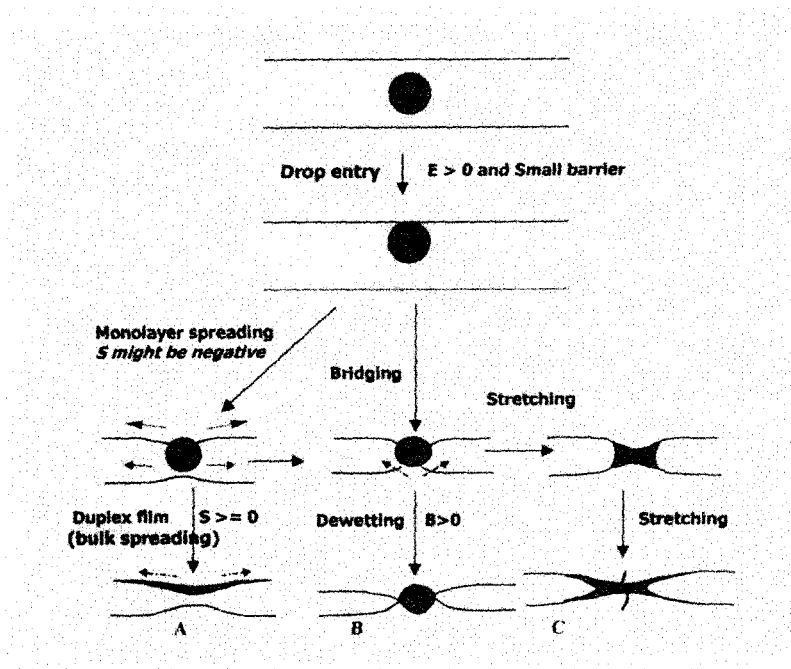


Fig 2.15 Schematic profile of several defoaming mechanisms (Zhang, 2002)

- (A) Spreading-fluid entrainment
- (B) Bridging-dewetting mechanism
- (C) Bridging-stretching mechanism

2.6 Foam flow in capillary tubes

From Hirasaki and Lawson [1985], a reasonable conceptual model of a natural porous medium is a bundle of interconnected capillaries of different sizes and containing constrictions. From their research, the apparent viscosity is the sum of three contributions (as shown in Fig. 2.16): those resulting from slugs of liquid between bubbles, the resistance to deforming the interface when a bubble passes through a capillary, and the surface tension gradient as surface active material is swept from the front of the bubble and accumulates at the back of the bubble.

The viscosity contribution from liquid slugs in capillary tube from Hirasaki and Lawson [1985] is:

$$\mu_{app}^{liq} = \mu L_s n_L \quad (2.8)$$

where L_s is the length of liquid slugs and n_L is the number of equivalent lamellae per unit length.

The contribution of the deformation of the foam bubble to apparent viscosity in capillary tube was also derived. In a capillary tube, for the bubbles shown in figure 2.17, the expression for the net dynamic pressure drop is:

$$\Delta p_{dynamic} = 2.26(\sigma / r_c)(3\mu U / \sigma)^{2/3}[(r_c / R)^2 + 1] \quad (2.9)$$

where U is the velocity of bubble, σ is the surface tension, r_c is the radius of curvature of gas-liquid interface and R is the capillary radius.

The apparent viscosity in a tube with the model above is derived from Poiseuille flow as:

$$\mu_{app}^{shape} = \frac{n_L \Delta p R^2}{8U} = 0.85 \frac{(\mu n_L R)}{(r_c / R)} (3\mu U / \sigma)^{-1/3} [(r_c / R)^2 + 1] \quad (2.10)$$

From Hirasaki and Lawson [1985], the apparent viscosity resulting from surface tension gradient is:

$$\mu_{app}^{grad} = (\mu n_L R)(3\mu U / \sigma)^{-1/3} \sqrt{N_s} \frac{(1 - e^{-N_L})}{(1 + e^{-N_L})} \quad (2.11)$$

where N_L is the dimensionless length of the thin film portion of bubble and N_s is the dimensionless number for surface tension gradient effect. The value of N_L describes the degree of mobility of the interface. The relationship between the two dimensionless numbers is:

$$N_L = \frac{-2L_B}{(P)_c (3\mu U / \sigma)^{1/3} r_c \sqrt{N_s}} \quad (2.12)$$

where $(P)_c$ is a coefficient.

When N_L is large, μ_{app}^{grad} is independent of the exact value of N_L . Then the value of N_s can be estimated. The value of coefficient $(P)_c$ is estimated when N_L is small.

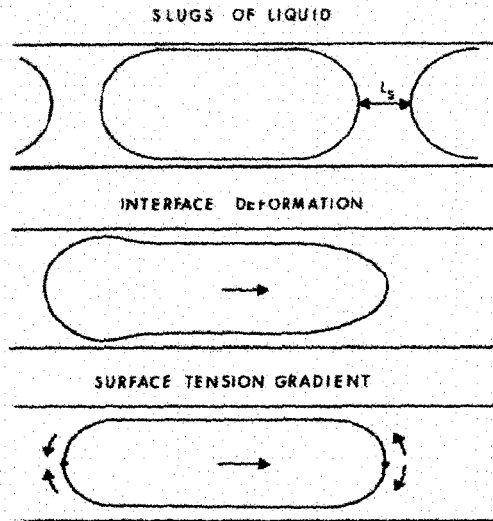


Fig 2.16 Mechanisms affecting apparent viscosity in smooth capillaries
(Hirasaki and Lawson, 1985)

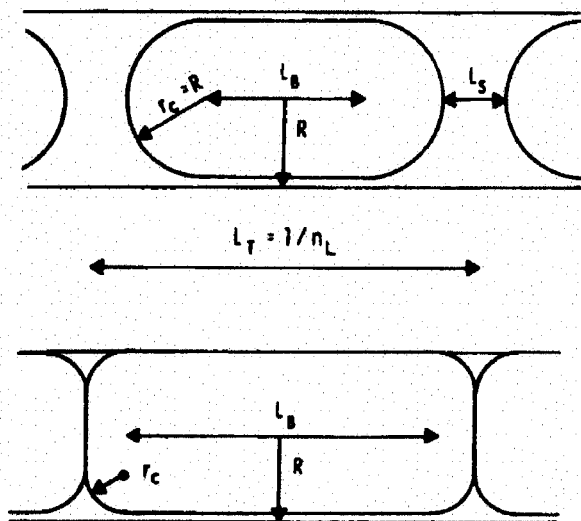


Fig. 2.17 Bubble configurations when the bubbles are separated and when they are touching (Hirasaki and Lawson, 1985)

Hiraskai and Lawson [1985] conducted some experiments on foam flow in capillary tubes and reached the following conclusions.

1. The foam texture (a measure of the bubble volume) is a key parameter in determining whether the foam exists as a bulk foam or a chain of bubbles that are separated by individual lamellae.
2. The dependence of apparent viscosity on the capillary radius at a constant velocity is proportional to: the 2.5 power of the radius for radii that are small compared to the bubble radius and the 2.0 power of the radius for radii that are large compared to the bubble radius.
3. The dependence of apparent viscosity on the foam texture is proportional to: the -2.0 power of the equivalent bubble radius for bubble radii that are small compared to the capillary radius and the -3.0 power of the equivalent bubble radius for bubble radii that are large compared to the capillary radius.
4. The dependence of apparent viscosity on the velocity is proportional to the $-1/3$ power of velocity when the foam is bulk foam or the velocity is low for individual lamellae, and to the $-2/3$ power of velocity for individual lamellae at high velocity.

2.7 Effect of heterogeneity on foam flow

Foam is used in EOR process to change the mobility of gas in the reservoir. The field situation is primarily heterogeneous and multidimensional. It is found the mobility of gas can be reduced more in high permeability regions than in low permeability regions. The reason is that the stability of foam is higher in high permeability regions than low permeability regions. Khatib *et al.* proposed the limiting capillary pressure mechanism in 1988, which is discussed below.

2.7.1 Capillary pressure's role in bulk foams

First let's discuss capillary pressure's role in foam stability outside porous media, or bulk foam. From Derjaguin-Laudau-Verwey-Overbeek (DLVO) theory, when gas/liquid interfaces are present, ionic surfactant molecules from an aqueous solution adsorb preferentially at the interface, thereby creating charged surfaces. The overlap of the electric fields from these charged layers imparts stability to a foam lamella. The double layer repulsion balances the van der Waals forces plus the capillary pressure, which acts to force the charged surfaces closer to one another and destabilize the system. As the capillary pressure increases, the work required for breaking the film decreases. Thus, the capillary pressure can

play a role in determining the stability of foams outside porous media. Khristov *et al.* [1988] presented the concept of the “critical” capillary pressure above which the lifetime of lamellae becomes exceedingly short. The critical capillary pressure varies with surfactant formulation-i.e., the type and concentration of surfactant and electrolyte.

The presence of salts may be good or bad for the stability of bulk foams. From DLVO theory, at higher electrolyte levels, the length over which the electric field from the charged surfactant layers decay should shorten and the repulsive forces should weaken. But this effect may be offset because salt raises the surface concentration of surfactant at the gas/liquid interfaces [Nilsson, 1957].

2.7.2 Limiting capillary pressure for foam in porous media

The stability of foams in porous media may likewise depend on capillary pressure. But in porous media, all lamellae do not coalesce at some “critical” capillary pressure. Instead, because lamellae are convected or generated in situ, the capillary pressure increases up to a limiting capillary pressure as foam generation creates stronger foam or the gas fractional flow is raised. With further decrease in gas mobility or increase in gas

fractional flow, the capillary pressure remains at its limiting value while the foam texture remains constant or becomes coarser respectively.

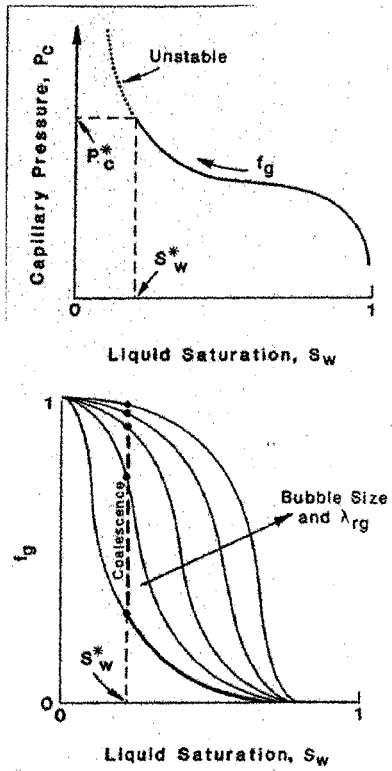


Fig 2.18 Sketches of capillary-pressure and fractional-flow curves operating during a two-phase displacement [Khatib, Hirasaki, Falls, 1988]

From Fig. 2.18, if the capillary pressure during a foam displacement can not exceed a limiting value P_c^* , because of the stability of lamellae, then the liquid saturation must be greater than or equal to the corresponding liquid saturation, S_w^* , because the capillary pressure is a monotonic function of saturation. Suppose that gas and liquid are flowing as a foam

of constant bubble size at a given gas velocity. As the gas fractional flow is raised, the liquid saturation declines until the limiting value S_w^* (at P_c^*) is attained. If the gas fractional flow is increased further, foam texture must coarsen to keep the capillary pressure from rising above the limiting value.

2.7.3 Behavior of foam in low-permeability media

From Khatib , Hirasaki and Falls [1988], the limiting capillary pressure is a decreasing function of gas flow rate and of the permeability. Then below some permeability, the limiting capillary pressure will become less than the capillary entry pressure, as shown in Fig. 2.19. When the capillary pressure is less than the capillary entry pressure, the implication is that flowing-foam lamellae are not stable and will coalesce. If the flowing foam coalesces, then either the gas will flow as a continuous phase or moving lamellae will have a short lifetime.

As shown in Fig. 2.20, Khatib and Hirasaki [1988] speculate on the consequences of gas flowing as a continuous phase whenever the permeability is less than the permeability at which the limiting capillary

pressure is equal to the capillary entry pressure. The limiting capillary pressure applies to the dynamic stability of flowing lamellae. Stationary lamellae, by contrast, have zero velocity and thus can be expected to be stable at capillary pressures in excess of the limiting capillary pressure for a flowing film. It is presumed that the stationary lamellae block some fraction of the gas-saturated pore space such that the relative gas mobility is at some reduced value and that the moving gas flows as a continuous phase. As a consequence, the gas mobility may have a dependence on permeability, as shown by the solid line in figure 3.5. This can explain why the mobility reduction effect of foam is better in high permeability regions than low permeability regions.

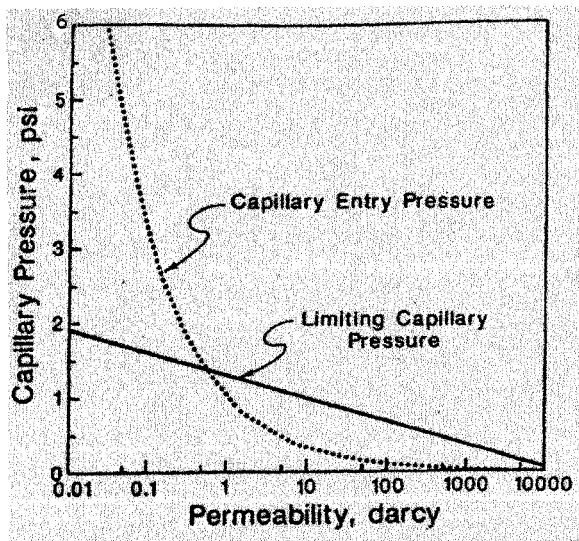


Fig 2.19 Relationship between capillary-entry pressure, limiting capillary pressure, and permeability [Khatib, Hirasaki, Falls, 1988]

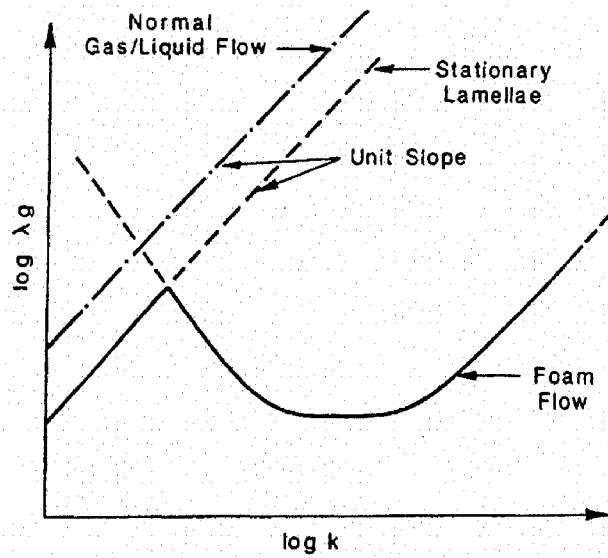


Fig 2.20 Schematic of the correlation between foam mobility and permeability [Khatib, Hirasaki, Falls, 1988]

2.7.4 Foam flow in heterogeneous porous media

Two kinds of heterogeneous systems have been used in previous laboratory studies to investigate the ability of foam to improve sweep efficiency in parallel cores with differing permeabilities. The cores can be either isolated or placed in contact where cross flow can occur, e.g., in composite cylindrical cores. As indicated below, some of the studies have dealt with gas injection, others with injection of acid solutions to increase permeability.

Casteel & Djabbarah [1988] used two parallel Berea cores with a 6.4 permeability ratio. They compared the use of foam with the water-alternating-gas process and showed that foam was preferentially generated in the more permeable core and could divert CO₂ towards the less permeable core. Llave et al. [1990] obtained similar results with parallel cores with a 4.6 permeability ratio. Zerhboub et al. [1994] studied matrix acidizing in a stratified system. They also showed clearly the effect of foam diversion. All these experiments, performed with parallel cores, considered only the case of porous media which were not in capillary contact, so that crossflow was prohibited.

Yaghoobi et al. [1996] used a short composite cylindrical core to study the influence of capillary contact. They observed a reduction of mobility in the higher permeability zone and called it “SMR”, Selective Mobility Reduction.

Siddiqui et al. [1997] investigated the diversion characteristics of foam in Berea sandstone cores of contrasting permeabilities. They found that the diversion performance strongly depended on permeability contrast, foam quality and total flow rate.

Bertin et al. [1999] studied foam propagation in an annularly heterogeneous porous medium having a permeability ratio of approximately 70. Experiments were performed with and without crossflow between the porous zones. In situ water saturations were measured continuously using X-ray computed tomography. They observed that foam fronts moved at the same rates in the two porous media if they were in capillary contact. On the other hand, when crossflow was prohibited due to the presence of an impervious zone between the layers, gas was blocked in the high permeability zone and diverted towards the low permeability core.

Osterloh and Jante [1992] identified two distinct foam-flow regimes: a high-quality (gas fractional flow) regime in which steady-state pressure gradient is independent of gas flow rate, and a low-quality regime, in which steady-state pressure gradient is independent of liquid flow rate. In each regime foam behavior is dominated by a single mechanism: at high qualities by capillary pressure and coalescence [Osterloh and Jante, 1992], and at low qualities by bubble trapping and mobilization [Cheng et al., 2000]. Cheng et al. [2000] found that foam diversion is sensitive to permeability in high quality regime and insensitive to permeability in low

quality regime. But in the low quality regime the harmful effect on diversion from crossflow is much less.

Nguyen et al. [2003] conducted experiments to study foam-induced fluid diversion in isolated and capillary-communicating double layer cores. They found that there existed a threshold injection foam quality below which foam no longer invaded the low permeability layer. This threshold depends on the permeability contrast and foam strength in the high permeability layer. The use of foam below the threshold quality is appropriate in foam acid diversion, where the presence of foam in the high permeability layer helps control the relative acid permeability, and acid can still penetrate the low permeability layer without resistance of foam.

Few studies have been reported of foam in fractures. Kavscek et al. [1995] experimentally studied nitrogen, water and foam flow through a transparent rough walled rock fracture with a hydraulic aperture of 30 μ m. In these experiments, foam flow resistance was approximately 100-540 times greater than that of nitrogen for gas fractional flow ranging from 0.60 to 0.99.

Our purpose is to understand the mechanisms of foam flow in fractures and predict foam diversion in heterogeneous fracture systems. We derive below a theory to predict the foam apparent viscosity, starting from the existing theory for foam flow in capillary tubes. We made a uniform fracture model and conducted experiments to verify the theory. Also a heterogeneous fracture model was set up and used to study foam diversion. Finally, we developed a model to predict the sweep efficiency in multiple heterogeneous fractures with log-normal distributed apertures.

2.8 Alkaline surfactant enhanced oil recovery process

Alkaline surfactant is a kind of chemical method in enhanced oil recovery that involves the injection of alkaline-surfactant solution into the reservoir. Both injection of surfactants and injection of alkaline solutions to convert naturally occurring naphthenic acids in crude oils to soaps can achieve ultralow interfacial tensions to get oil recovered. Most of the work at present was directed toward developing micellar-polymer processes to recover residual oil from sandstone formations using anionic surfactants. However, Nelson et al. [1984] recognized that in most cases the soaps formed by injecting alkali would not be at the "optimal" conditions needed to achieve low tensions. They proposed that a

relatively small amount of a suitable surfactant be injected with the alkali so that the surfactant/soap mixture would be optimal at reservoir conditions. With polymer added for mobility control the process would be an alkali-surfactant-polymer (ASP) flood. The use of alkali also reduces adsorption of anionic surfactants on sandstones because the high pH reverses the charge of the positively charged clay sites where adsorption occurs.

The initial portion of a Shell field test, which did not use polymer, demonstrated that residual oil could be displaced by an alkaline/surfactant process. Several ASP field projects have been conducted with some success in recent years in the US and Canada [Vargo et al., 2000, Wyatt et al., 2002]. Pilot ASP tests in China have recovered more than 20% OOIP in some cases, but the process has not yet been applied there on a large scale [Wang et al 1999, Qiao et al 2000, Chang 2006].

The application of surfactant processes including ASP to carbonate reservoirs received little attention until the last few years, probably owing to concern that the main surfactants being considered, e.g., alkyl/aryl sulfonates, would form calcium and magnesium sulfonates that would

either precipitate or partition into the oil phase. An exception was the work of Adams and Schievelbein [1984], who found from laboratory experiments and two well pair tests that oil could be displaced in a carbonate reservoir using a mixture of petroleum sulfonates and alkyl ether sulfates or alkyl/aryl ether sulfates.

Carbonate reservoirs are typically mixed wet and often fractured as well. As a result, considerable effort has been directed toward promoting spontaneous imbibition of aqueous solutions by adding surfactants to alter wettability. Austad and coworkers [2003] suggested using cationic surfactants to promote desorption of acids on carbonate rock surfaces, making the rock more water wet. Others have investigated the effectiveness of various surfactants in altering wettability [Chen et al., 2001, Xie et al., 2005]. Hirasaki and Zhang [2004] showed that if sodium carbonate was used as the alkali and injected with a suitable anionic surfactant, the usual positive charge of carbonate rocks could be reversed with the results that surfactant adsorption was greatly decreased and oil wet surfaces were modified to intermediate wet. They found that a significant amount of oil could be recovered from an initially oil wet carbonate core placed in an imbibition cell containing a suitable

aqueous solution of surfactant, sodium carbonate and sodium chloride. The wettability modification allowed the surfactant solution to enter and the resulting low interfacial tension reduced capillary forces to the point that oil rose to the top of the core, where it was released. No oil was recovered when a sodium chloride solution was used instead. They proposed that such alkaline/surfactant solutions could be injected into fractured carbonate formations to increase recovery. Seethepalli et al [2004] and Adibhatla et al. [2005] pursued a similar approach experimentally and performed simulations of how such a process would perform for field conditions.

2.9 Enhanced oil recovery in fractured carbonate reservoir

The formation of interest is a fractured and preferentially oil-wet carbonate, where water flooding is not effective because water flows preferentially in the fractures and negative capillary pressure keeps water from entering the matrix, which results in a large amount of residual oil trapped in the matrix below oil-water contact. The average matrix permeability is 100 md, but the fracture permeability is greater than 1,000 md [Chen, 2000]. When water invades the reservoir, it flows into fractures instead of matrix, which leads to a high residual oil saturation.

With this background, it is evident that a cost effective enhanced oil recovery method for the targeted reservoir is needed. In the last decade, extensive research on alkaline/surfactant flooding has been carried out worldwide, Bahrain [Zubari and Sivakumar, 2003], Canada [e.g. Taylor and Nasr-El-Din, 1996], China [e.g. Han et al., 1997], France [e.g. Baviere et al., 1995], Saudi Arabia [e.g. Al-Hashim et al., 1996], USA [e.g. Nelson, 1989], to name a few. Alkaline/surfactant flooding combining principal technologies of several traditional chemical methods has great prospect for increasing oil recovery.

Clark et al. [1988] estimated the ultimate recoveries of water, polymer, alkaline/polymer, and alkaline/surfactant/polymer flooding for West Kiehl field, and alkaline/surfactant/polymer flooding was expected to increase ultimate recovery dramatically.

Olsen et al. [Olsen et al., 1990], too, worked on an oil-wet carbonate reservoir. They compared oil recovery of alkaline/surfactant/polymer flooding with that of alkaline/ polymer and polymer flooding, and found alkaline/surfactant/polymer flooding has a much better post-water-flood recovery than the other two. They concluded that a cost effective

alkaline/surfactant/polymer flooding could be designed for application in a carbonate reservoir.

Delshad et al. [Delshad et al., 1998] predicted oil recovery of a Chinese oil field by computer simulation. Among water, alkaline, surfactant/polymer, and alkaline/ surfactant/polymer flooding, alkaline/surfactant/polymer flooding exhibited the best simulation result.

Chapter 3

FOAM FLOW IN HOMOGENEOUS FRACTURE

3.1 Foam apparent viscosity in homogeneous fracture

Gas has a very low viscosity compared with oil and water. However, when gas is a dispersed phase, as in foam, its apparent viscosity is greatly increased, i.e., its mobility is greatly reduced. Hirasaki and Lawson [1985] described a mathematical model for apparent viscosity in a smooth capillary tube for bubbles large enough that they travel sequentially along the tube. They found that the most important variable affecting foam apparent viscosity in uniform, smooth capillaries is foam texture or bubble size, which determines the number of interfaces per unit length. Dynamic changes at these interfaces strongly influence apparent viscosity, which is the sum of three contributions as in Fig. 3.1:

- 1) Slugs of liquid between gas bubbles resist flow.
- 2) Viscous and capillary forces result in interface deformation against the restoring force of surface tension. The different curvatures at the front and rear of a moving bubble dictate the pressure drop required for bubble motion.

- 3) The surfactant is swept to accumulate at the back and be depleted at the front of the bubble, which causes a surface tension gradient that resists flow.

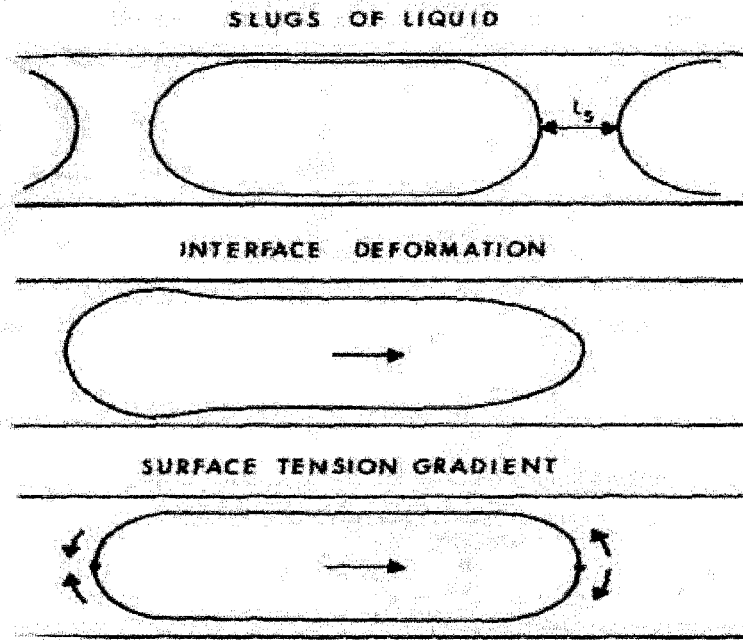


Fig. 3.1 Mechanisms affecting apparent viscosity in smooth capillaries

(Hirasaki and Lawson, 1985)

The goal of our research is to find the optimum condition to divert the greatest amount of surfactant solution into thinner fracture regions. For that purpose, we first adapt the above model for capillary tubes to the

case of a uniform fracture and describe experiments to confirm the validity of the model and determine the parameters involved. Then we extend both model and experiments to parallel flow in fractures of different thickness.

As indicated above, there are three contributions to the apparent viscosity of foam in a circular smooth capillary tube. The first is that from liquid between the bubbles, which is given by equation (3.1). This equation is also applicable to flow in a wide fracture of uniform thickness.

$$\mu_{app}^{liq} = (1 - f_g) \mu^{liq} \quad (3.1)$$

where μ^{liq} is the viscosity of pure liquid and f_g is the gas fractional flow.

The contribution of deformation of the foam bubble to apparent viscosity in a uniform fracture can be predicted by comparing with that from foam flow in a capillary tube. From Hirasaki and Lawson [1985], the equation for the net dynamic pressure drop across a single bubble is:

$$\Delta p_{dynamic} = 2.26 \left(\frac{\sigma}{r_c} \right) \left(\frac{3\mu^{liq}U}{\sigma} \right)^{2/3} [(r_c / R)^2 + 1] \quad (3.2)$$

Here U is the velocity of the bubble, σ is the surface tension, r_c is the radius of curvature of gas-liquid interface and R is the capillary radius. When the bubbles are not in contact $r_c = R$ and this equation simplifies to Bretherton's result [1961]. For flow of large bubbles between parallel plates, a similar equation applies but without the term in brackets as above because the radius of curvature across the width of the channel is much greater than r_c :

$$\Delta p_{dynamic} = 2.26 \left(\frac{\sigma}{r_c} \right) \left(\frac{3\mu^{liq}U}{\sigma} \right)^{2/3} \quad (3.3)$$

The apparent viscosity from the contribution of foam bubble deformation in a uniform fracture can be predicted from the equations for plane-Poiseuille flow:

$$\mu_{app}^{shape} = \frac{n_L \Delta p_{dynamic} b^2}{12 U} = \frac{0.57 \mu^{liq} (n_L b) \left(\frac{3\mu^{liq}U}{\sigma} \right)^{-1/3}}{\left(\frac{r_c}{b} \right)} \quad (3.4)$$

where n_L , the number of equivalent lamellae per unit length, is a function of the number of bubbles per unit area and b is the fracture aperture or the distance between the two parallel plates. If the bubbles are distributed uniformly, from the derivation in Appendix A, one finds

$$n_L = \left[\frac{3f_g b}{4\pi r_B^3} \right]^{1/2} \quad (3.5)$$

where f_g is the gas fractional flow and r_B is the equivalent bubble radius. The equivalent bubble diameter is assumed to be larger than the aperture. If the bubbles are not in contact, the radius of curvature, r_c , is equal to the half aperture of the fracture, and substitution of equation (3.5) into equation (3.4) yields

$$\frac{\mu_{app}^{shape}}{\mu^{liq}} = 0.56 \left(\frac{3\mu^{liq} U}{\sigma} \right)^{-1/3} f_g^{1/2} \left(\frac{b}{r_B} \right)^{3/2} \quad \text{where } b/(2r_B) \leq 1 \quad (3.6)$$

The total apparent viscosity can be obtained from measuring the pressure difference across the model. That is, from plane-Poiseuille equations:

$$\mu_{app} = \frac{b^2 |\nabla p|}{12U} \quad (3.7)$$

where $|\nabla p|$ is the pressure gradient.

By comparing the sum of μ_{app}^{shape} and μ_{app}^{liq} with the value of μ_{app} , the contribution from surface tension gradient was found to be insignificant in our system.

3.2 Experimental methods

The fracture model used is shown in Fig. 3.2. It consists mainly of two parallel glass plates. Changing the gasket thickness between the plates can change the aperture of the fracture. The thick glass is from Lone Star Glass Company, Houston, TX. It is borosilicate glass with 35.56 cm length and 20.32 cm width. Its thickness is 6.35 ± 0.3 mm. The surface of the glass is polished. For experiments with a homogeneous fracture, the uniformly thick gasket keeps a uniform distance between the plates.

A schematic diagram of the equipment for the foam experiments is shown in Fig. 3.3. A Harvard syringe infusion pump (Model 22) is used to inject

surfactant solution and a Matheson mass flow controller (Model 8270) is used to inject air into the foam generator. Relatively uniform bubbles can be generated only when the air and liquid are introduced on opposite sides of the frit in the foam generator. Choosing frits with different pore sizes can generate different sizes of bubbles. The borosilicate frits are from Chemglass Company, Vineland, NJ. Two grooves were made along the inlet and outlet of the fracture model to assure uniform pressures at both locations.

Homogeneous Fracture Model

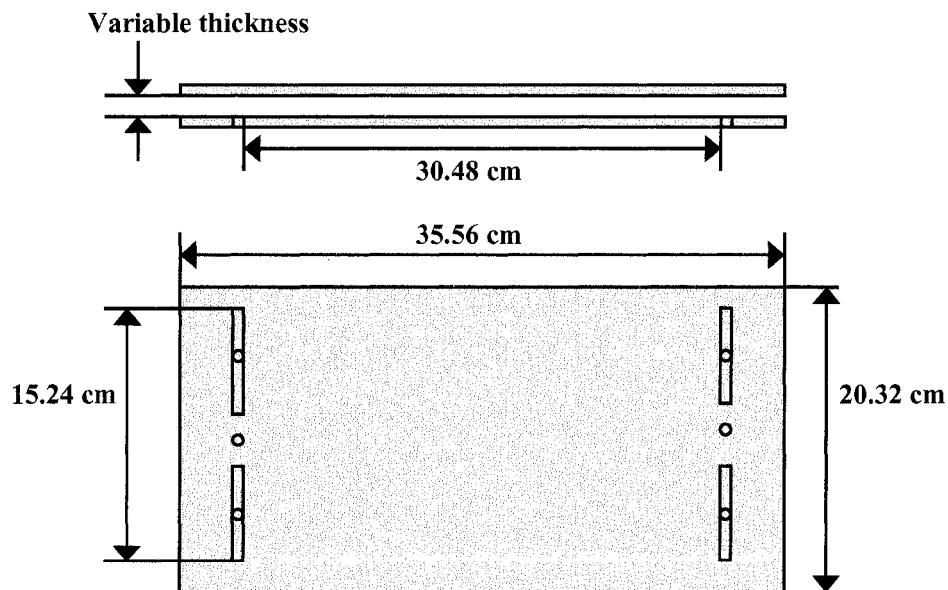


Fig. 3.2 Detailed diagram of homogeneous fracture model

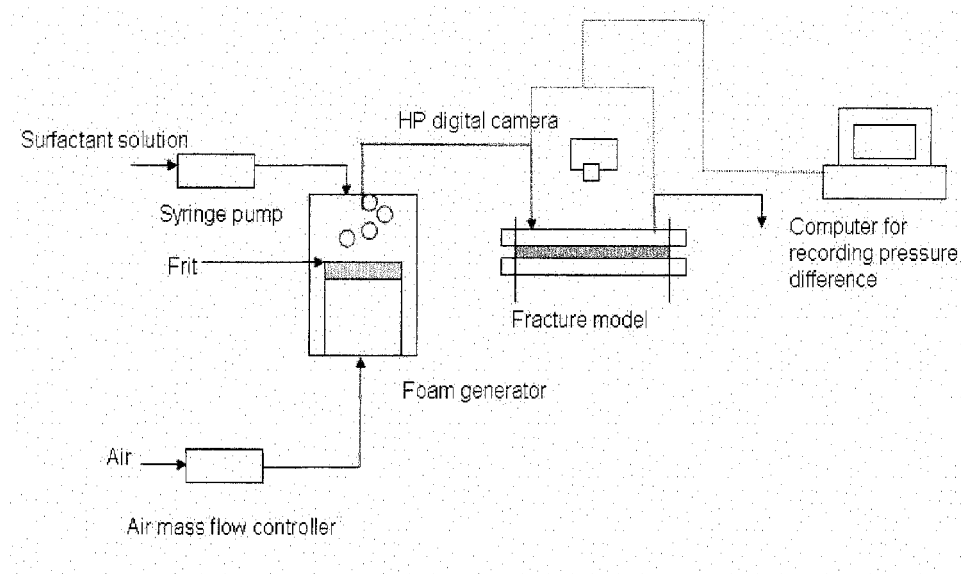


Fig 3.3 Set –up diagram for foam mobility control experiment in fracture model

The surfactant solution in the experiments was 0.5% C13-4PO and 0.5% STEOL CS330. C13-4PO is from Harcros Company, and its chemical description is propoxylated iso-C13 alcohol ether sulfate, ammonium salt. STEOL CS330 is from Stepan Company and its chemical description is C12-3EO sulfate. The solution contained 0.23% NaCl, 0.07% CaCl_2 and 0.04% MgCl_2 . The bubble diameters in the experiment ranged from 0.4 to 1.0 mm. The aperture was 0.1 mm or 0.2 mm for homogeneous fracture experiments. The gas fractional flow range was from 0.0 to 0.9. The values used for the viscosity of solution and surface tension were 0.001 Pa's and 28 mN/m from measurement.

3.3 Foam bubble size measurement in fractures

Two different methods were used to determine the average bubble size: image analysis and capillary tube experiments. From analysis of images taken just after foam flow has stopped, the average bubble size and bubble size distribution can be obtained with the help of image analysis software “IPTK”, which was developed by Reindeer Graphics Inc., Asheville, NC. The average bubble size may also be obtained by counting the number of lamellae in a given capillary tube length by letting foam flow into capillary tubes with diameters less than the bubble diameter. The mean bubble sizes obtained from image analysis and capillary tube experiments are in good agreement as shown in Fig. 3.4. The bubble size shown is the equivalent spherical diameter. The standard deviation of the bubble size distribution is about 20%. From Fig. 3.4, the mean bubble size and standard deviation remain constant at different flow rates and different gas fractional flow. Other experiments showed similar behavior as long as the bubble equivalent diameter was less than 5 times the aperture.

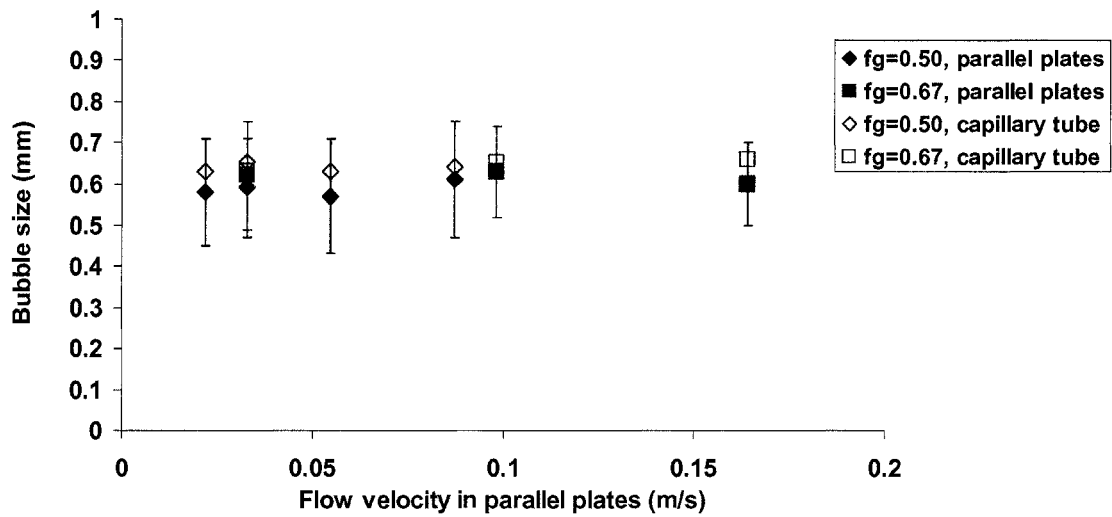


Fig 3.4 Bubble size measurement results from image processing method and capillary tube method match each other

3.4 Foam apparent viscosity in homogeneous fracture experiment results

Experiments were conducted to investigate the effects of flow rate, bubble size, gas fractional flow, and aperture on the apparent viscosity of foam flowing in uniform fractures. From the experiments, the most important variable affecting foam viscosity in a homogeneous fracture system is foam texture. Foam of finer texture has more lamellae per unit length and, as a result, greater resistance to flow. The foam bubbles in our experiments are individual bubbles because the aperture is smaller

than the equivalent diameter of the bubbles. No aggregation or coalescence of bubbles was observed.

Results for a homogeneous fracture with an aperture of 0.2mm are shown in Fig. 3.5 ~ Fig. 3.8. The data fit the theory (based on contributions from liquid and bubble deformation without the contribution from the surface tension gradient) quite well at low flow rates. Because the theory is based on Hele-Shaw flow, which is valid for creeping flow, the data begin to deviate from the theory when the Reynolds number exceeds about 1~10, depending on bubble size and gas fractional flow. Here the Reynolds number is defined as

$$\text{Re} = \frac{\rho^{liq} b U}{\mu^{liq}} \quad (3.8)$$

where ρ^{liq} is the density of the liquid. At the velocity $U = 0.1 \text{ m/s}$, the Reynolds number Re is about 10. As Fig. 3.5 shows, the bubbles produce a shear thinning effect.

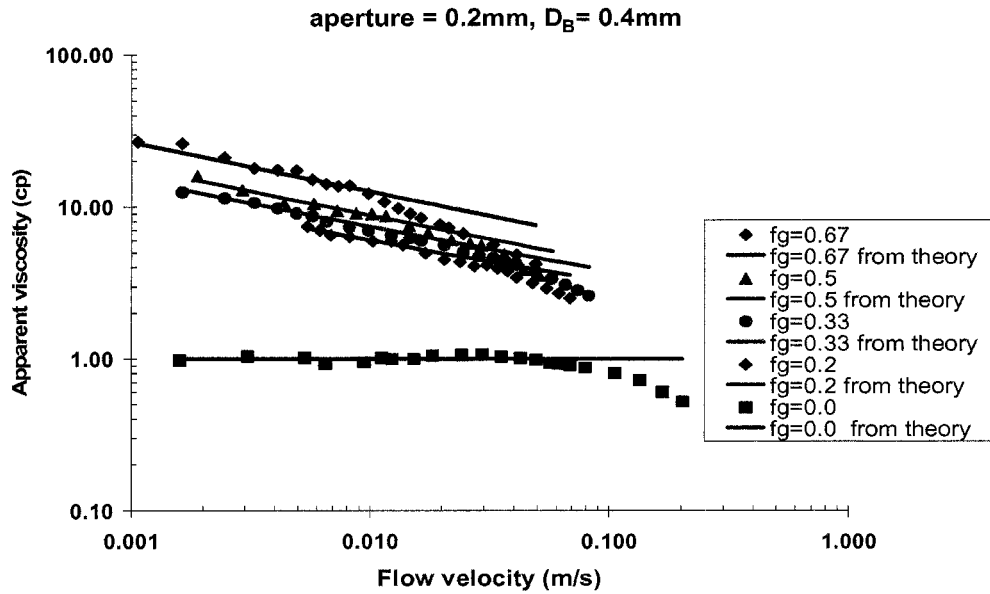


Fig. 3.5 Effect of flow rate and fractional flow on apparent viscosity for aperture = 0.2 mm, mean bubble diameter $D_B = 0.4$ mm

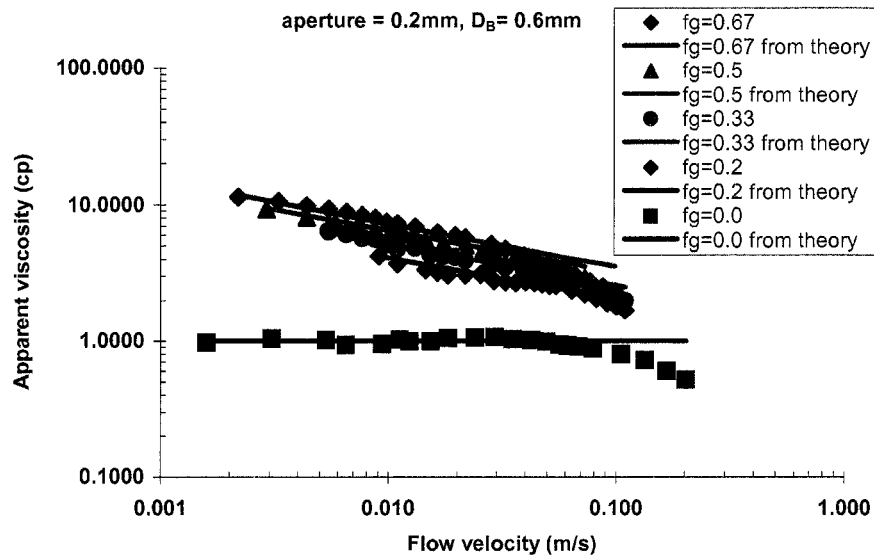


Fig. 3.6 Effect of flow rate and fractional flow on apparent viscosity for aperture = 0.2 mm, mean bubble diameter $D_B = 0.6$ mm

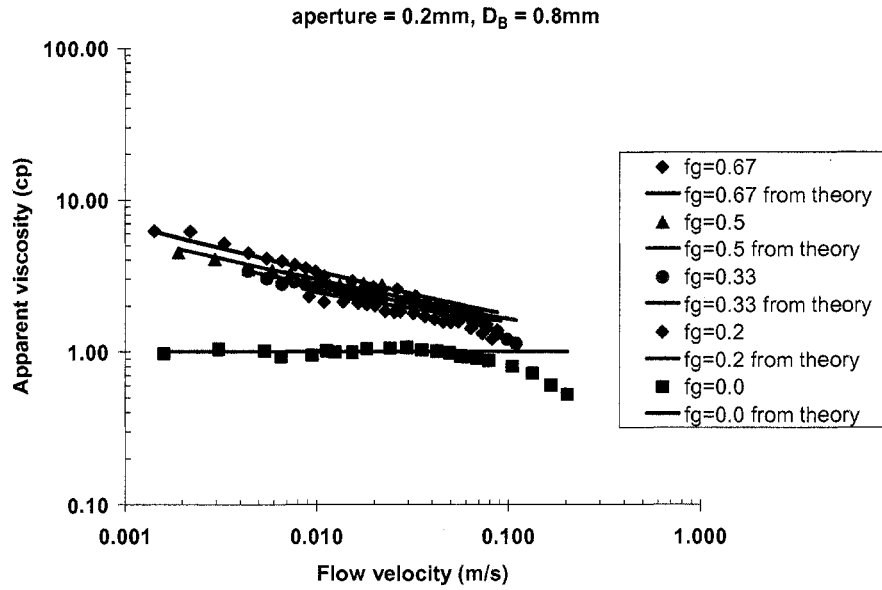


Fig. 3.7 Effect of flow rate and fractional flow on apparent viscosity for aperture = 0.2 mm, mean bubble diameter $D_B = 0.8$ mm

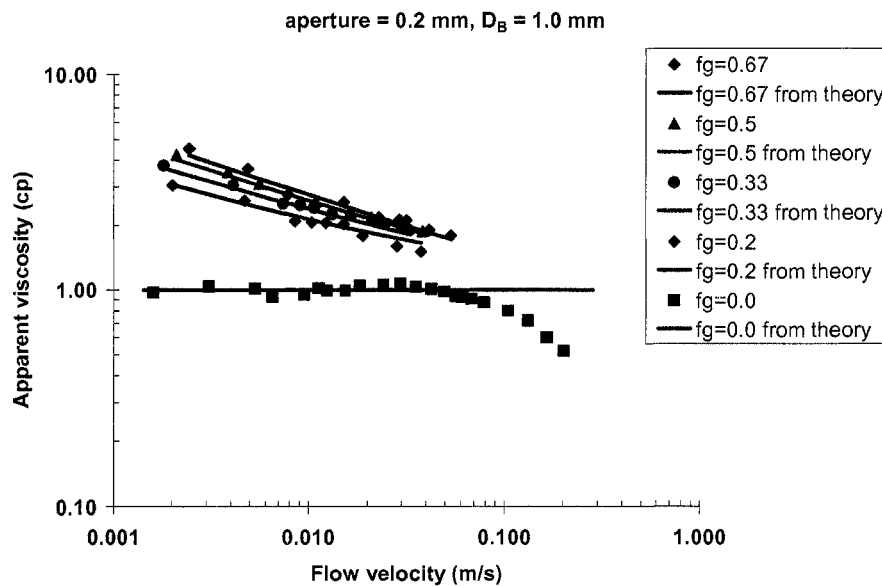


Fig. 3.8 Effect of flow rate and fractional flow on apparent viscosity for aperture = 0.2 mm, mean bubble diameter $D_B = 1.0$ mm

Fig. 3.5 ~ Fig. 3.8 also shows the effect of gas fractional flow on apparent viscosity. With the increase of gas fractional flow or foam quality, the number of lamellae per unit length or number of bubbles per unit area increases, which causes apparent viscosity proportional to the half power of gas fractional flow in equation (3.6).

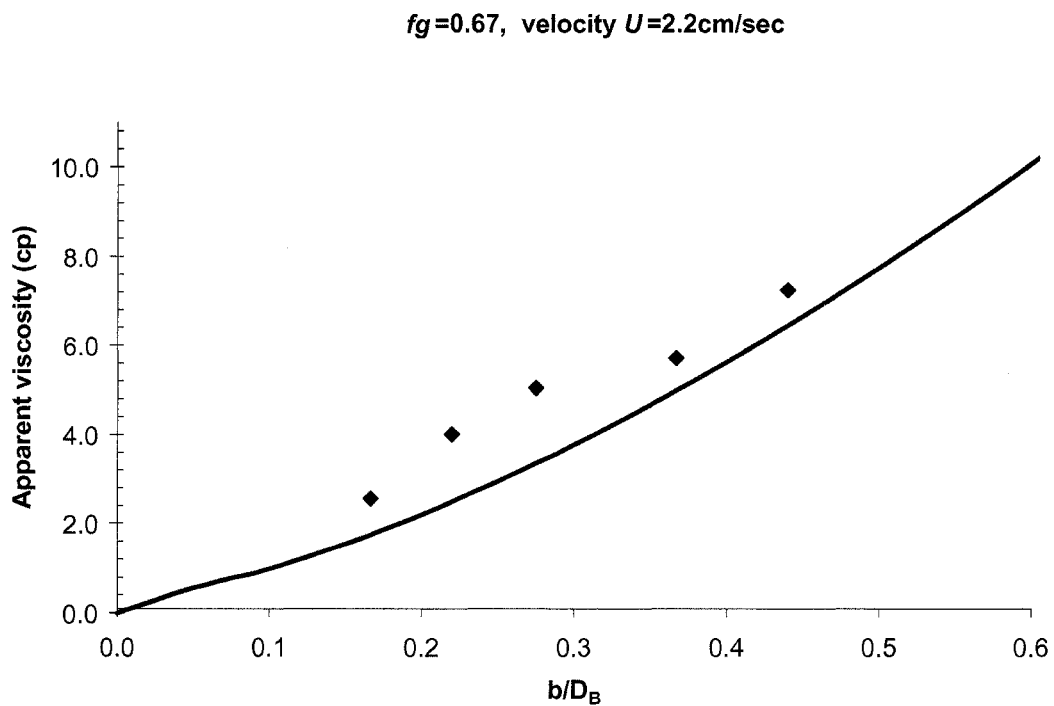


Fig. 3.9 Effect of ratio of aperture/bubble size on apparent viscosity

Fig. 3.9 shows the effect of the ratio of aperture to bubble size on apparent viscosity. The number of lamellae per unit length or of bubbles per unit area increases with decrease of bubble size and increase of aperture at fixed fractional flow. From equation (3.6), the contribution to

apparent viscosity from bubble deformation is proportional to the $3/2$ power of the ratio of aperture b to bubble size r_B . As a result, apparent viscosity would be significantly higher for smaller bubbles only slightly greater than aperture thickness. On the other hand, the apparent viscosity is larger for large apertures. This feature is important in foam application, because it indicates that foam of the same bubble size and gas fractional flow can reduce fluid flow in high permeability regions and divert flow into low permeability regions. Experiments were conducted to investigate the effects of flow rate, bubble size, gas fractional flow, and aperture on the apparent viscosity of foam flowing in uniform fractures. From the experiments, the most important variable affecting foam viscosity in a homogeneous fracture system is foam texture. Foam of finer texture has more lamellae per unit length and, as a result, greater resistance to flow. The foam bubbles in our experiments are individual bubbles because the aperture is smaller than the equivalent diameter of the bubbles. No aggregation or coalescence of bubbles was observed.

3.5 Bulk foam apparent viscosity

Princen [1983] modeled the theory for rheology of foams and highly concentrated emulsions. Hirasaki and Lawson [1985] developed the model to describe bulk

foam apparent viscosity in a capillary tube. But the theory can be applied only to bubbles with the shape of pentagonal dodecahedrons, which are obtained only at quite high gas fractional flow and all the bubbles in the system are closely-packed.

Many semi-empirical expressions are available for describing the shear viscosity of concentrated dispersions of hard spheres. The most widely used is the functional form suggested by Krieger and Dougherty [1972].

$$\eta_r = (1 - K\phi)^{-2.5/K} \quad (3.9)$$

Where η_r is the relative viscosity, which is the ratio of the viscosity of emulsion to the viscosity of water. ϕ is the volume fraction of emulsion in water. K is the crowding factor and equal to the reciprocal of the dense random packing limit volume fraction ϕ_{\max} , at which η_r diverges to infinity. For random close packing of monodisperse hard spheres, they found $\phi_{\max} = 0.64$ and $K = 1.56$.

Mooney [1951] developed another expression for the relative viscosity of emulsions where the particles behave as rigid spheres.

$$\eta_r = \exp\left[\frac{2.5\phi}{1 - K\phi}\right] \quad (3.10)$$

The crowding factor K in the above two equations can be smaller when the particles are not uniformly distributed or the particles are deformable because these can cause an increase of the dense random packing limit volume fraction.

Pal [1992] studied the rheology of polymer-thickened emulsions and found the increase of the viscosity ratio of continuous phase to dispersed phase enhances the internal circulation effect which leads to a decrease in the relative viscosity. He suggested the following equation.

$$\eta_r^{1/K_I} = \exp\left[\frac{2.5\phi}{1-K\phi}\right] \quad (3.11)$$

where K_I is the factor which takes into account internal circulation effects and is given by

$$K_I = \left[\frac{1 + 0.4(\eta_c / \eta_d)}{1 + (\eta_c / \eta_d)} \right] \quad (3.12)$$

In the above equation, η_c is the viscosity of the continuous phase and η_d is the viscosity of the dispersed phase. Pal [1992] also suggested a crowding factor $K = 1.04$, which means the dense random packing limit volume fraction $\phi_{\max} = 0.96$.

The apparent viscosity for bulk foam flow in fractures was measured at different aperture, flow velocity and bubble size as in Fig. 3.10. The experiment set-up is the same as the experiment for individual lamellae except the frits with smaller pore size were used. The theory predictions from Krieger and Dougherty equation, Mooney equation and Pal's model are also plotted in Fig. 3.10. The experimental measurement matches the prediction from Pal's model. The highest gas fractional flow in our bulk foam experiments is 0.67 because we found bubbles began to coalesce for gas fractional flow over 0.67.

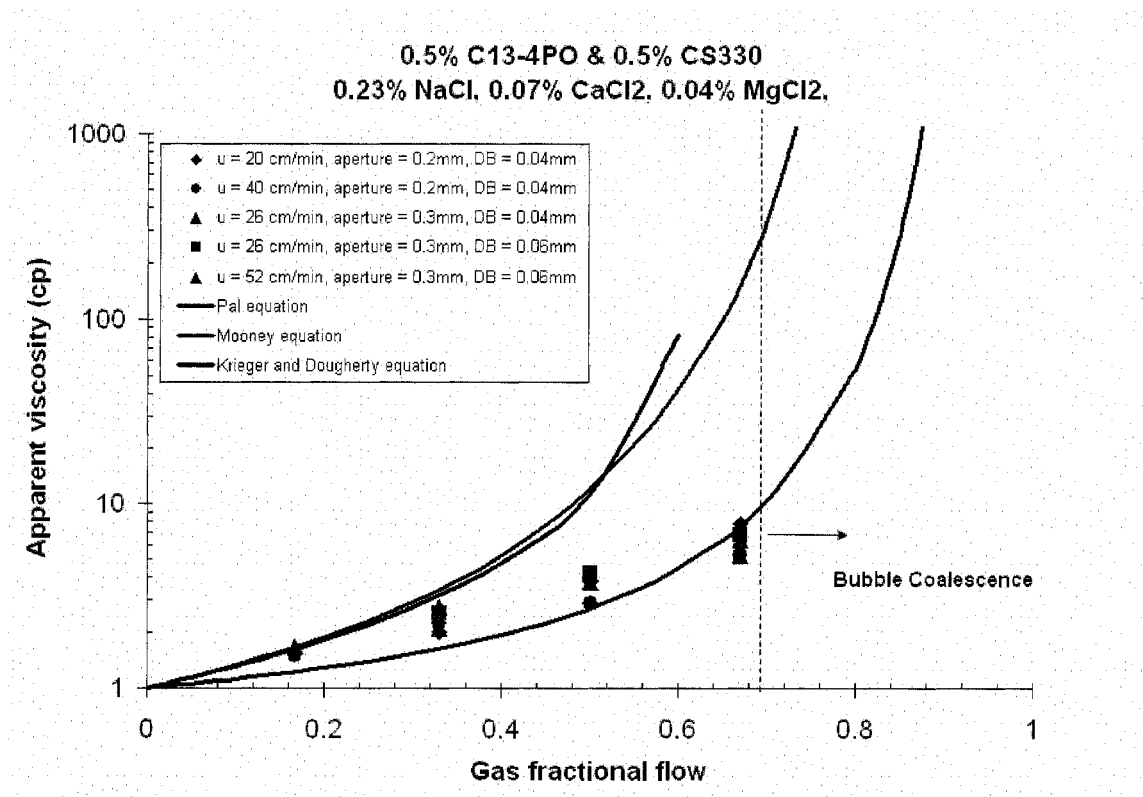


Fig 3.10 Bulk foam apparent viscosity in fractures measurement and prediction

From Fig. 3.10, the theory predictions from Krieger and Dougherty equation or Mooney equation have deviation from the experimental results even we set the dense random packing limit volume fraction $\phi_{\max}=0.99$ and crowding factor $K=1.01$. For Pal's model, we assume in the bulk foam case the dispersed phase is gas and the continuous phase is water. Because the viscosity of water is much larger than that of gas, K_f is close to 0.4. We still use 0.96 as the dense random packing limit volume fraction. Then the crowding factor K is 1.04. Because the viscosity of the dispersed phase is small in the foam case, internal circulation doesn't contribute significantly to the viscosity. There is not much internal circulation in the system because the surfactant films are coherent, which will resist tangential flow at the interface. So from Pal's model the internal circulation contribution is not important for foams where the dispersed phase is gas, i.e., that the model is consistent with our experiments.

One feature of the apparent viscosity prediction from Pal's model is that the bubble size doesn't need to be uniform in a fracture only if the diameter of each bubble is smaller than the aperture because the apparent viscosity is dependent on the gas fractional flow only. From Pal [1992], the emulsions in his experiment were polydisperse with respect to droplet size.

3.6 Contrary diversion effect

From Fig. 3.9, the foam has higher apparent viscosity in larger aperture region than in smaller aperture region when the foam bubble size, gas

fractional flow are the same, which implies that foam can divert the fluid from the larger aperture region to smaller aperture region. But at some condition, the foam apparent viscosity in the thinner layer may be higher than that in thicker layer can cause the contrary diversion, that is, the fluids is diverted from thinner layer to thicker one and decrease the sweep efficiency. This may happen when the apertures in a heterogeneous fracture system has a wide distribution and the foam bubble size is less than some big apertures, which means the bulk foam exists in the big aperture regions. As in Fig 3.10, the bulk foam apparent viscosity in big aperture regions is less than the apparent viscosity of individual lamellae in some smaller aperture regions. This causes the fluid is diverted from bigger aperture regions to some smaller aperture regions. The other condition at which the contrary diversion may happen is that the bubble diameters in each layer is at some constant ratio to the aperture of each layer which can cause the higher apparent viscosity in smaller apertures. This will be further discussed in chapter 4.

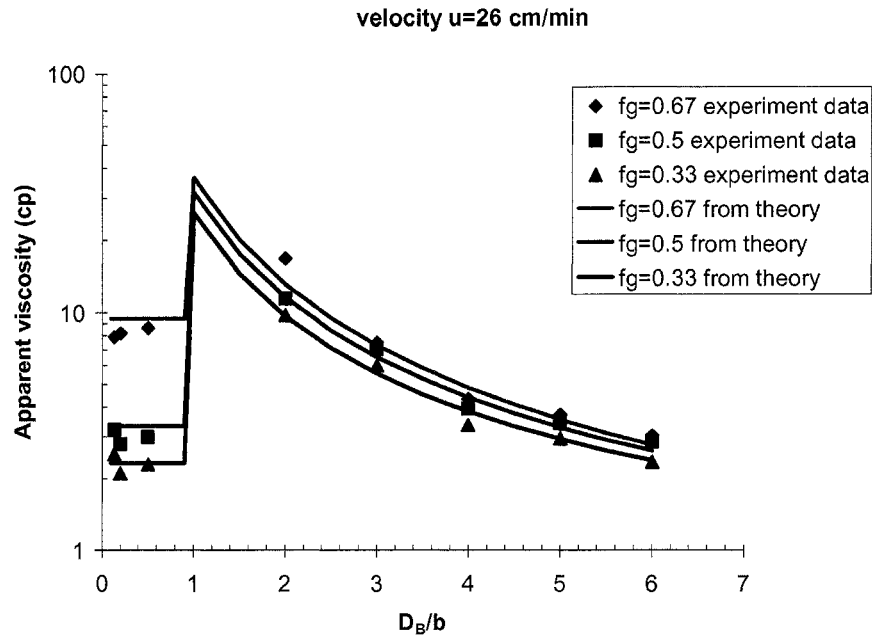


Fig 3.10 Apparent viscosity at different ratio of foam bubble diameter to aperture and different gas fractional flow. When the apparent viscosity increases with the increase of d_b/b , the contrary diversion happens.

Chapter 4

FOAM DIVERSION IN HETEROGENEOUS FRACTURES

4.1 Foam apparent viscosity in heterogeneous fractures

Consider flow into two fractures of different thickness. The velocities in both fractures need to be determined to get the apparent viscosity either by theory or measurement. If only water or surfactant solution is flowing and if the pressure gradient is the same in the two regions, the velocity ratio can be obtained from:

$$\frac{U_1}{U_2} = \left(\frac{b_1}{b_2}\right)^2 \quad (4.1)$$

The velocity ratio can be found for foam flow. If the contribution to apparent viscosity from bubble deformation dominates, combining equations (3.6) and (3.7) yields equation (4.2).

$$b^{-1/2} U^{2/3} = 0.21 (\mu^{liq})^{-2/3} f_g^{-1/2} r_B^{3/2} \sigma^{-1/3} |\nabla p| \quad (4.2)$$

If it is further assumed that gas fractional flow and the pressure gradient are the same in both regions, the right side of this equation is the same for both regions. Thus, the ratio of equation (4.2) for the two regions gives

$$\frac{U_1}{U_2} = \left(\frac{b_1}{b_2}\right)^{3/4} \quad (4.3)$$

Then from overall material balance, the velocities in both fractures can be estimated. Moreover, taking the ratio of equation (3.6) for the two regions and eliminating the velocity ratio with equation (4.3), one finds that the apparent viscosity from the deformation contribution is proportional to $5/4$ power of aperture as in equation (4.4). This result shows the possibility of foam diversion into the thinner fracture because of the higher resistance to flow in the thicker fracture.

$$\frac{\mu_{app,1}}{\mu_{app,2}} = \left(\frac{b_1}{b_2}\right)^{5/4} \quad (4.4)$$

4.2 Prediction of sweep efficiency in heterogeneous fractures

By using a similar method to that described by Lake [1989], we developed a mathematical model to describe foam flooding in heterogeneous fractures with different apertures. We assumed no crossflow between fractures, the same pressure drop across each fracture, plug flow in each region and foam apparent viscosity determined by the velocity of foam flow at steady state, i.e., the velocity after all layers have been swept.

First, we apply this model in heterogeneous fractures with two regions of different apertures. We assume that foam completely displaces the water initially present in each region as it advances. Suppose $b_1 > b_2$. Then integration of the equation to the time when $x_1 = 1$ yields (see Appendix B for derivation of the equations in this section)

$$x_2 = \frac{[M_2^2 + \frac{k_2 \mu_{app,1} (1 - M_2)(1 + M_1)}{k_1 \mu_{app,2}}]^{1/2} - M_2}{1 - M_2} \quad (4.5)$$

The dimensionless time in injected liquid fracture volumes when this occurs is

$$\text{Dimensionless time} = (x_2 b_2 + b_1)(1 - f_g) / (b_1 + b_2) \quad (4.6)$$

From this time until that when $x_2 = 1$ for the thinner fracture, v_1 in the thicker fracture is given by equation (4.4) with $x_1 = 1$.

Then similarly we can get the dimensionless time in injected liquid fracture volumes when $x_2 = 1$:

$$\text{Dimensionless time} = (z_1 b_1 + b_2)(1 - f_g) / (b_2 + b_1) \quad (4.7)$$

where z_1 exceeds 1 by the dimensionless length of a region of thickness b_1 needed to hold the foam produced from fracture 1 up to that time.

$$z_1 = 1 + \frac{k_1 \mu_{app,2}}{k_2 \mu_{app,1}} \left[\frac{(1 + M_2)}{2} - \frac{(1 + M_1)(k_2 \mu_{app,1})}{2k_2 \mu_{app,2}} \right] \quad (4.8)$$

4.3 Fractures with log-normal distribution apertures

Normally there are more than two fractures. For multiple fractures, the key is to get the number of fractures that have been swept at some FWR, the ratio of foam to water being produced. The number N of fractures where foam has broken through at some FWR is given by

$$FWR = \sum_{i=1}^N Q_i / \sum_{i=N+1}^{N_L} Q_i \quad (4.9)$$

where Q_i is the flow rate in the i th fracture and N_L is the total number of fractures. Then by a derivation similar to that above for the two heterogeneous fractures, the sweep efficiency and the dimensionless time can be obtained. There is a difference when we calculated the sweep efficiency in multi-layer heterogeneous fracture system from that in two layer heterogeneous fractures. Because the foam enhanced sweep is used together with spontaneous imbibition process to recover residual oil in matrix, the volume contacted by each fracture in the matrix is much larger than the volume of each fracture and more important than the fracture volume. So in the calculation for the sweep efficiency, we assume

each fracture layer contacts the same volume of matrix. The dimensionless time is the total fracture volumes of fluid injected.

$$\text{Sweep efficiency} = \frac{N + \sum_{i=N+1}^{N_L} x_i}{N_L} \quad (4.10)$$

$$\text{Dimensionless time} = \frac{\sum_{i=1}^{N_L} z_i b_i}{\sum_{i=1}^{N_L} b_i} \quad (4.11)$$

Olso [2001], Andres [2001], Baker, et. al. [2001], Wilson [1970] and Gale [1987] have found that the fracture aperture distribution of reservoirs is approximately log-normal. Such a log-normal aperture distribution can be described by the function

$$C = \frac{[1 + \text{erf}(\tau / \sqrt{2})]}{2} \quad (4.12)$$

$$\text{where } \tau = \frac{\ln(b / \bar{b})}{\sqrt{\sigma_N^2}}$$

The function $C(b)$ is the fraction of the samples that have aperture less than b , i.e., the cumulative probability function. The parameter \bar{b} is the median or log-mean aperture. The parameter σ_N^2 is the variance of the distribution. If the log-mean value \bar{b} and variance σ_N^2 are known, different values of b can be obtained and used in equation (4.10) and equation (4.11) to get the sweep efficiency and dimensionless time.

4.4 Experimental methods

The fracture model used is shown in Fig. 4.1. It consists mainly of two parallel glass plates. Changing the gasket thickness between the plates can change the aperture of the fracture. The thick glass is from Lone Star Glass Company, Houston, TX. It is borosilicate glass with 35.56 cm length and 20.32 cm width. Its thickness is 6.35 ± 0.3 mm. The surface of the glass is polished. The thin glass is Schott D-263 borosilicate glass from Precision Glass & Optics Company, Santa Ana, CA. It is 25.4 cm long and 7.62 cm wide. It is 0.10 ± 0.01 mm thick. It is not quite long enough to span the flow area. The procedure for making the heterogeneous fracture is: 1. Adhere the thin glass plate described above to half of one of the thick glass plates by Norland optical adhesive; 2. Roll the thin glass on the

thick glass to remove any air and excess adhesive between them; 3. Cure the adhesive by a high intensity ultraviolet lamp (Model Spectroline SB-100P) for over 48 hours.

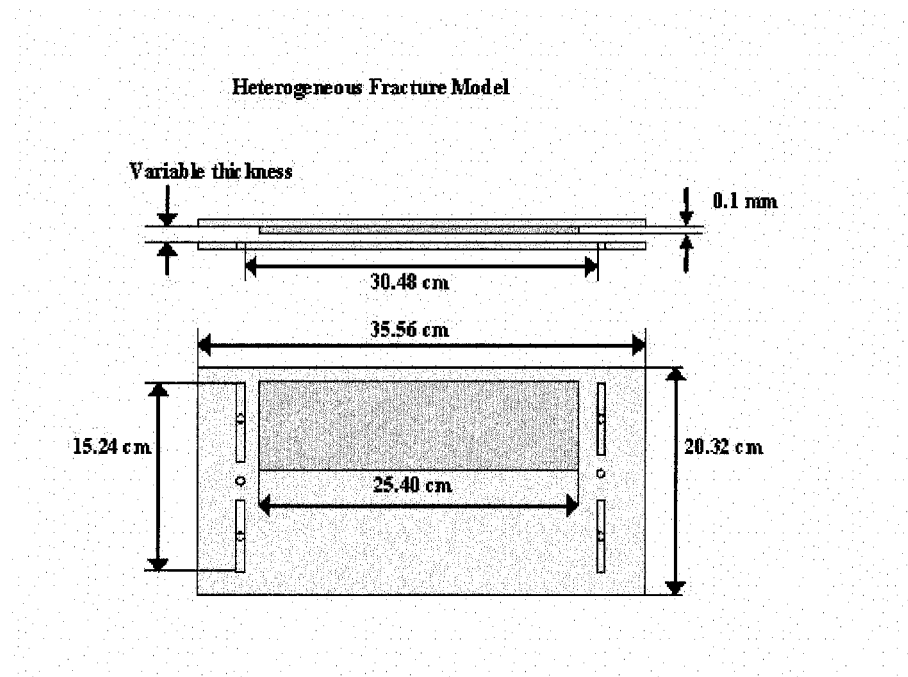


Fig 4.1 Detailed diagram of heterogeneous fracture model

4.5 Experimental results for apparent viscosity and sweep in heterogeneous fractures

Experiments with the heterogeneous fracture model were performed for average bubble diameters of 0.4 and 0.6mm, which are larger than the thicker aperture to meet the conditions of our theory. The Reynolds

numbers were 0.22 and 0.44. Two different aperture ratios were used in the experiments, 1:2 and 1:3.

4.5.1 Apparent viscosity

The apparent viscosity in each region can be calculated from equation (3.7), using the pressure difference obtained in experiments. We assume that gas fractional flow is the same in thinner and thicker apertures and that velocity in each layer can be obtained from equation (4.3) and material balance, as indicated above. Also the apparent viscosity can be estimated from the sum of equations (3.6) and (3.1). We consider first the case in which both regions of the fracture are fully filled with foam, so that there are minimal lateral pressure gradients and no cross flow. The theoretical and experimental results are compared in Figs 4.2 and 4.3. For the range of experimental conditions listed at low Reynolds' number (less than 1) the apparent viscosity from measurement of pressure difference fits well with that from theory prediction. This confirms that the assumption of equal gas fractional flow is valid.

From Figs 4.2 and 4.3, we can see the effects of the aperture ratio on the magnitude of diversion in heterogeneous fractures. The diversion

depends on the apparent viscosity difference between the two regions. If we ignore the contribution of liquid slug to the total apparent viscosity, equation (4.4) predicts that the apparent viscosity is proportional to the $5/4$ power of aperture thickness. So the apparent viscosity ratio is largest in Fig. 5.3, which is with 3:1 aperture ratio.

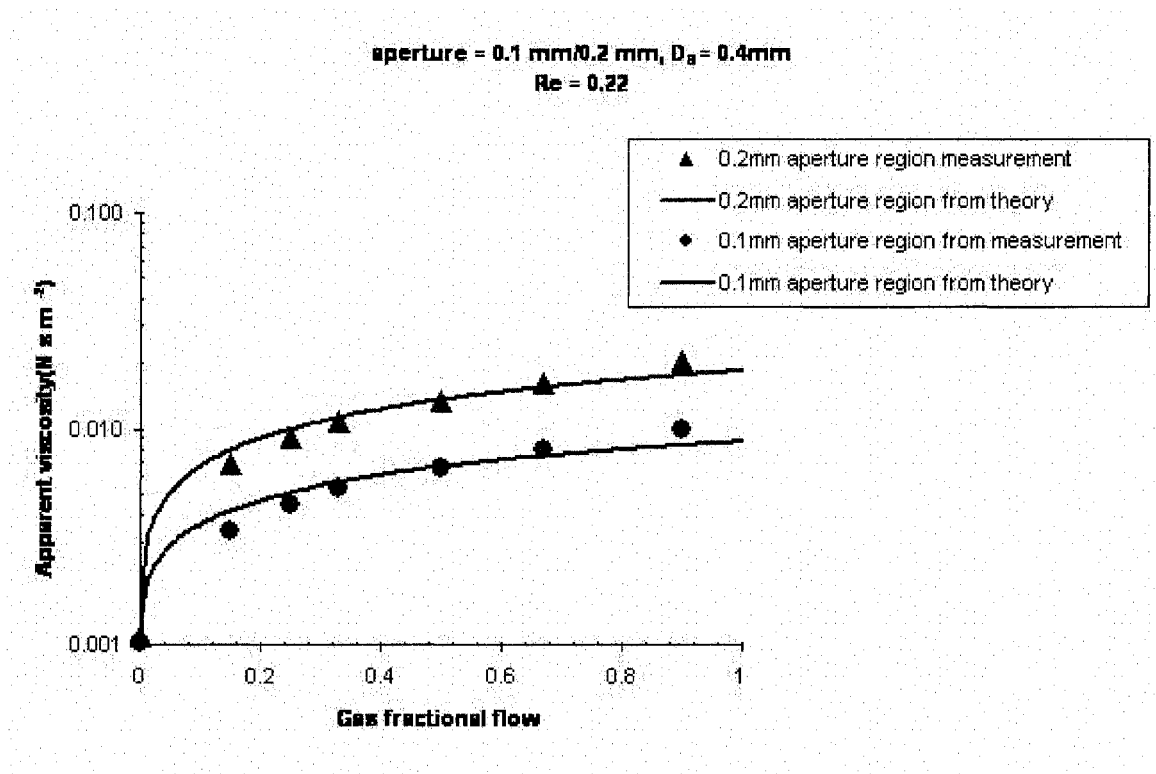


Fig 4.2 Apparent viscosity for aperture ratio of 0.1 mm/0.2 mm, bubble size = 0.4 mm and $Re = 0.22$

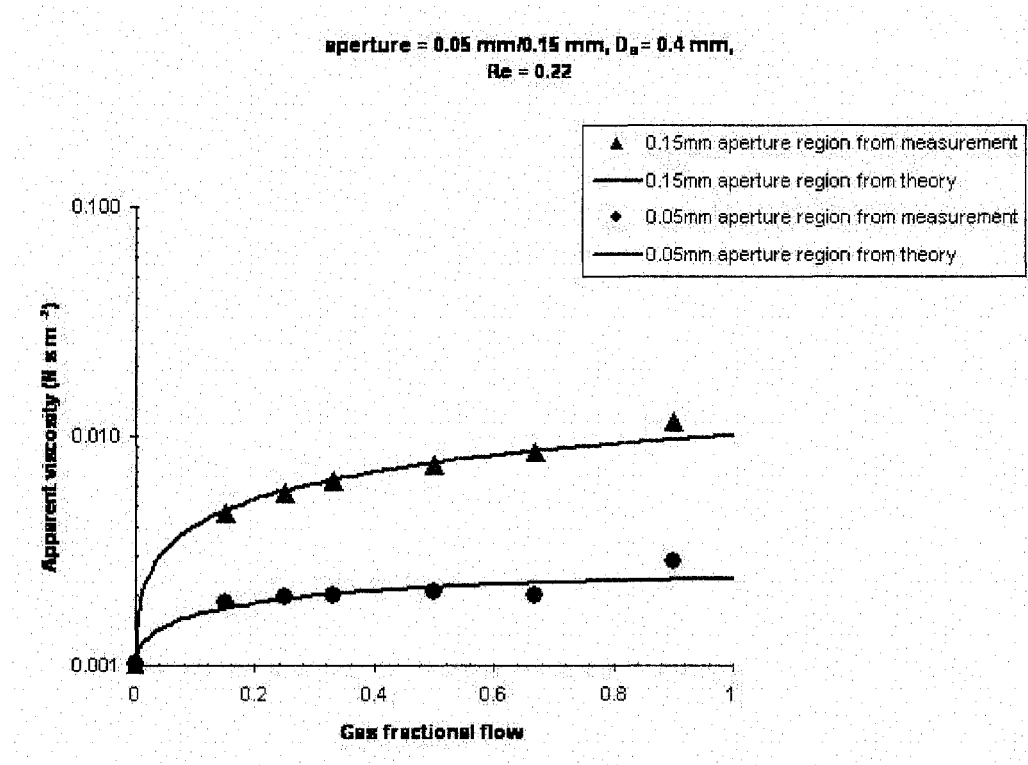


Fig 4.3 Apparent viscosity for aperture ratio of 0.05 mm/0.15 mm, bubble size = 0.4 mm and $Re = 0.22$

4.5.2 sweep efficiency

Photographs were taken during experiments to investigate the sweep by foam and surfactant solution in heterogeneous fractures. An example of foam/surfactant solution sweep is shown in Fig. 4.5. For comparison, the picture of sweep by surfactant solution alone is shown in Fig. 4.4. We use “fracture volume” to measure the amount of foam or liquid needed for sweeping the fractures. “Fracture volume” PV is defined as the volume

equal to open space in fractures. “Liquid fracture volume” LPV is the volume of liquid equal to open space in fractures. The relationship between fracture volume and liquid fracture volume is shown in equation (4.13).

$$LPV = PV * (1 - f_g) \quad (4.13)$$

The injection of foam bubbles together with surfactant solution greatly improves the sweep over the injection of surfactant solution only. From Fig. 4.4 for 0.05 mm/0.15 mm fracture, at Reynolds number 0.22, it takes about 6.6 fracture volumes of surfactant solution to sweep the 0.05 mm aperture region, while theory predicts that 7.0 fracture volumes are needed. With gas fractional flow 0.9 and bubble size at 0.4 mm in diameter, only 0.15 liquid fracture volume of surfactant solution is needed, as shown in Fig. 4.5. The amount of surfactant solution needed to sweep both regions is reduced by a factor of more than 40. This large difference is partly the result of the higher apparent viscosity in the thicker region and partly because less liquid is required to fill a given volume when foam is used.

Experiments were also conducted for other gas fractional flows with aperture ratios of 2 and 3. The results are shown in Fig. 4.6. It is easily seen that high gas fractional flow can give better sweep efficiency, i.e., reduction in the amount of surfactant solution required to sweep both portions of the heterogeneous fracture. As might be expected, more surfactant solution is required for the higher aperture ratio.

Fig. 4.7 shows the comparison between the theoretical predictions and experimental results for foam/surfactant sweep in a heterogeneous fracture with 1:3 aperture ratio. Agreement is good. This validates the assumption of minimal crossflow. It also indicates that the assumption of equal gas fractional flow in different layers is reasonable for these conditions.

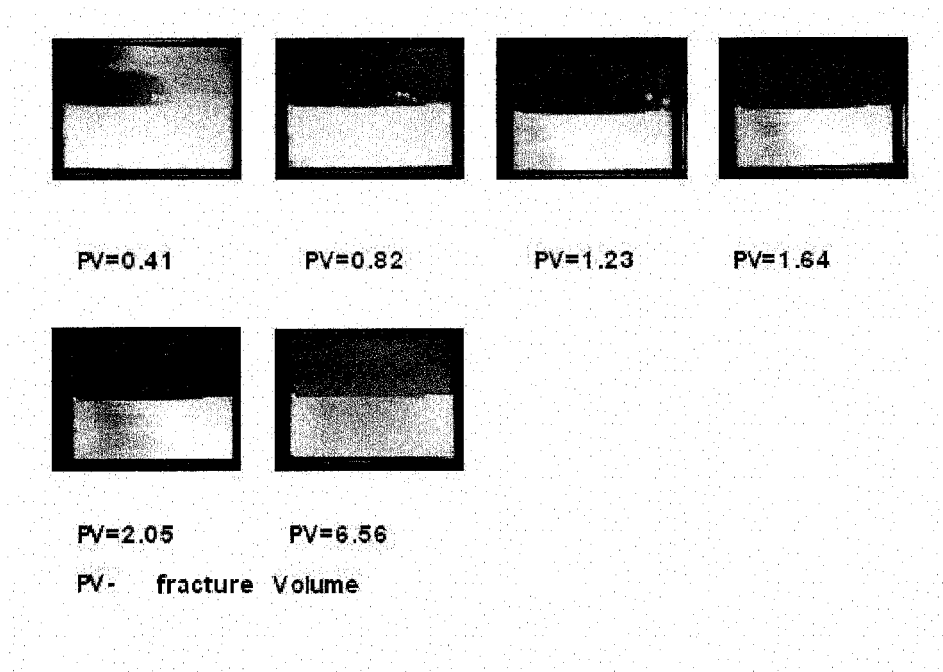


Fig 4.4 Surfactant solution sweeping heterogeneous fracture, $Re = 0.22$, fracture aperture ratio = 0.05 mm(top)/0.15 mm(bottom). PV refers to fracture volume of the entire heterogeneous fracture.

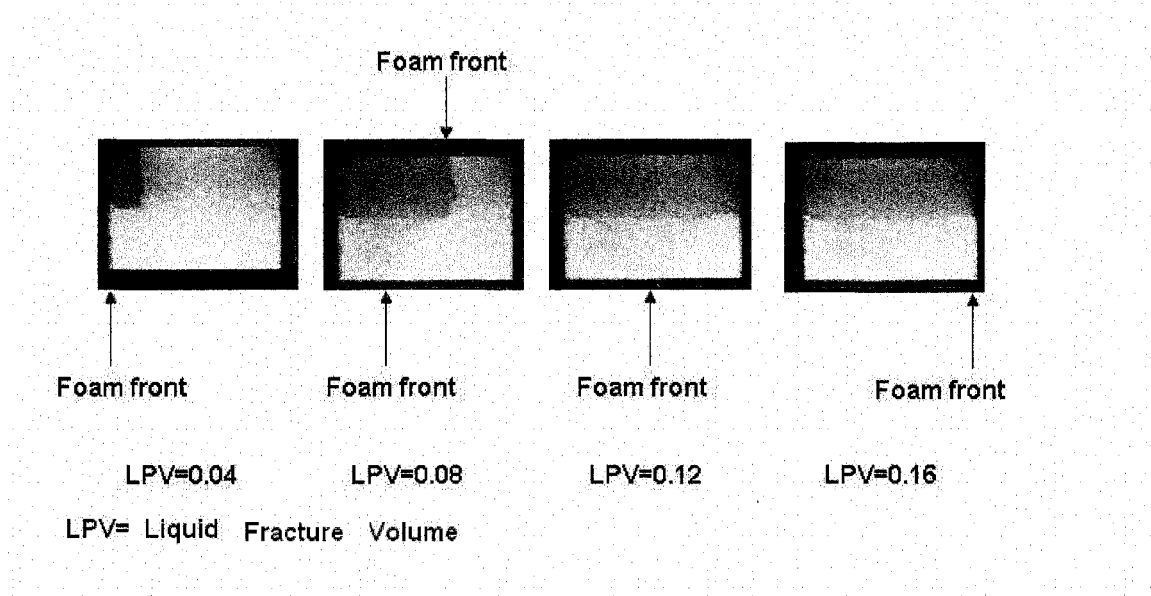


Fig 4.5 Foam/surfactant solution sweeping heterogeneous fracture, $Re = 0.22$, $f_g = 0.9$, fracture aperture ratio = 0.05 mm(top)/0.15 mm(bottom), $D_b = 0.4$ mm (Note: LPV is the liquid fracture volumes injected)

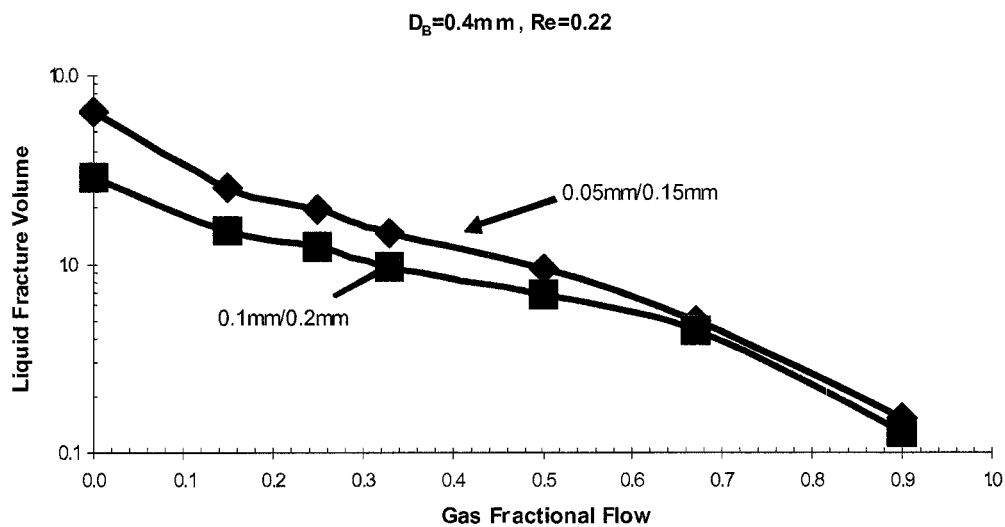


Fig 4.6 Surfactant solution sweeping heterogeneous fracture at different fracture aperture ratio (for thinner region only)

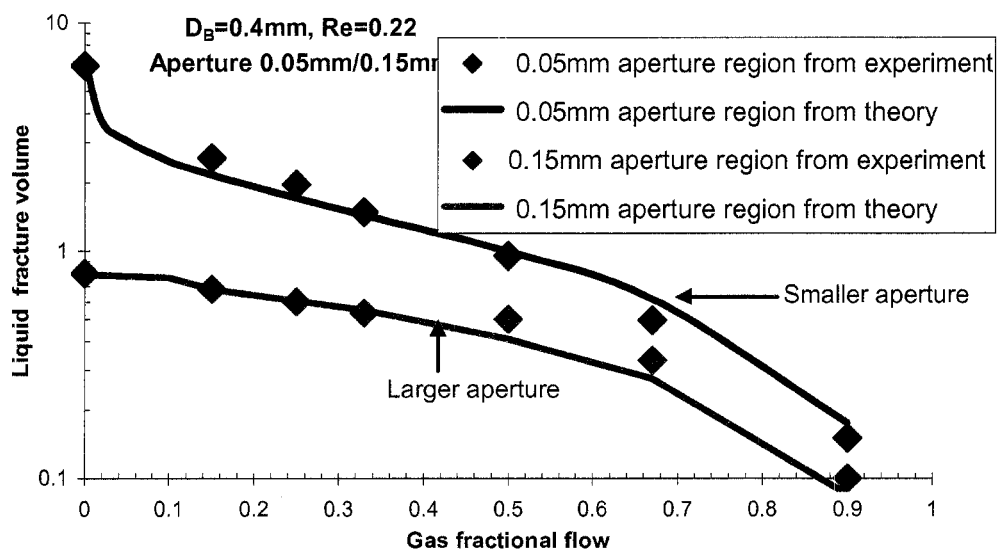


Fig 4.7 Comparison between the calculation and the experiment results for foam/surfactant sweep in heterogeneous fractures with 1:3 aperture ratio

4.6 Sensitivity of foam bubble size to sweep efficiency in heterogeneous reservoirs

The fracture apertures in a fractured reservoir are believed to be distributed in log-normal distribution. We consider a heterogeneous fracture system with 50 layers having different apertures. The variance σ_N^2 is 0.81, which is the most heterogeneous fracture aperture distribution from literature. At different foam bubble size, different apparent viscosity of foam can be got in different layers. Here we studied the sweep efficiency sensitivity to bubble size in this heterogeneous fracture system based on the assumptions that the pressure difference in different layers is the same and that the gas fractional flow in the different layers is the same.

Let's first simplify the consideration to two layers with different apertures to study the mechanism of the effect of bubble size. Consider two layers in a heterogeneous fracture system filled with water with permeability ratio of r_{12} defined in equation (4.14). Layer 1 is the thicker layer while layer 2 is the thinner one.

$$r_{12} = \frac{k_1}{k_2} = \left(\frac{b_1}{b_2} \right)^2 \quad (4.14)$$

When the thinner layer is swept, the hypothetical foam front in thicker layer from equation (4.8) is:

$$z_1^f = 1 + \frac{k_1 \mu_{app,2}}{(k_2 \mu_{app,1})} \left[\frac{(1 + M_2)}{2} - \frac{(1 + M_1) k_2 \mu_{app,1}}{(2 k_1 \mu_{app,2})} \right] \quad (4.15)$$

If the fracture is swept by water, then $M_1 = M_2 = 1$ and the above equation can be changed to

$$z_1^w = k_1 / k_2 \quad (4.16)$$

Let p be the sweep improvement coefficient between the foam sweep and water sweep.

$$z_1^w = p z_1^f \quad (4.17)$$

If there is any improvement in sweep by foam over water, p is greater

than 1. And $M_1 = \frac{1}{\mu_{app,1}}$, $M_2 = \frac{1}{\mu_{app,2}}$ because the water is displaced.

$$p = \frac{z_1^w}{z_1^f} = \frac{\left(\frac{k_1}{k_2}\right)}{\left\{1 + \frac{k_1 \mu_{app,2}}{(k_2 \mu_{app,1})} \left[\frac{(1 + M_2)}{2} - \frac{(1 + M_1) k_2 \mu_{app,1}}{(2 k_1 \mu_{app,2})} \right] \right\}} = \frac{2 k_1 \mu_{app,1}}{(k_2 \mu_{app,1} + k_1 \mu_{app,2} + k_1 - k_2)} \quad (4.18)$$

By algebraic manipulation, the following equation describing the sweep improvement coefficient in the heterogeneous system may be obtained:

$$p = \frac{2}{\left[\frac{\mu_{app,2}}{\mu_{app,1}} + \frac{1}{\mu_{app,1}} \left(1 - \frac{1}{r_{12}}\right) + \frac{1}{r_{12}} \right]} \quad (4.19)$$

where $r_{12} = \frac{k_1}{k_2}$.

If foam sweep has improvement over water sweep, the value of

$\left[\frac{\mu_{app,2}}{\mu_{app,1}} + \frac{1}{\mu_{app,1}} \left(1 - \frac{1}{r_{12}}\right) + \frac{1}{r_{12}} \right]$ needs to be smaller than 2.

From this, it is found that two factors affect the sweep by foam in heterogeneous fractures with a given permeability ratio. The first one is the viscosity ratio of foam in different layers, and the second is the foam viscosity in the thicker layer.

4.6.1 Foam bubble size with some constant ratio (>1) to aperture.

When foam bubble sizes in different layers are at a constant ratio to the apertures of these layers, i.e., $\frac{b}{r_B}$ is constant, the lamellae bubbles per unit length or number of bubbles per unit area in different layers decreases with the increase of aperture from equation (3.5). This may happen when the foam is generated in each fracture layer in situ by some mechanism and few interconnections exist between different fracture layers.

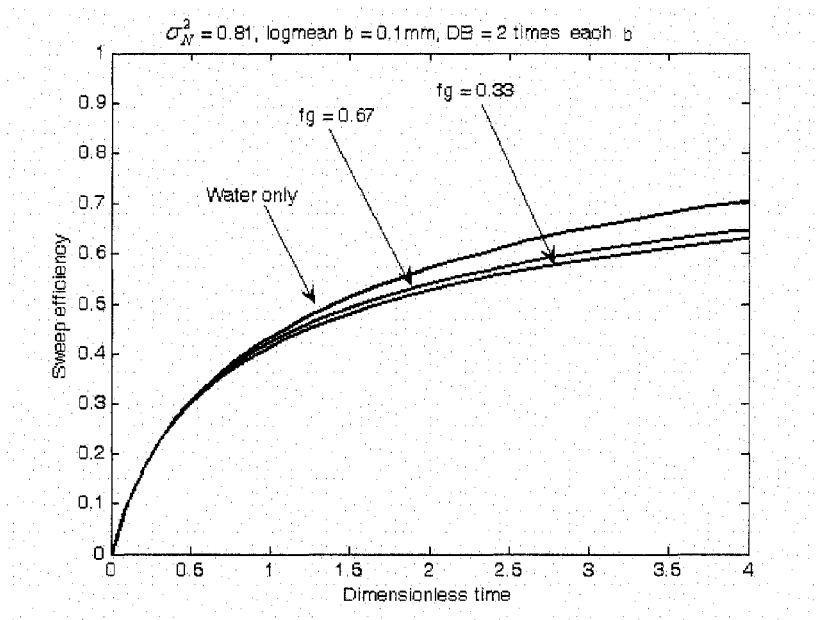


Fig 4.8 Sweep efficiency by foam with bubble size 2 times aperture in each layer

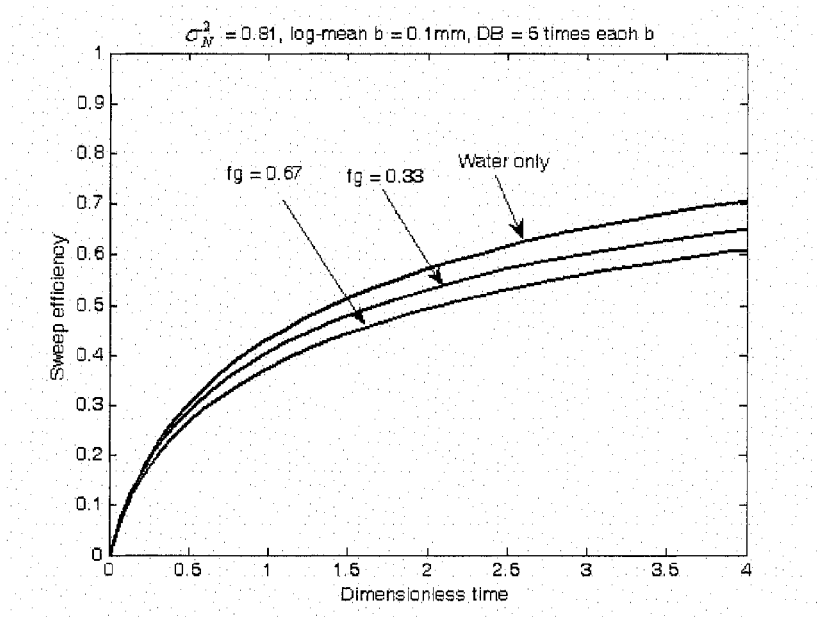


Fig 4.9 Sweep efficiency by foam with bubble size 5 times of aperture in each layer

So higher apparent viscosity will be obtained in thicker layer and the foam will divert the liquid from thinner layers to thicker ones, which will lower the sweep efficiency by foam. Then from Fig.4.8 to Fig.4.9, higher gas fractional flow gets lower sweep efficiency. The foam apparent viscosity ratio in different layers is derived in equation (4.20) from equation (3.6) and equation (3.7) when we assume the gas fractional flow and bubble diameter to the aperture are the same in each layer.

$$\frac{\mu_{app,2}}{\mu_{app,1}} = \frac{b_1}{b_2} \quad (4.20)$$

In the heterogeneous fractures with log-normal distributed apertures, if we consider the variance $\sigma_N^2 = 0.81$, the largest aperture is over 6 times the mean aperture, then $\frac{\mu_{app,2}}{\mu_{app,1}} = \frac{b_1}{b_2} \gg 2$, which causes $p \ll 1$ according to equation (4.19). So the foam sweep at this condition has lower sweep efficiency than water sweep. And the value of $\frac{1}{\mu_{app,1}}$, which is the inverse of the apparent viscosity of thicker layer and mainly a function of gas fractional flow and bubble size to aperture ratio, is much smaller

than $\frac{\mu_{app,2}}{\mu_{app,1}}$. This means the apparent viscosity ratio factor here decides

the sweep improvement coefficient and causes the contrary diversion which may be found from Fig. 4.10 where the apparent viscosity increases with the number of layers (higher number layer has smaller aperture).

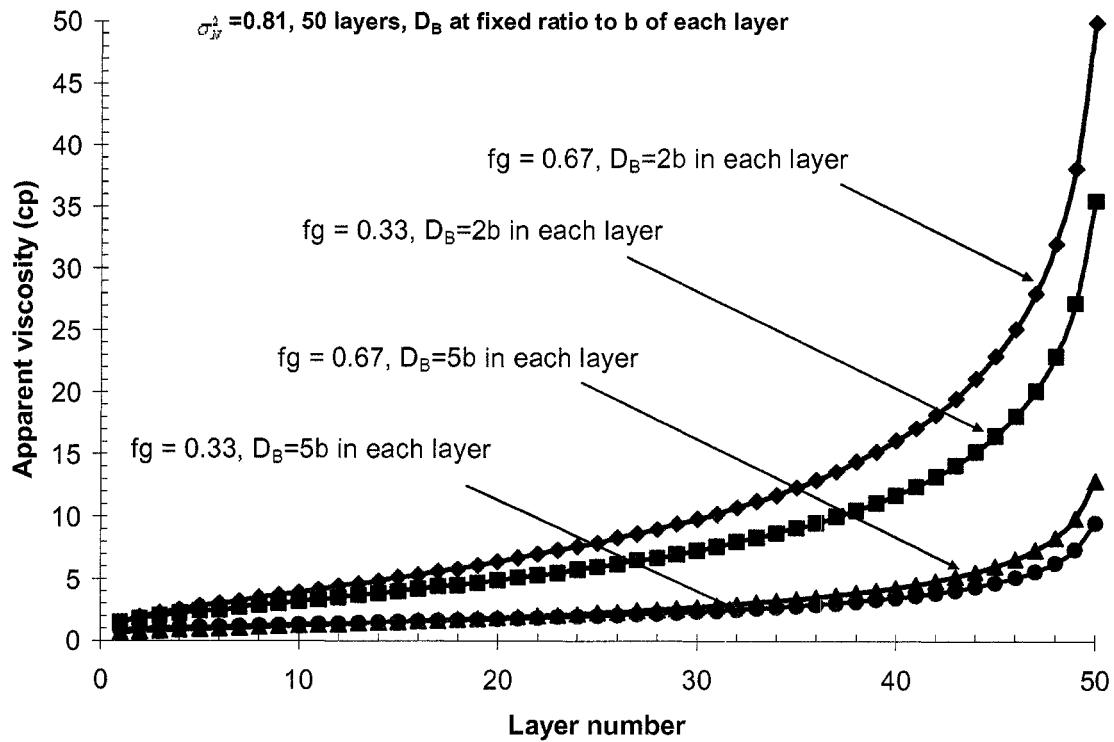


Fig 4.10 Apparent viscosity in a heterogeneous fracture system with $\sigma_N^2=0.8$ when the bubble diameter in a fixed ratio to the aperture of each layer.

4.6.2 Foam bubbles at constant size ($>$ aperture) in different layers

The foam bubble size in different layers is the same when the foam is injected and fractures don't affect bubble size in smooth fractures. Then the apparent viscosity ratio in different layers as shown by equation (4.4) is proportional to the $\frac{5}{4}$ power of the aperture ratio, which means the apparent viscosity of foam in thicker layer is higher than in the thinner layer. So the higher gas fractional flow gets higher sweep efficiency.

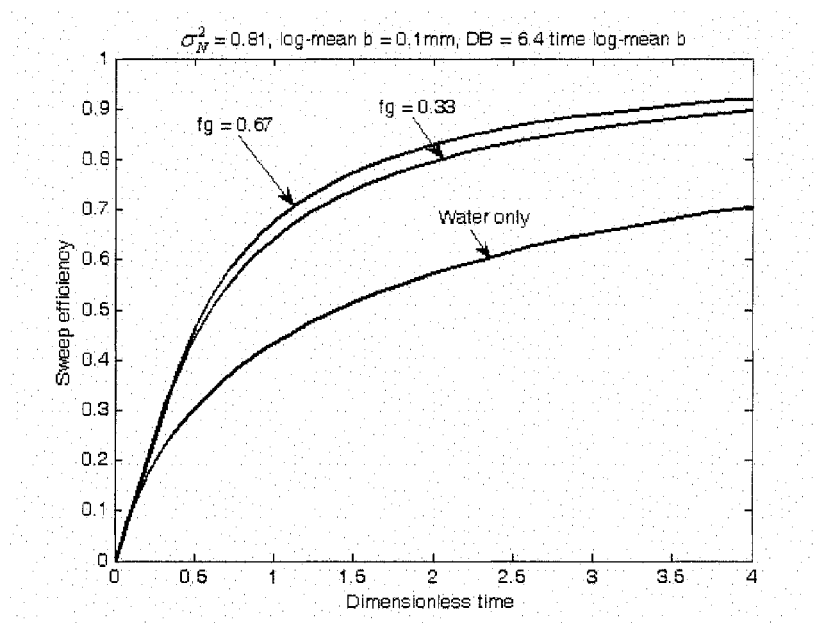


Fig 4.11 Sweep efficiency by foam with bubble size 6.4 times of the log-mean aperture which is equal to the largest aperture in the heterogeneous fracture system

In Fig. 4.11, the foam bubble diameter is equal to the largest aperture in the heterogeneous system, the sweep efficiency at different gas fractional flows is above 0.9 at 4 total fracture volume foam injection while the sweep efficiency by water is about 0.7 at 4 total fracture volume injection. The advantage of having the uniform bubble diameter larger than any aperture is that the contrary diversion is avoided because the apparent viscosity is higher in larger aperture layer as in Fig. 4.12 and the fluid is diverted from larger aperture layer to smaller aperture layer. But the sweep efficiency decreases with the further increase of the bubble diameter. From Fig. 4.13, when the bubble diameter is 25 times of the log-mean aperture, the sweep efficiency by different gas fractional flow is close to water only sweep efficiency. The reason is that the apparent viscosity of foam is lower when the bubble diameter is larger. If the bubble diameter is too big, the apparent viscosity can be even lower than the viscosity of water. For the case when the bubble diameter is larger than any aperture in the system, the foam with bubble diameter equal to the largest aperture can supply the highest sweep efficiency because its apparent viscosity is highest.

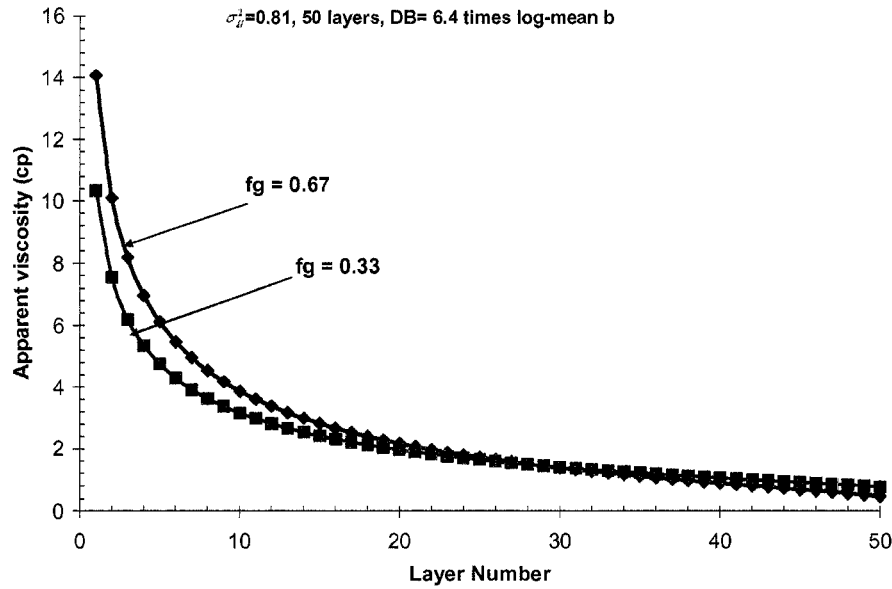


Fig 4.12 Apparent viscosity in a heterogeneous fracture system with $\sigma_N^2 = 0.81$ when the bubble diameter is equal to the largest aperture in the heterogeneous system.

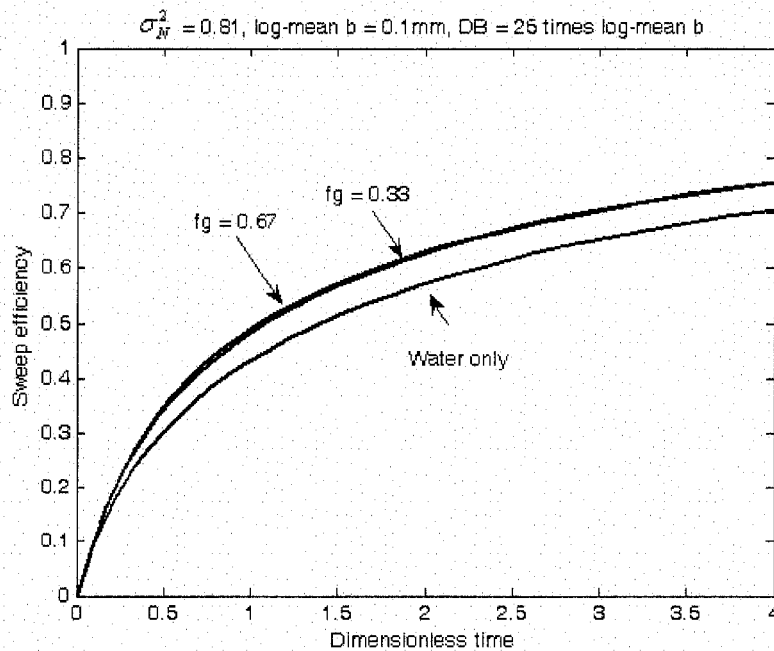


Fig 4.13 sweep efficiency by foam with bubble size 125 times of aperture

4.6.3 Foam bubbles at constant size (< aperture) in different layers

When the foam bubble diameter is less than any aperture in the heterogeneous fracture system, bulk foam is obtained. For this case,

$\frac{\mu_{app,2}}{\mu_{app,1}}$ is a constant because $\mu_{app,1}$ for bulk foam is determined only by gas

fractional flow according to equation (3.11). That is, the apparent viscosity is the same in each layer at the same gas fractional flow, as shown in Fig. 4.15. The sweep efficiency is higher at higher gas fractional flow because foam apparent viscosity is higher. From Fig. 4.14, the sweep efficiency by bulk foam is lower than for the case of individual lamellae in each layer with the bubble diameter is close to the largest aperture (Fig. 4.11) because bulk foam doesn't have any diversion effect.

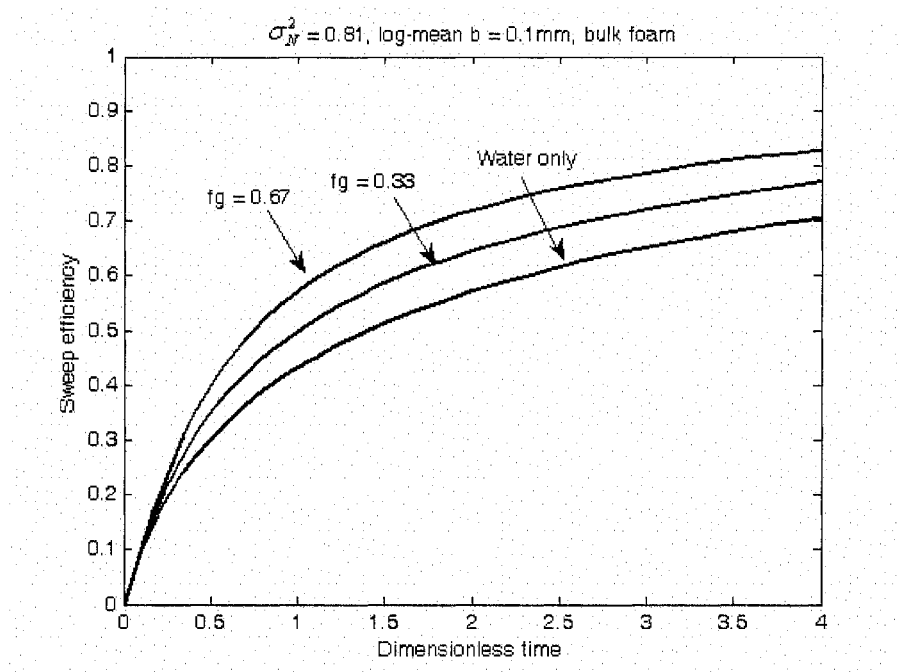


Fig 4.14 sweep efficiency by bulk foam

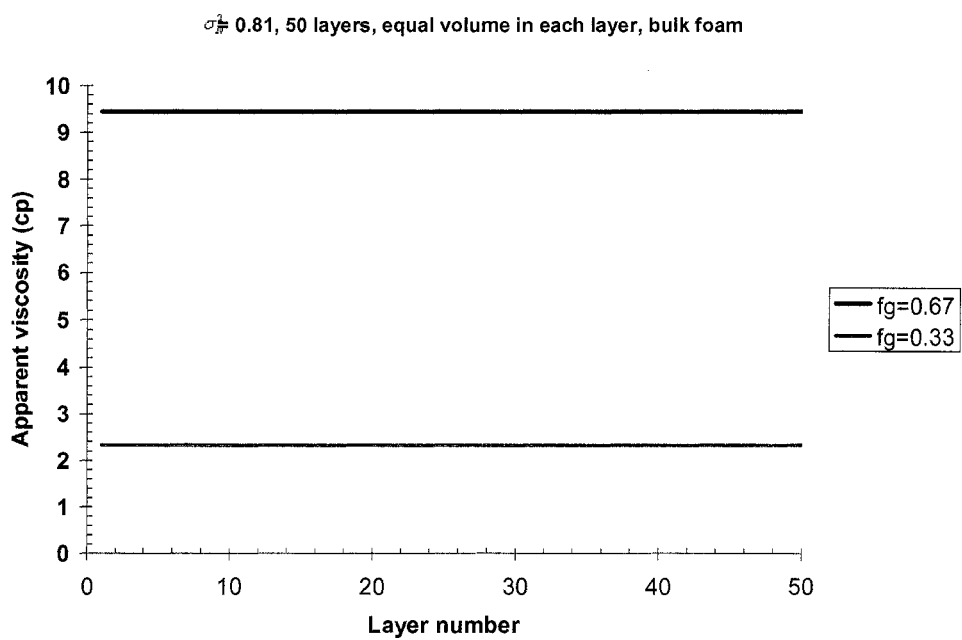


Fig. 4.15 Apparent viscosity in a heterogeneous fracture system with

$\sigma_N^2=0.8$ when the bubble diameter is smaller than any aperture

4.6.4 Foam bubbles at constant size ($>$ some apertures and $<$ some apertures) in different layers

Because bubble size can affect the number of layers containing bulk foam and $\mu_{app,1}$ is related to gas fractional flow, the sweep improvement is related to bubble size and gas fractional flow as in Fig. 4.16 and Fig. 4.18. From Fig. 4.17, we can find the foam apparent viscosity μ_{app} discontinuity when the foam bubble diameter D_B is equal to the aperture b because the model is switched from bulk foam model to individual lamellae model. In this case, the foam apparent viscosity μ_{app} is less in largest apertures. Then as described in chapter 3, in those cases where foam bubble diameter D_B is only slightly greater than aperture b , contrary diversion effect can also be produced. With the increase of bubble size, we can find from Fig. 4.17 and Fig. 4.19, the contrary diversion effect is less with the increase of bubble size because fewer layers have the bulk foam. Although the highest apparent viscosity decreases with the increase of bubble size, the decrease in the contrary diversion effect improves the sweep efficiency.

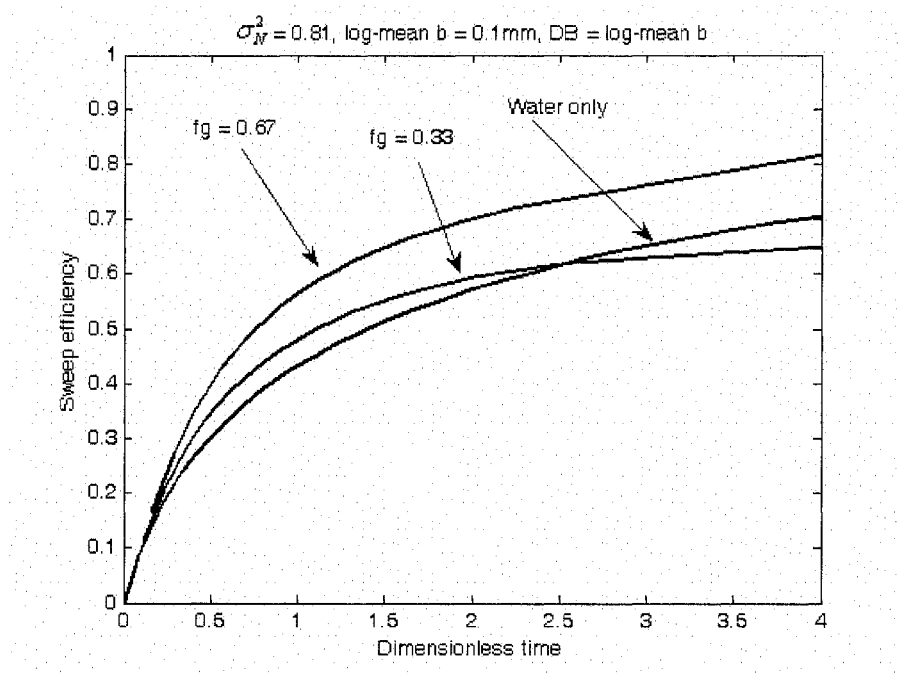


Fig 4.16 sweep efficiency by foam with bubble size equal to log-mean aperture

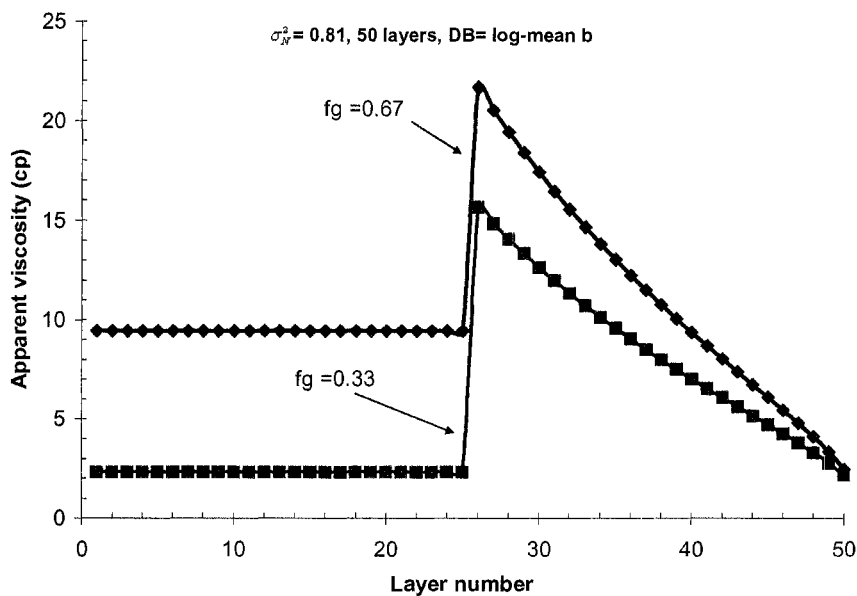


Fig 4.17 Apparent viscosity in a heterogeneous fracture system with $\sigma_N^2=0.8$ when the bubble diameter is equal to the log-mean aperture

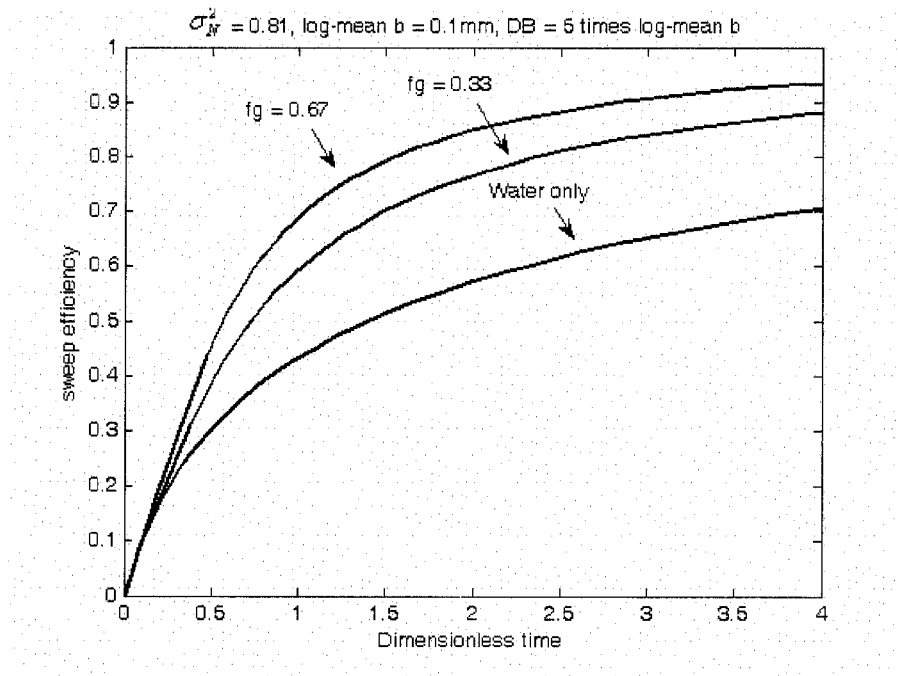


Fig 4.18 sweep efficiency by foam with bubble size 5 times log-mean aperture

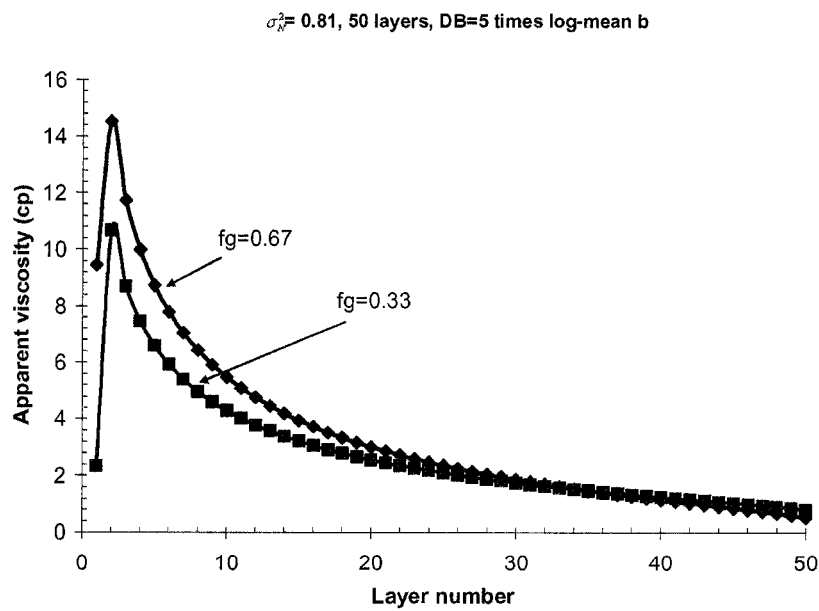


Fig 4.19 Apparent viscosity in a heterogeneous fracture system with $\sigma_N^2=0.8$ when the bubble diameter is equal to 5 times log-mean aperture

Fig 4.20 shows the sweep efficiency at different fracture volumes of injected fluid by water flooding or by foam flooding at gas fractional flow 0.67 and different bubble sizes. When the bubble diameter is 5 times the log-mean aperture, the sweep efficiency is the highest because only one layer in this case has bulk foam and shows the contrary diversion effect. Moreover, the bubble size is relatively small, which yields a high apparent viscosity compared to the 25 times log-mean aperture case. The sweep efficiency by bulk foam is the next, and the foam with bubble diameter equal to log-mean aperture is the third because the contrary diversion effect decreases its sweep efficiency. So it is recommended to use the bubble with bubble diameter equal or close to the largest aperture to get highest sweep efficiency because the contrary diversion effect is smallest and apparent viscosity is relatively high from not too big bubbles.

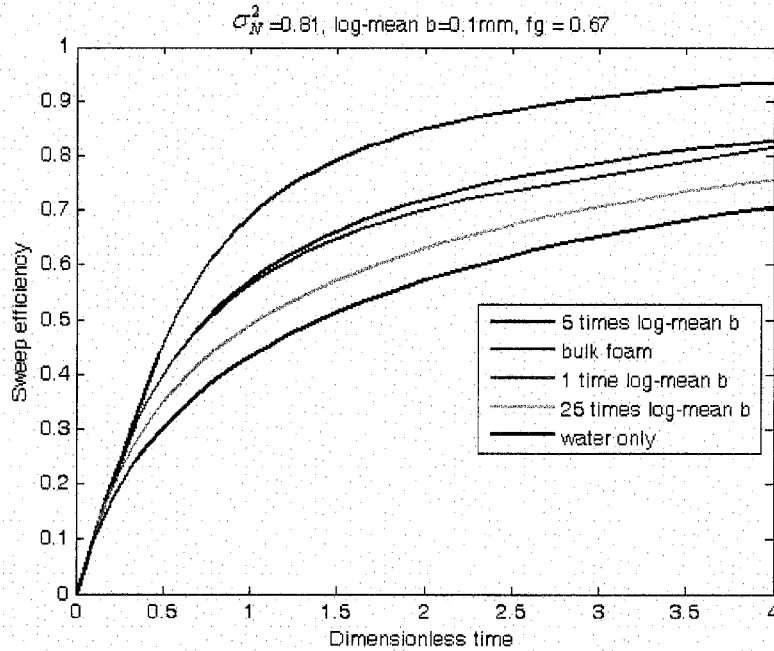


Fig 4.20 Comparison of sweep efficiency at different bubble size

The above conclusion is based on the assumption that the gas fractional flow in different layers is the same. If higher gas fractional flow exists in thicker layers because of the higher entry capillary pressure in thinner layers, the apparent viscosity ratio is higher and is good for the liquid diversion to thinner layers, which increases the sweep efficiency.

Chapter 5

SURFACTANT EVALUATION FOR FOAM-AIDED ALKALINE/SURFACTANT ENHANCED OIL RECOVERY PROCESS

5.1 Selection of surfactants

Selection of surfactants is crucial to foam-aided alkaline/surfactant enhanced oil recovery process. The surfactant in this process should meet the requirements 1) to get ultra-low interfacial tension and 2) generate strong foam. Traditionally, the most commonly used surfactants for alkaline/surfactant flooding are sulfonated hydrocarbons. Their advantages are [Salter, 1986] 1) they are very effective in lowering interfacial tension; 2) they are inexpensive, especially petroleum sulfonates; and 3) they are reported to be chemically stable. But the problem of sulfonates is that they have poor hardness tolerance and salinity tolerance [Green and Willhite, 1998].

Because of their known tolerance to divalent ions, exothylated (EO) and propoxylated (PO) sulfates were evaluated by Gale et al. [1981], Osterloh and Jante [1992], Wellington and Richardson [1995] and Aoudia et al. [1995]. Sulfates rather than sulfonates were evaluated in this research

due to their easier synthesis when ethoxylated or propoxylated and because the target application is a low temperature carbonate reservoir where sulfate hydrolysis is not a problem.

Another important property of PO surfactants is that they decrease hydrophile-lipophile balance (HLB) while not compromising solubility. In the alkaline/surfactant EOR process, both natural surfactants and synthetic surfactants exist. Natural surfactants are mostly very hydrophobic. It is found that the closer the HLB of the added synthetic surfactants are to the natural soap, the smaller influence water/oil ratio (WOR) and surfactant concentration have on the process [Zhang et al., 2005]. The decrease of HLB by increasing straight hydrocarbon chain length of the surfactant will result in the precipitation of surfactants. The addition of PO groups helps to overcome this dilemma [Minana-Perez et al., 1995]. Branching of the hydrocarbon chain also opposes precipitation and formation of highly viscous liquid crystalline phase.

From the work of Zhang et al. [2005], two surfactant formulations were considered as candidates in alkaline/surfactant enhanced oil recovery process. The surfactants involved are identified in Table 5.1.

Trade name	Structural name
CS-330	Sodium dodecyl 3EO sulfate
C13-4PO	Ammonium iso-tridecyl 4PO sulfate
TC blend	1:1 blend weight ratio of C13-4PO and CS330
N67-7PO	Ammonium C16-17 7PO sulfate
IOS	Sodium C15-18 internal olefin sulfonate
NI blend	4:1 weight ratio of N67-7PO and IOS

Table 5.1 Surfactants used in the experiments for alkaline-surfactant EOR process

The sources of CS330 and C13-4PO have been introduced in chapter 3. N67-7PO is developed by Shell Chemical with Procter and Gamble and IOS is from Westhollow technology center, Houston, TX.

Zhang et al. [2005] optimized the formulation by two steps: phase behavior tests followed by interfacial tension measurements. For foam work, we tested the foam strength and foam stability with the presence of residual oil of the optimized surfactant formulation.

During the alkaline/surfactant EOR process, it is important to keep the surfactant solution as one phase to assure that all the oil is contacted by a solution of the proper composition and that no highly viscous phase forms. We made the solutions with 3% N67-7PO&IOS at different mixing ratios of N67-7PO and IOS at 1% Na_2CO_3 and different NaCl concentration. Fig. 5.1 shows the phase behavior at ambient temperature of aqueous solutions containing 3% of mixtures of N67-7PO and IOS as a function of added NaCl for a fixed 1% concentration of Na_2CO_3 . IOS exhibits precipitation above about 4% NaCl. In contrast, no precipitation occurs and a surfactant-rich liquid phase less dense than brine forms as NaCl content increases for solutions containing N67-7PO and its mixtures having up to 75% IOS. The line is drawn for conditions where separation of a second bulk phase was seen. The solutions appeared cloudy at salinities slightly below the line, indicating that some small droplets of the new phase were present. The phase transition occurs at higher salinities as IOS is initially added to N67-7PO, reaching a maximum near 8% NaCl for a 1:1 blend. For the 4:1 mixture of N67-7PO&IOS, it occurs at about 6% NaCl. For N67-7PO alone, but not for the mixtures, some cloudiness was observed after several months even at low salinities.

Fig. 5.2 shows behavior when CaCl_2 is added to 0.5% mixtures of the two surfactants with 2% NaCl present but no Na_2CO_3 . A solid precipitate is observed for IOS alone and the mixture containing 80% IOS for CaCl_2 concentrations exceeding about 0.1 and 0.25% respectively. Except when IOS content falls below 10% tolerance to calcium ions is about 1% for mixtures having higher contents of N67-7PO. For these mixtures separation of a viscous, surfactant-rich phase more dense than brine occurs at high concentrations of CaCl_2 .

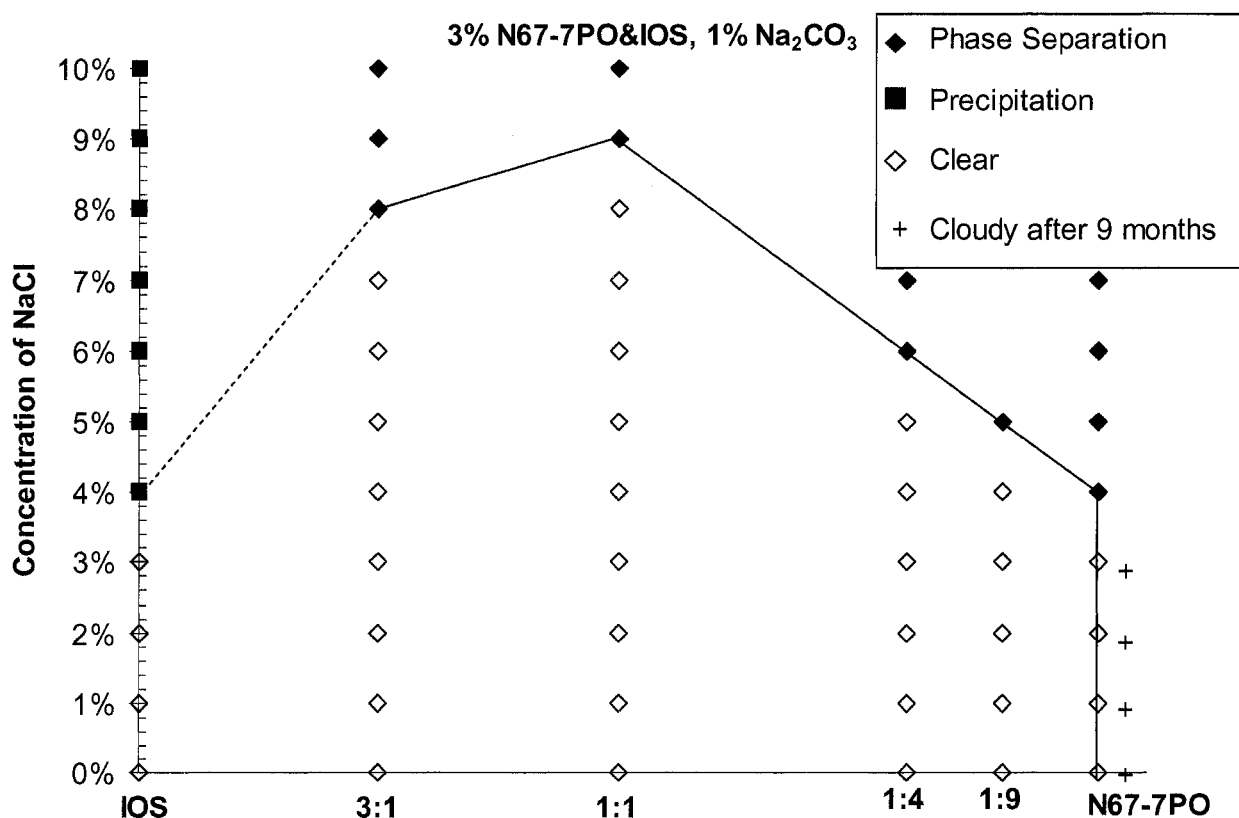


Fig. 5.1 Aqueous phase behavior of N67-7PO&IOS blends, 1% Na_2CO_3 + various NaCl

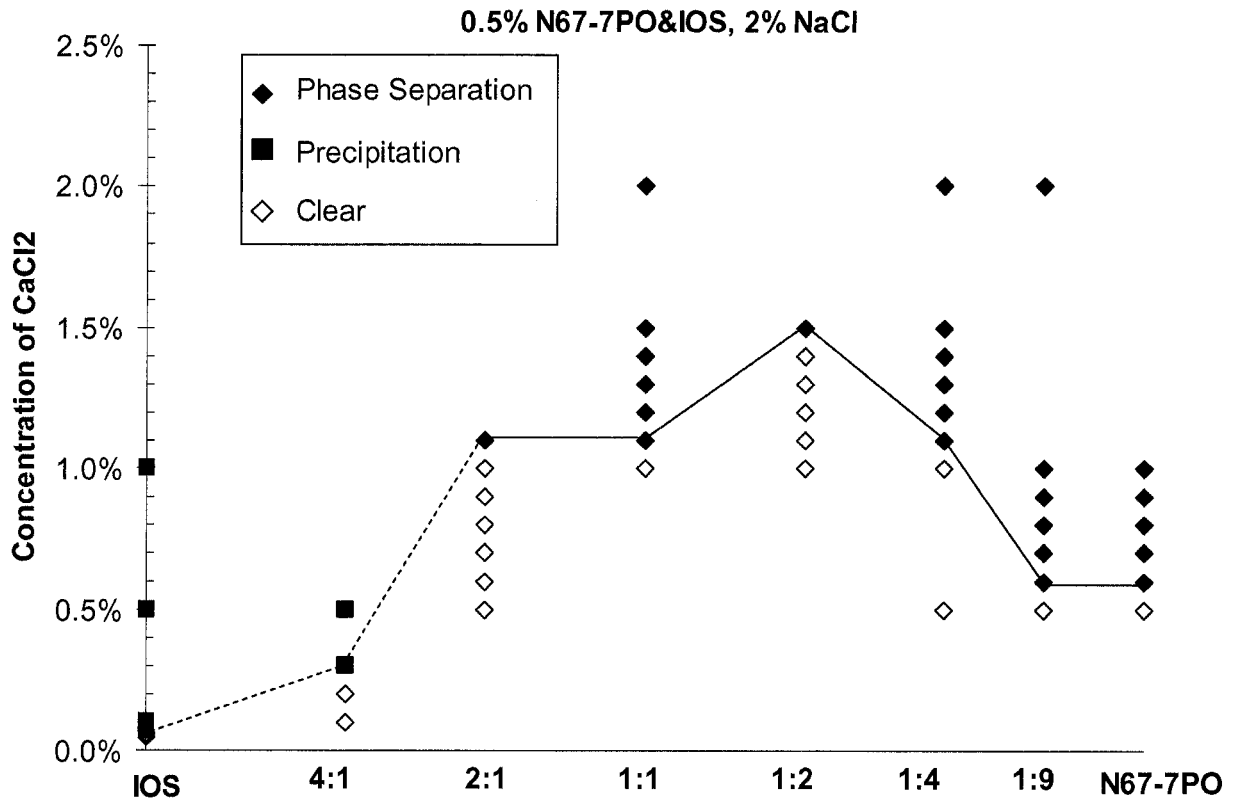


Fig. 5.2 Aqueous phase behavior of N67-7PO&IOS blends, 1% Na₂CO₃ + various CaCl₂

5.2 Foam strength with different surfactants

From the description in chapter 4, foam can greatly improve the sweep efficiency in fracture network. But the success of the foam sweep depends strongly on the strength and stability of foam, which is related to the surfactant composition and salinity. The surfactant composition and salinity in chapters 4 and 5 are from an aquifer remediation project and were used in the fracture study because they had been demonstrated

to form strong foam in sand packs. The surfactant used in the EOR process needs to be tested near the reservoir salinity. We tested the strength of foam by coinjection of surfactant solution and air into a horizontal sand pack initially filled with surfactant and brine at 2% NaCl and 1% Na_2CO_3 to generate foam and measuring the pressure difference across the sand pack to get the apparent viscosity of foam. The surfactants tested were various mixtures of N67-7PO and IOS for total surfactant concentration of 0.5 wt% at the salinity 1% Na_2CO_3 and 2% NaCl. The sand pack is 1 foot long and its permeability is 40 darcy.

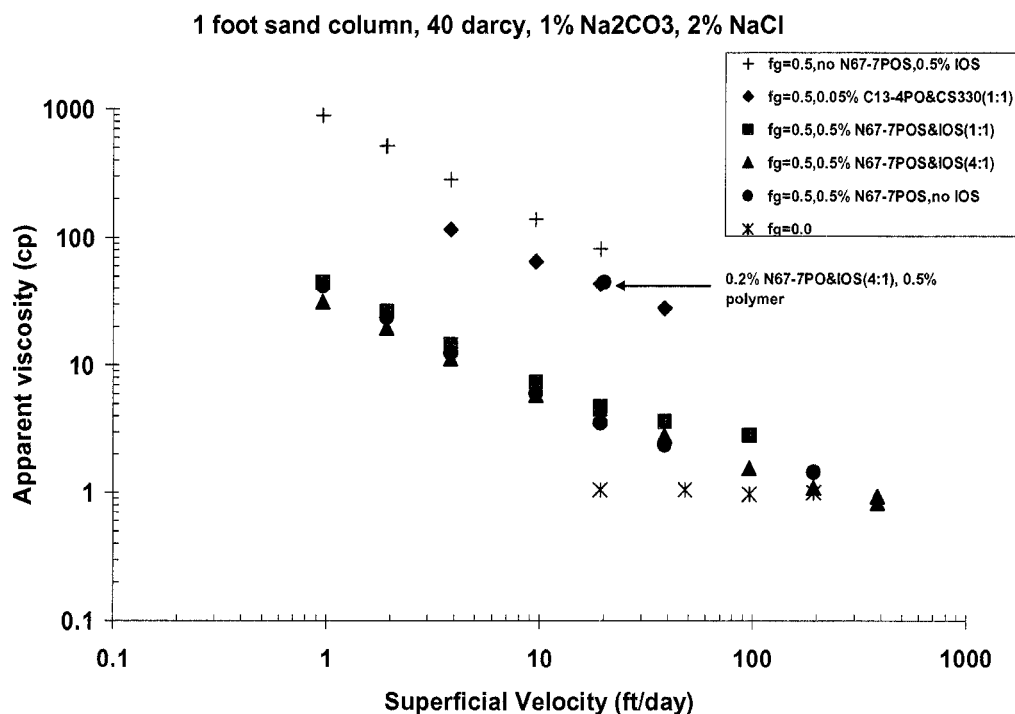


Fig 5.3 Foam strength at different surfactant composition

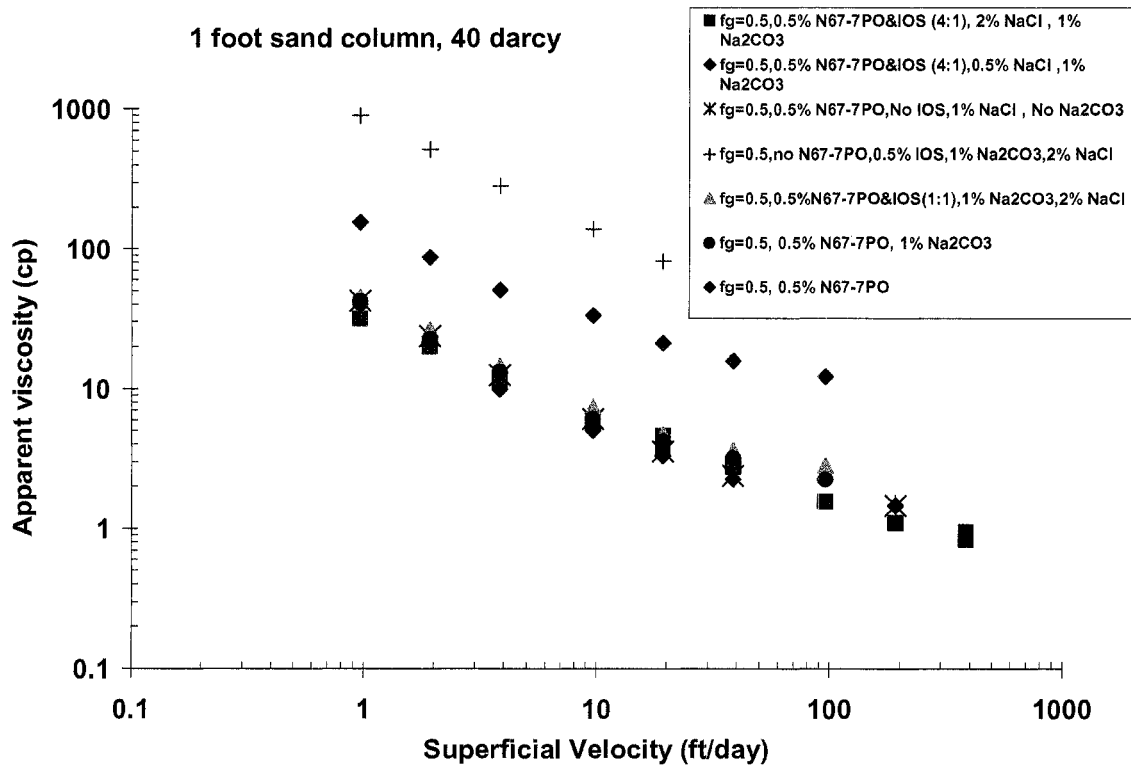


Fig 5.4 Foam strength at different salinity

Fig. 5.3 shows the results of foam strength tests for different surfactant compositions and different velocities at the same salinity. With total surfactant concentration 0.5%, at mixing ratio N67-7PO with IOS at 1:1 to 4:1, the foam apparent viscosity is almost the same as N67-7PO itself at concentration 0.5%. The foam strength produced by the NI blend is weaker than that by the TC blend at a lower concentration and the same salinity. The other finding is that IOS alone is a strong foamer. At the superficial velocity around 1 ft/day, the apparent viscosity of foam by IOS

can be close to 900 cp. One reason may be that IOS is hydrophilic, i.e., well below its optimal salinity with most oils at the conditions studied. Such surfactants are generally good foamers. Fig. 5.4 indicates for the mixture of N67-7PO and IOS, the foaming ability is not affected by different salinity. So the conclusion is that the foaming ability of the mixture of N67-7PO and IOS is limited by the foaming ability of N67-7PO. The reason may be that N67-7PO is hydrophobic with a branched hydrophobe that prevents formation of a compact surfactant monolayer.

Although from the above discussion, N67-7PO or NI blend is not a strong foamer compared with IOS or TC blend, it can still get around 20~30 cp apparent viscosity at low velocities typical of real reservoir conditions. From our study of foam diversion in heterogeneous fractures in Chapter 4, when the foam apparent viscosity is around 20 cp, we can obtain 20~40 times reduction in the liquid volume required to sweep heterogeneous fractures with 1:2 or 1:3 fracture aperture ratios. Then the foam by NI blend is strong enough to divert the surfactant solution into the thinner fractures. And by the work of Zhang et. al. [2005], at the salinity of 2% NaCl and 1% Na_2CO_3 , which is close to the targeted reservoir formation salinity, solution of the NI blend can get the ultra-low

interfacial tension with the reservoir crude oil. Although TC blend or IOS can generate stronger foam, their optimum salinities are much higher than the formation salinity. So NI blend can be used in alkaline-surfactant EOR process with spontaneous imbibition in fractured oil reservoir to get both ultra-low interfacial tension and foam mobility control.

But in forced convection oil displacement in matrix, the foam strength by NI blend or N67-7PO is not enough at the salinity 2% NaCl and 1% Na₂CO₃ because the foam in matrix is needed to displace viscous crude oil instead of water in fractures. Polymer may be blended with NI blend to get NI/polymer foam which has a close apparent viscosity to IOS foam at 20 ft/day as shown in Fig. 5.3.

5.3 Foam stability with the presence of residual oil

The foam was not only to be used in spontaneous imbibition process in fractured reservoir to divert surfactant solution into thinner apertures, but also to be used as mobility control agent in forced convection alkaline-surfactant flooding processes in reservoirs with few or no fractures. For the latter case, the foam may contact crude oil not displaced by the alkaline/surfactant slug, which makes the study of the

foam stability with the presence of residual crude oil necessary. The foam stability for different surfactants with the presence of residual oil was tested in a short sand pack. A short sand pack is used to avoid the long periods of time that would have been required to test various surfactants in the 1-ft long sand pack. The set up for the experiment is shown in Fig. 5.5.

The porous medium consists of a 1.5 inch long and 0.5 inch diameter cylinder packed with 50-mesh size sand. Pore volume for the short sand pack is about 5 ml. Foam is generated in the sand pack by co-injection of surfactant solution and air. The surfactant is injected by an ISCO pump, and air is injected by an air flow controller. Two pressure transducers measure the pressure drop across the tubing and the injection pressure to the sand pack. Foam quality is measured by passing foam from the tubing through an inverted burette containing an IPA/water mixture, which breaks the foam. The ratio of the volume of air collected to the amount of liquid displaced gives the quality of foam.

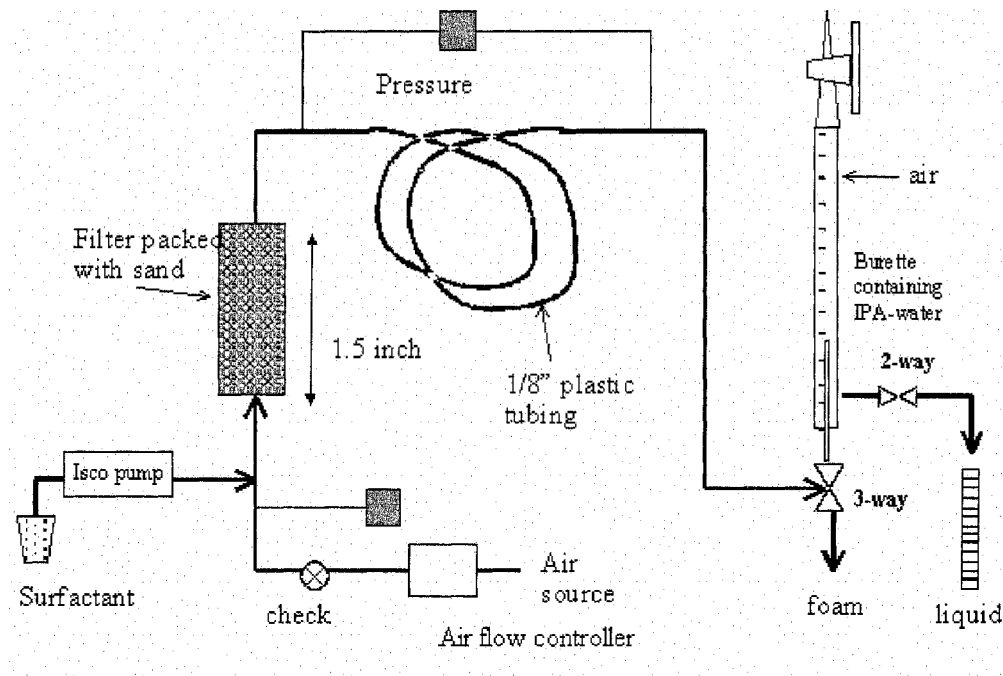


Fig 5.5 Short sand pack setup

To test the foam stability in the presence of residual oil, first, the foam strength without the presence of oil is measured for comparison at some constant gas fractional flow. Second, the water-saturated pack is filled with hexadecane. Then water is used to flush the sand pack to achieve residual oil saturation. Foam is then generated at the same gas fractional flow. The steady state pressure readings are recorded to compare the foam strength with or without residual oil in the sand pack.

The results are shown in Fig 5.6. IOS seems to be the best foamer among the various blends of N67-7PO with IOS. Even after contacting with residual oil, the foam produced by IOS still has a higher apparent viscosity than that formed by any other foamer. N67-7PO and the blend of N67-7PO&IOS (4:1) can get almost the same apparent viscosity with or without residual oil. But that doesn't necessarily mean that foam generated with N67-7PO or the N67-7PO&IOS (4:1) is more stable when the residual oil is present. Because the salinity we used is close to the optimal salinity of N67-7PO and N67-7PO&IOS (4:1), almost all residual oil is displaced by the initial surfactant injected so that little oil is present at the final steady state conditions. And the foam with N67-7PO or N67-7PO&IOS(4:1) is weak compared with that with IOS in Fig. 5.3. So it is reasonable to use IOS as foamer. The reason for IOS has good stability at the residual crude oil is that oil has difficulty entering air/water surface for IOS because of electrical contribution of disjoining pressure in pseudoemulsion film for the ionic surfactant.

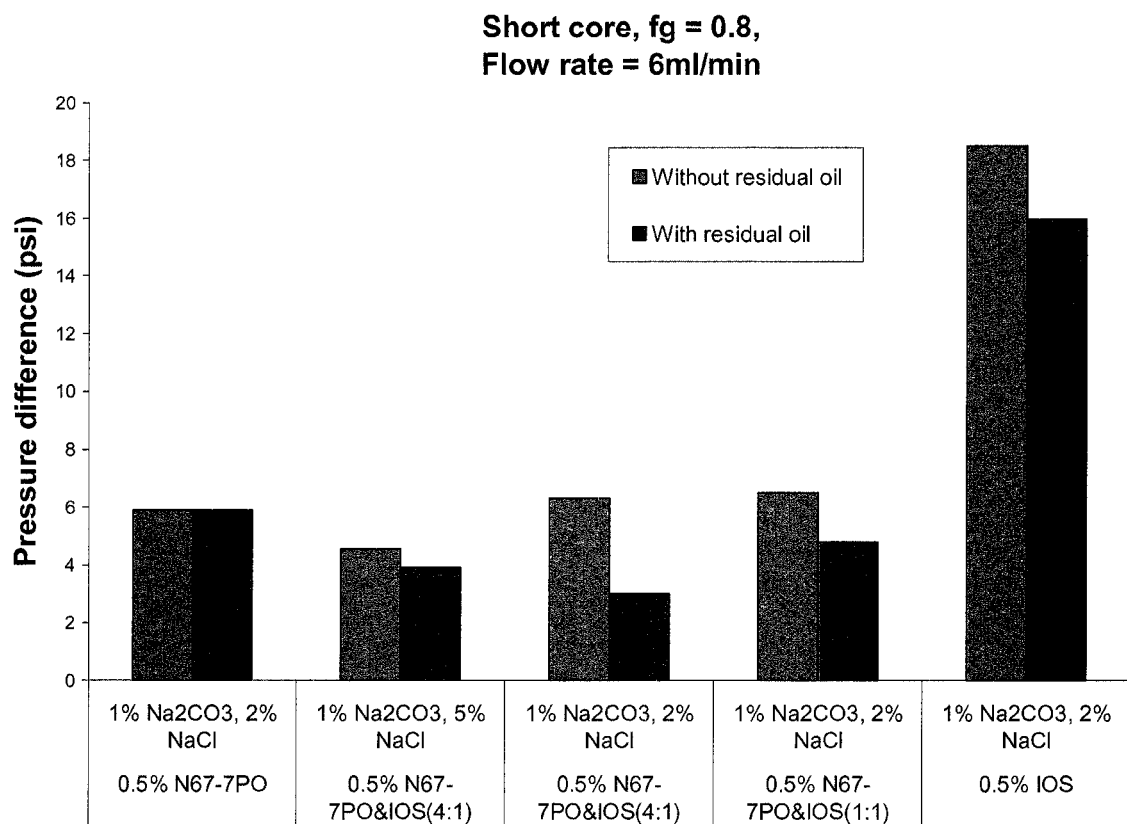


Fig 5.6 Comparison of foam strength with or without residual oil by different surfactant or surfactant blends

Chapter 6

ALKALINE/SURFACTANT/ POLYMER/FOAM

ENHANCED OIL RECOVERY PROCESS

Alkaline/surfactant injection is a chemical method in enhanced oil recovery. Polymer is usually injected following the alkaline/surfactant slug to act as mobility control agent. Here we did experiments with both polymer and foam as mobility control agents for the alkaline surfactant EOR process because foam has higher apparent viscosity in high than in low permeability region and can divert more surfactant solution into low permeability region.

For all the experiments, crude oil samples MY-4 or MY-6 from a West Texas field were used. Both came from the same well, and have very similar properties. API gravity is 28, and acid number is 0.20 mgKOH/g. Water was deionized with a conductivity of 4-7 mS/cm. Anhydrous sodium carbonate powder (99.8% purity with 0.005% calcium), NaCl (certified for biological work), and $\text{CaCl}_2 \cdot 2\text{H}_2\text{O}$ (ACS certified) were all obtained from Fisher Scientific. A partially (25-30%) hydrolyzed

polyacrylamide, Flopaam 3330S, with a molecular weight of approximately 8 million was obtained from SNF Floerger. The surfactant was NI blend.

6.1 Alkaline/ surfactant/ polymer EOR process

An Alkaline/surfactant/polymer (ASP) process was conducted at ambient temperature using upward flow in a vertical, 40-darcy silica sand pack one foot long and one inch in diameter. After the sand pack was saturated with 2% NaCl brine, MY-4 crude oil (viscosity 19 cp) was injected. Waterflooding at ambient temperature and superficial velocity 10 ft/day with 3 PV of 2% NaCl brine reduced oil saturation to 25%.

Next the ASP slug (0.5 PV) containing 0.2% NI blend, 1% Na_2CO_3 , 2% NaCl and 0.5% (5000 ppm) Flopaam 3330S was injected at an superficial velocity of 5 ft/day, followed by 1.0 PV of a drive with no surfactant or alkali but with the same NaCl and polymer concentrations and approximately the same viscosity (43 cp) as the slug. The relatively high polymer concentration and viscosity of both slug and drive were used owing to the high viscosity of the crude oil. The two series of photos in Figs. 6.1 and 6.2 illustrate the formation and propagation of the oil bank and the effluent samples. Fig. 6.3 shows cumulative recovery of the

waterflood residual oil. The oil bank broke through at approximately 0.8 PV and surfactant at 0.9 PV (based on the first observation of a colored microemulsion containing solubilized oil instead of transparent brine in the effluent) from Fig. 6.2. The process recovered 95% of the residual oil with 80% as clean oil. The small amount of oil solubilized in the aqueous effluent was not measured and hence not included in these numbers.

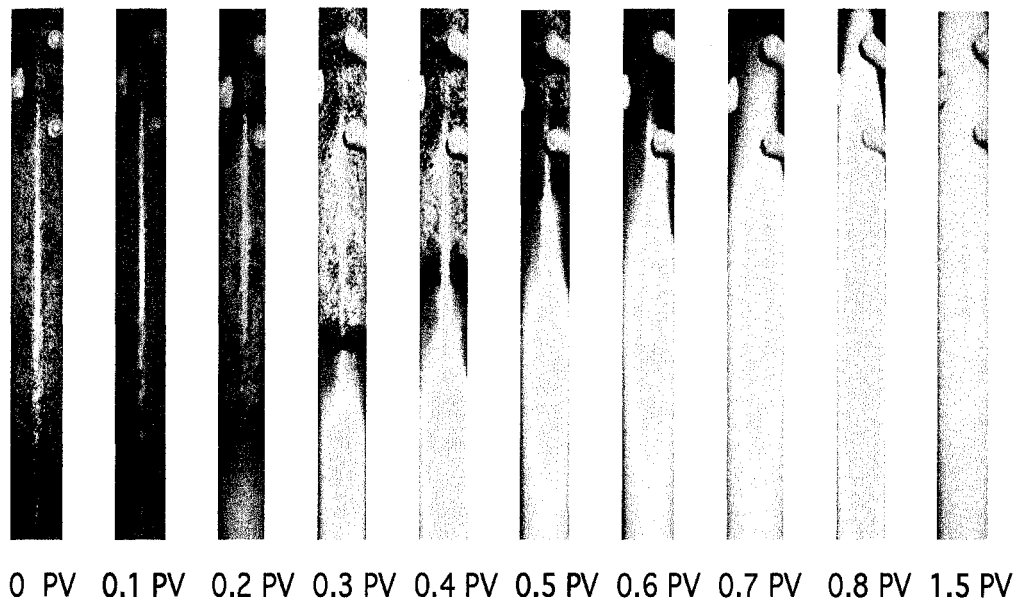


Fig. 6.1 Photos showing behavior during ASP flood of silica sand pack

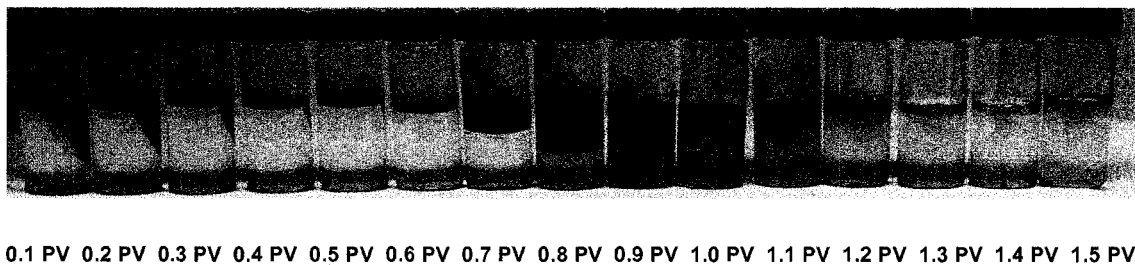


Fig. 6.2 Effluents for different pore volume for ASP experiment

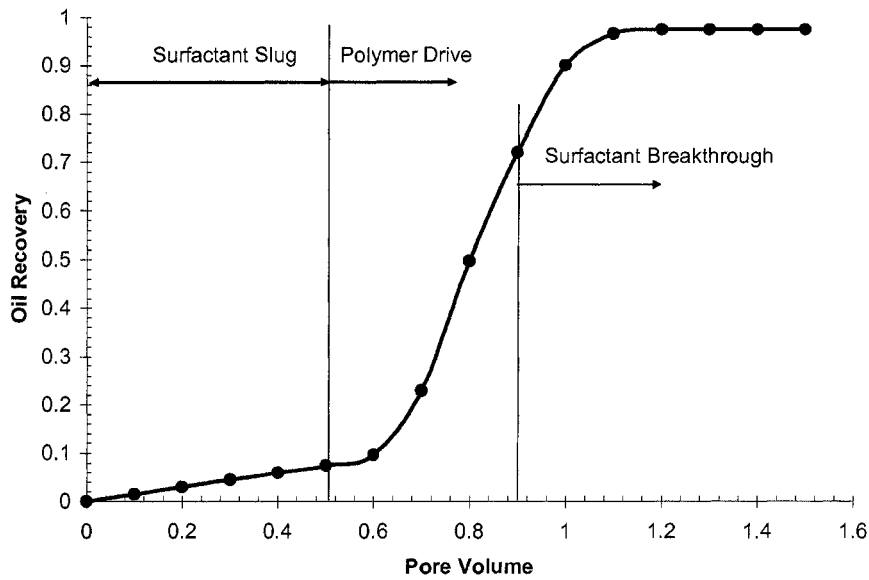


Fig. 6.3 Measured cumulative oil recovery for ASP flood in silica sand pack.

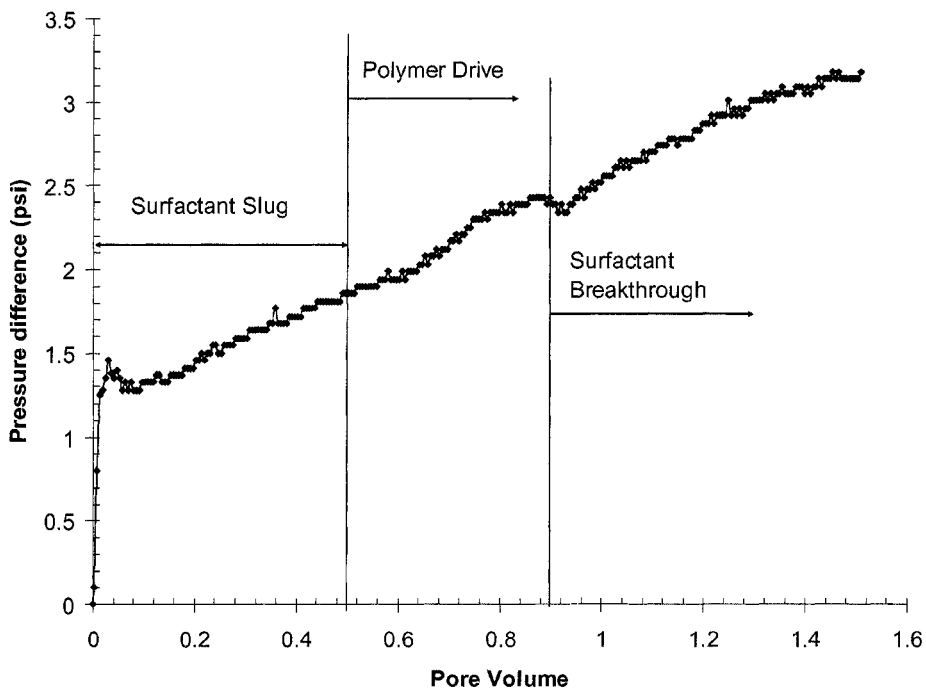


Fig. 6.4 Time-dependence of pressure drop during ASP flood in silica sand pack.

Fig. 6.4 shows that the pressure drop across the sand pack increased steadily during injection of the first pore volume of viscous slug and drive fluid, then remained nearly constant at 3 psi. That is, no highly viscous phases or emulsions developed.

Another ASP flood in a similar silica sand pack was made with the same procedure and compositions except that NaCl content of the brine was 4% instead of 2%. As Fig 6.5 shows, considerable oil traveled behind the oil bank, which was much less distinct than in Fig. 6.1. Moreover, pressure drop rose to 25 psia, nearly an order of magnitude greater than before. The high pressure drop indicates that a highly viscous phase or emulsion was present, presumably owing to separation of the surfactant slug into polymer-rich and surfactant-rich phases at this salinity (shown in Fig. 6.6). The pressure drop rose sharply as the concentrated polymer phase was displaced by the polymer drive in Fig. 6.7.

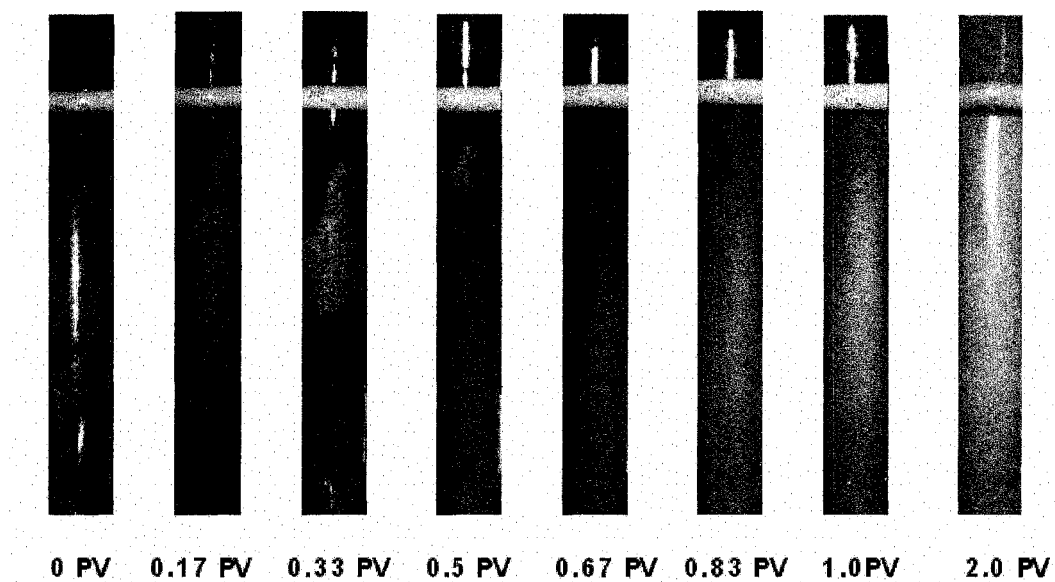


Fig 6.5 Photos of unsuccessful ASP flood at 4% NaCl

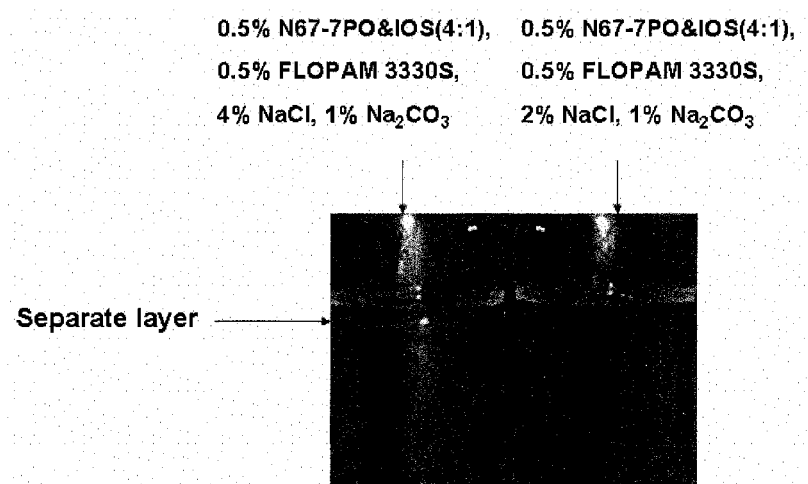


Fig 6.6 Photo of phase separation with polymer at 4% NaCl

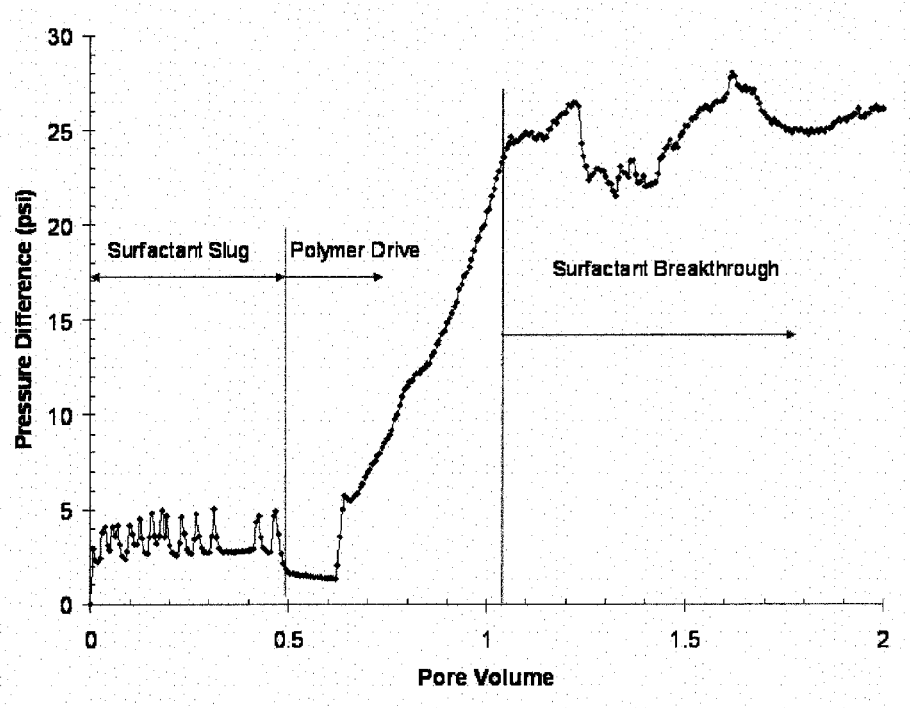


Fig. 6.7 Time-dependence of pressure drop during unsuccessful ASP flood

6.2 Foam drive possibility in alkaline/surfactant/polymer process

In normal alkaline/surfactant/polymer process, polymer is used as mobility control agent to be injected together with surfactant and also as drive. However polymer is expensive. We investigated the possibility of using foam to replace polymer as drive.

The experiment was performed in a horizontal one-dimensional 1-foot long sand pack. The sand pack's permeability is 40 darcy. It was

presaturated with a polymer/surfactant solution to simulate a situation when residual crude oil saturation was zero behind the surfactant/polymer slug. The polymer in this slug is 0.5% FLOPAM 3330S. The surfactant is 0.5% N67-7PO&IOS (4:1). The salinity is 2% NaCl and 1% Na₂CO₃. By measurement, the viscosity of the polymer/surfactant solution is 43 cp at 24 C and shear rate 66 s⁻¹.

The experiment was performed at constant pressure drop between 4.0 and 4.5 psi. The foam was generated in the sand pack by co-injection of surfactant solution and air at gas fractional flow 0.67. We tried three different surfactants using the same salinity as in the slug: 1% IOS, 0.5% CS330, 0.5% C13-4PO&CS330 (1:1). The surfactant blend N67-7PO&IOS was not included although it has good performance in displacing oil. As described as in chapter 5, the foam produced by the blend of N67-7PO&IOS is weak. The experimental results are shown in Fig. 6.8. About 0.1~0.2PV of co-injected fluid was needed to get the pressure drop up to 4.5 psi. Then by changing the flow rate, the pressure drop was kept between 4.0~4.5 psi. The foam produced by 1% IOS broke through around 1 PV, 0.5% CS330 at 0.9 PV and 0.5% C13-4PO&CS330 (1:1) at 0.8PV. We also tried to use the foam generated by 1% N67-7PO&IOS

(4:1) and found the pressure drop never exceeded 1.5 psi before foam breakthrough.

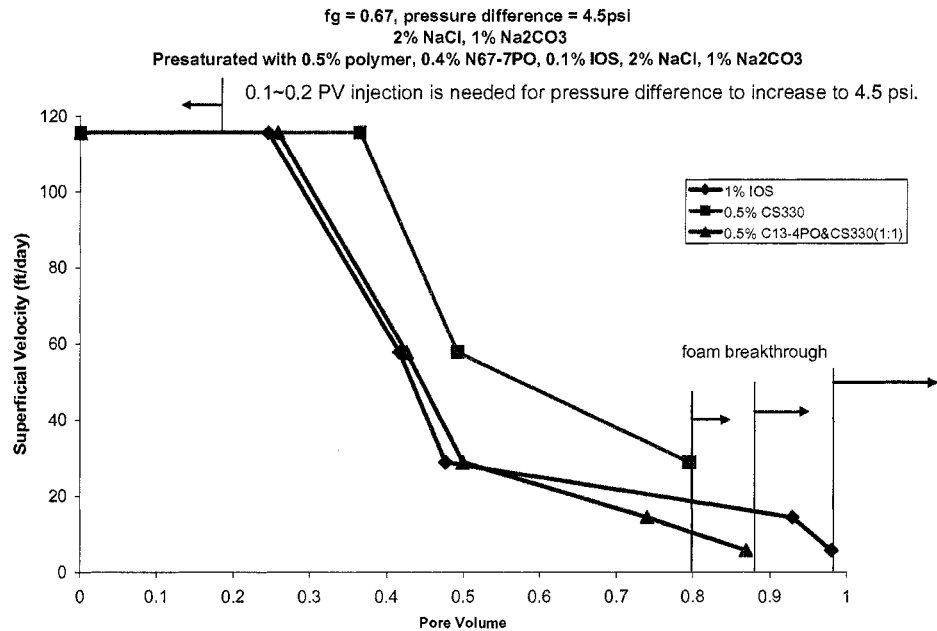


Fig. 6.8 Foam sweep the sand pack presaturated with polymer/surfactant

Fig. 6.9 shows the apparent viscosity during the sweeping the sand pack by foam. At the time of foam breakthrough, the apparent viscosity is about 40 cp for 0.5% CS330 and 200 cp for 1% IOS and 0.5% C13-4PO&CS330 (1:1). The viscosity of the polymer/surfactant solution is 43 cp. If we assume the apparent viscosity of the system at the foam breakthrough is equal to the foam apparent viscosity, the latter is close to or higher than the viscosity of the polymer/surfactant solution. But we

did see the fingering at the interface of the foam and polymer/surfactant. The reason may be that the foam front is not as strong as the steady foam behind and the N67-7PO in the system may weaken the foam front.

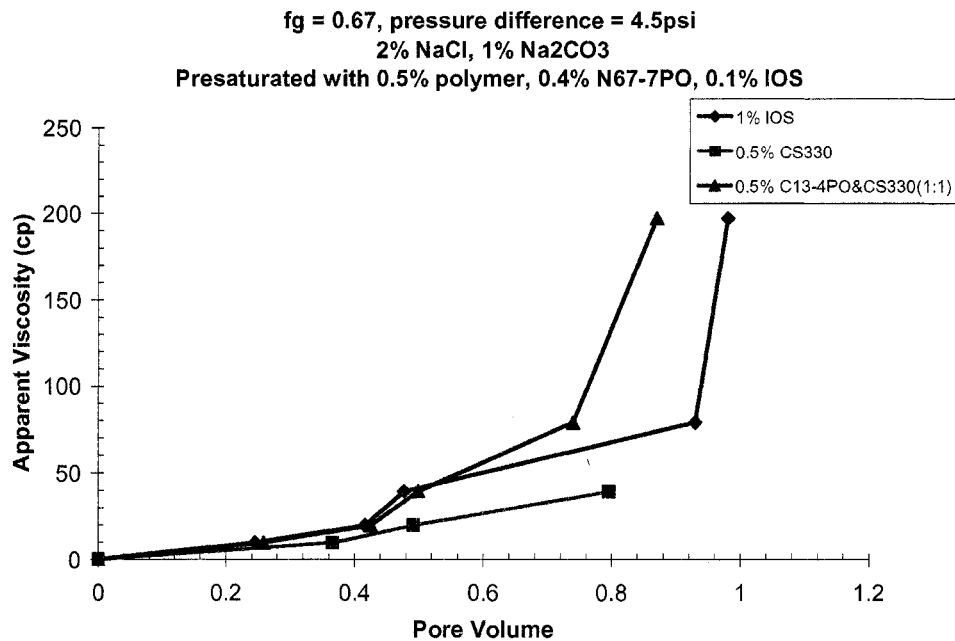


Fig. 6.9 Apparent viscosity during the sweeping the sand pack presaturated with polymer/surfactant

The results in Fig. 6.8 show that it is possible to use foam instead of polymer as drive in ASP process. Although the cost of surfactant is comparable to polymer at the same concentration, lower surfactant concentrations are possible. Also less surfactant solution is required

because a substantial portion of the drive fluid would be the gas in the foam bubbles.

6.3 Foam drive in alkaline/surfactant/polymer process

To continue to investigate the possibility of using foam to replace polymer as drive in ASP process, we did an experiment which involved crude oil. The experiment was performed in a one dimensional sand pack in vertical position. The sand pack is 1 foot long with 40 darcy permeability. The procedure for the alkaline-surfactant-polymer-foam experiment is:

1. Fill the sand pack with CO₂;
2. Fill the sand pack with water;
3. Fill the sand pack with crude oil;
4. Use brine to flood the sand pack at 10 ft/day superficial velocity until no oil comes out;
5. Inject alkaline/NI blend/polymer solution into sand pack to displace oil for 0.5 PV at superficial velocity 5 ft/day;
6. Inject IOS/polymer solution as drive for 0.2 PV at superficial velocity 5 ft/day;

7. Co-inject IOS solution and air into sand pack as drive at gas fractional flow 0.67 and superficial velocity 20 ft/day.

The brine in this experiment contains 2% NaCl. The alkaline/surfactant/polymer solution includes 1% Na_2CO_3 , 0.2% N67-7PO&IOS at 4:1 mixing ratio, 0.5% polymer at 2% NaCl. The viscosity for the solution is 46.5 cp from measurement by a viscometer at the shear rate 50 s^{-1} . The crude oil is MY-4 and its viscosity is 19cp. The surfactant/polymer solution in step 6 is 0.5% IOS and 0.5% polymer at 2% NaCl. Its viscosity is 46.1cp from measurement. The reason that we include step 6 is that we want to construct a barrier between NI blend and IOS because from chapter 5 we found N67-7PO can make the foam weak. The co-injection of air and surfactant solution is at gas fractional flow 0.67. The surfactant solution in step 7 is 0.5% IOS at 2% NaCl and 1% Na_2CO_3 . The residual saturation after brine flooding is 25% from material balance calculation.

The ASPF displacement picture is shown in Fig. 6.10. From the picture, the oil bank is pretty clear but there was a tail after the oil bank. The reason may be that the injected for this experiment (but not others)

crude oil contained some viscous emulsion. But we can see that the shape of the tail didn't change after the foam drive began. This shows the foam drive forms a plug flow in the sand pack. From Fig. 6.11, at around 1.5 PV, almost all the residual oil was recovered. The big tail can also be found from the effluents shown in Fig. 6.12.

Fig. 6.13 shows the pressure history during the ASPF experiment. The first 0.7 PV is alkaline/surfactant/polymer slug and polymer drive injection. The pressure difference during this time period gradually increases. When the air/surfactant co-injection begins, the pressure difference decreases first and then increases up to around 3 psi and stays there. That shows the steady foam forms.



Fig. 6.10 Photos showing behavior during ASPF flood of silica sand pack

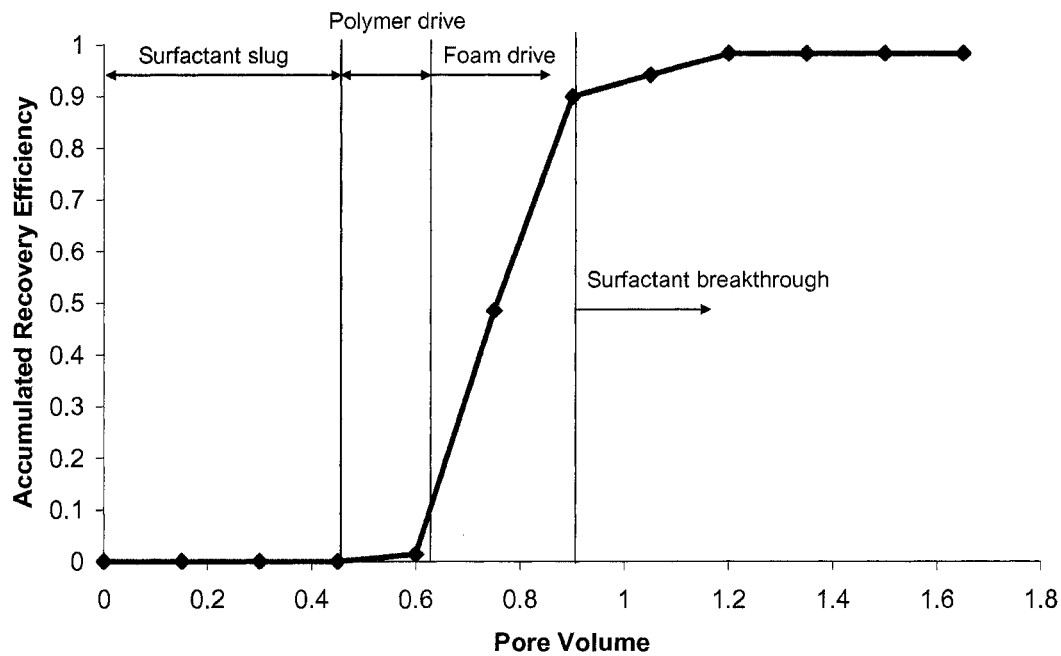


Fig. 6.11 Recovery history for ASPF experiment

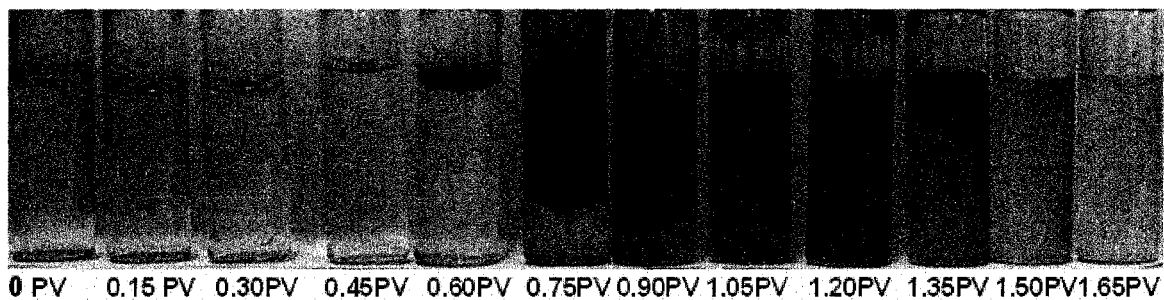


Fig. 6.12 Effluents for different pore volume for ASPF experiment

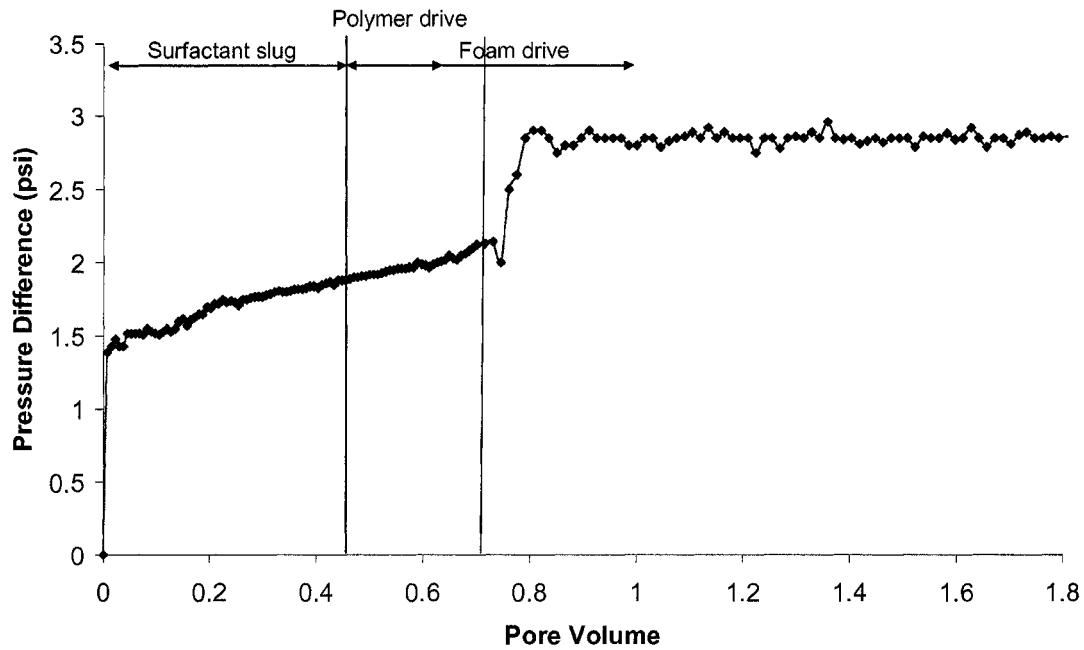


Fig. 6.13 Pressure history for ASPF experiment

The second ASPF experiment was performed for two reasons: first to test the reproducibility of the ASPF experiment result, second to optimize the process by using less surfactant slug. Different from the first ASPF experiment, the second experiment uses only 0.3 PV alkaline/surfactant/polymer as surfactant slug which includes 0.2% NI blend at 4:1 ratio of N67-7PO to IOS, 1% Na_2CO_3 and 2% NaCl, followed by 0.2 PV IOS/polymer containing 0.2% IOS and 2% NaCl. The polymer concentration in the surfactant slug and polymer drive is 0.5% which supplies 47 cp viscosity. The foam is generated by alternating injection of

air and 0.2% IOS at 2% NaCl at the volume ratio of 2:1. The superficial velocity for the injection of surfactant slug and polymer drive is 5 ft/day. Air is injected at 20 ft/day and surfactant solution is injected at 10 ft/day.

From the pictures showing the behavior during the ASPF flood in Fig 6.14, the oil bank is not as clear as in Fig. 6.1. The reason may be that the surfactant slug is small and the oil recovered in the oil bank is less than the previous experiments with 0.5 PV surfactant slugs. From Fig. 6.17 which shows the pressure history, the pressure difference increased gradually after the air injection which means the foam was formed. But after the injection of surfactant solution, the pressure difference increased greatly. The reason may be that the foam bubbles began to move by the injection of surfactant solution and the foam bubbles coalesce when the air was injected.

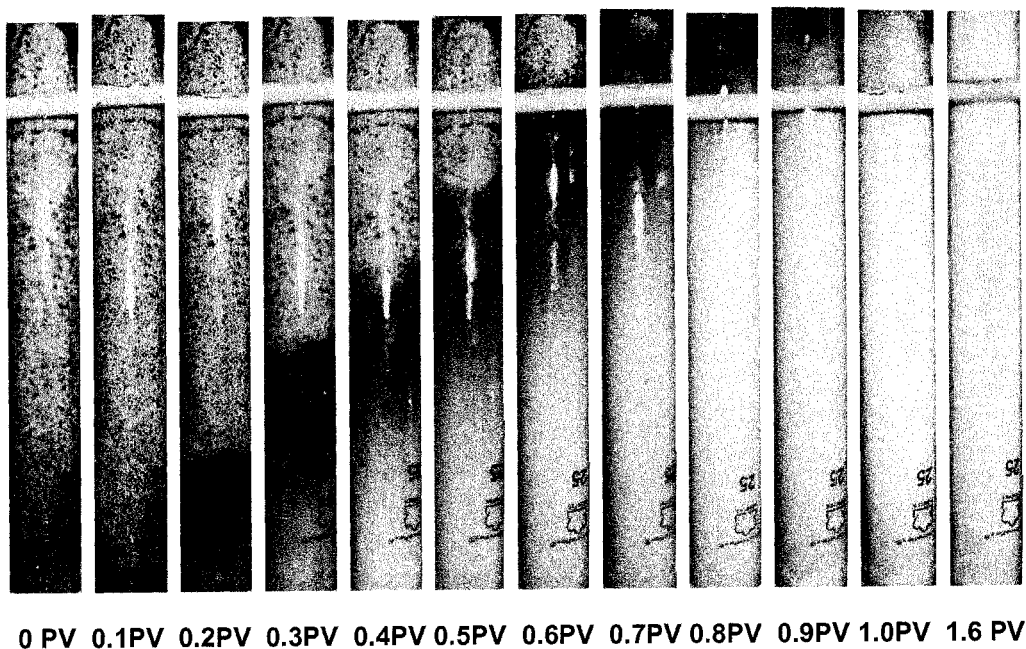


Fig. 6.14 Photos showing behavior during ASPF flood of silica sand pack at optimized condition

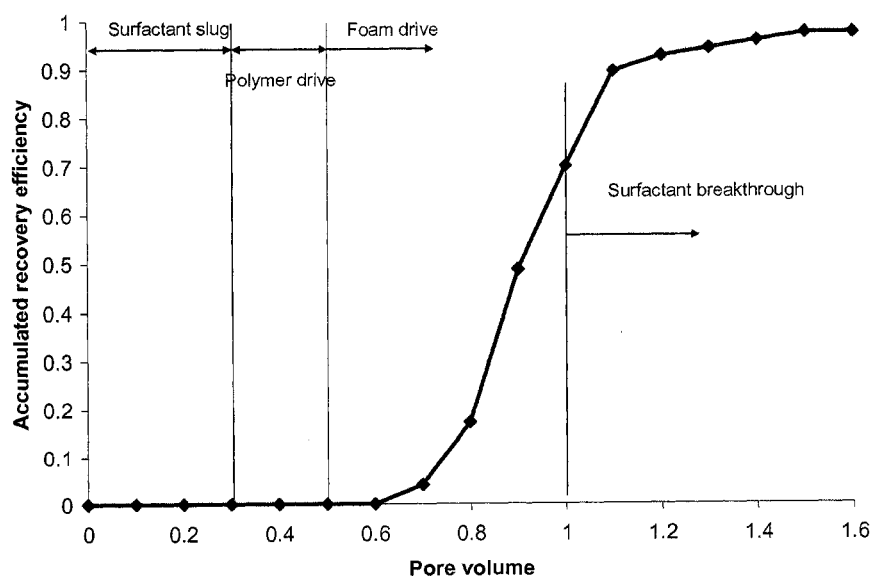


Fig. 6.15 Recovery history for ASPF experiment at optimized condition



0.1PV 0.2PV 0.3PV 0.4PV 0.5PV 0.6PV 0.7PV 0.8PV 0.9PV 1.0PV 1.1PV 1.2PV 1.3PV 1.4PV 1.5PV 1.6PV 1.7PV

Fig. 6.16 Effluents for different pore volume for ASPF experiment at optimized condition

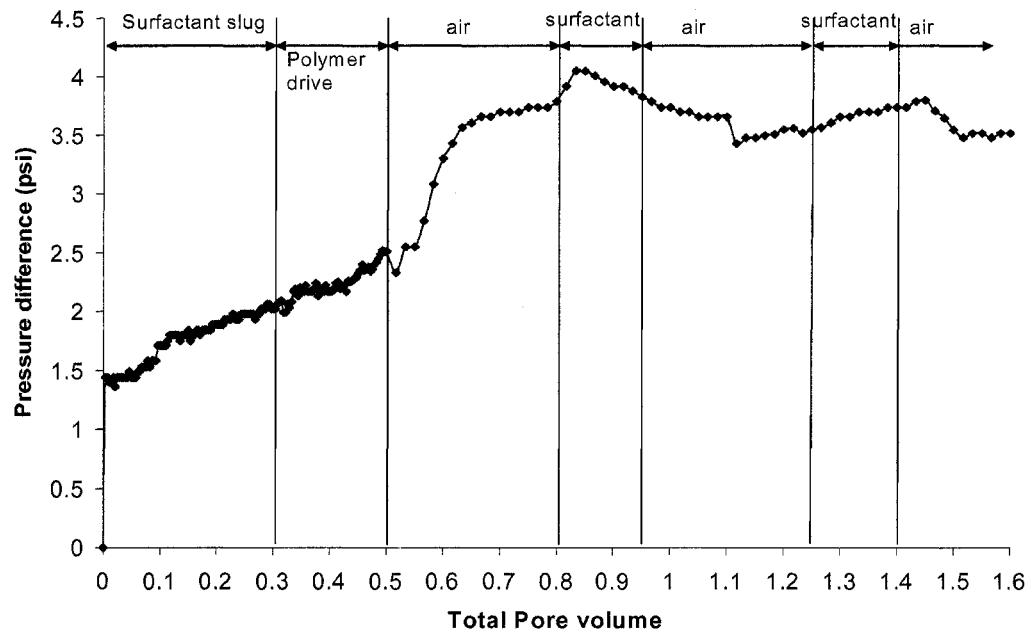


Fig. 6.17 Pressure history for ASPF experiment at optimized condition

The above two experiments give similar results: the recovery efficiency is above 90%, more than 70% of recovered oil is clean oil, and all the oil is recovered within 1.6 total pore volume and most within 1.1 total pore volume. The differences between the two experiments are that the

surfactant slug in the second experiment is 0.3 PV which is 0.2 PV less than in the first experiment, and the foam in the second experiment is generated by surfactant/air alternate injection while in the first one the foam is generated by co-injection of surfactant solution and air. The 0.3 PV surfactant slug is enough to recover the residual oil from the experiment. The pressure difference during the foam injection increases up to 2 times of that during surfactant slug and polymer slug injection, which shows the foam apparent viscosity is slightly greater than the viscosity of the polymer.

6.4 Alkaline/surfactant/polymer/foam process

Although the foam drive is proven to be feasible in the previous experiments to replace polymer drive, the unique advantage of foam in ASPF process is not fully utilized if foam is only used as drive. The reason is that the entire alkaline /surfactant slug is injected before the foam drive begins with the result that foam has no effect on slug distribution among layers. The foam has higher apparent viscosity in the high permeability region so foam with slug injection should be able to divert more of the slug into low permeability region. Then foam can work best in the heterogeneous system to get higher oil recovery by increasing the

sweep efficiency. We did two experiments to test the foam strength in two sand packs with different permeability. From the description in chapter 6.1, the blend of N67-7PO and IOS at 4:1 ratio at the salinity 1% Na_2CO_3 and 2% NaCl can get ultra low interfacial tension between oil and water and displace the oil nearly completely. But NI blend is a weak foamer. So we try to use NI blend with polymer together as foamer.

The experiment for foam flooding to displace residual crude oil was performed in a one dimensional vertical sand pack. The sand pack has 40 darcy permeability. The procedure for doing the experiment is:

1. Fill the sand pack with CO_2 .
2. Fill the sand pack with brine at 2% NaCl.
3. Fill the sand pack with MY-6 crude oil at 10 ft/day.
4. Use brine (2% NaCl) to flood the sand pack at 10 ft/day until no oil comes out.
5. Alternate the injection at 20 ft/day into the sand pack of 0.2% NI blend with 0.5% polymer at 1% Na_2CO_3 and 2% NaCl for 0.1 PV, and air for 0.1 PV. Totally 0.6 PV of NI/polymer and air is injected.

6. Alternate the injection into the sand pack of 0.2% IOS at 1% Na_2CO_3 and 2% NaCl for 0.1 PV, and air for 0.1 PV. The superficial velocity is 20 ft/day.

6.4.1. 40 darcy sand pack

The pictures taken during the experiment are shown in Fig 6.18, and the effluents' pictures are shown in Fig 6.19. From measurement, the sand pack has 25% residual oil saturation after water flooding. The cumulative recovery efficiency for the flooding is shown in Fig 6.20 and the pressure history is shown in Fig 6.21.

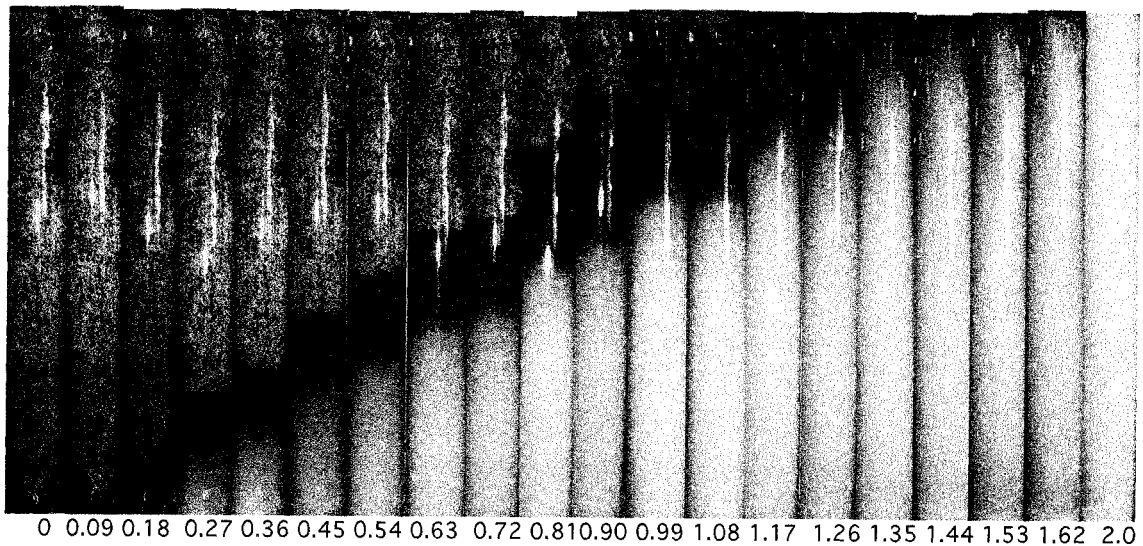


Fig. 6.18 Pictures for the displacement of residual crude oil by polymer/foam in 40 darcy sand pack (Unit: PV)

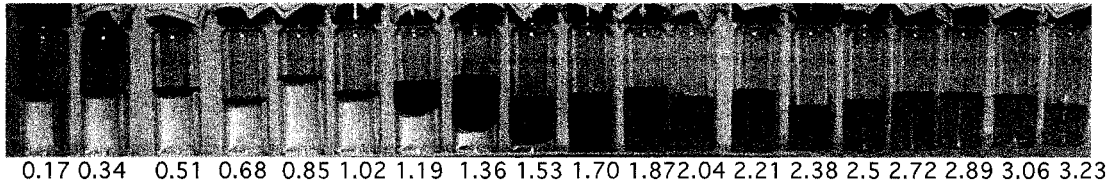


Fig. 6.19 Pictures for effluents for polymer/foam flooding in 40 darcy sand pack (Unit: PV)

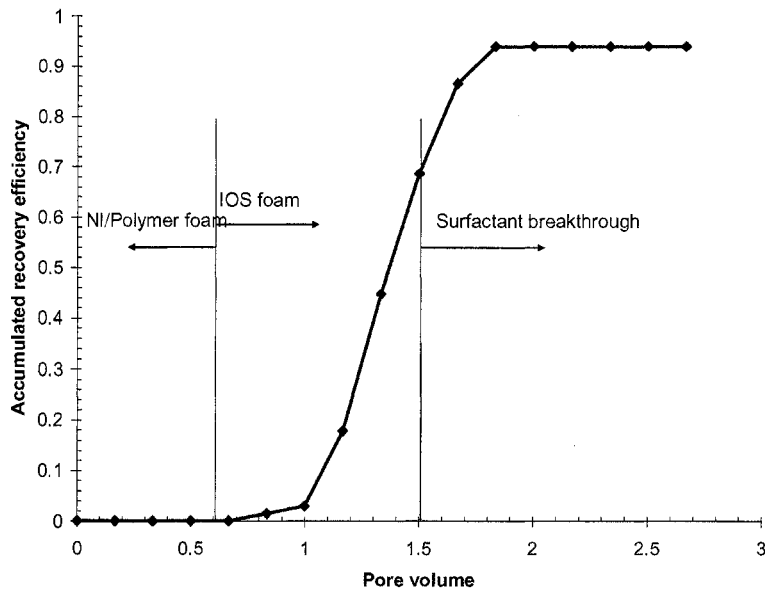


Fig. 6.20 Recovery efficiency for polymer/foam flooding in 40 darcy sand pack

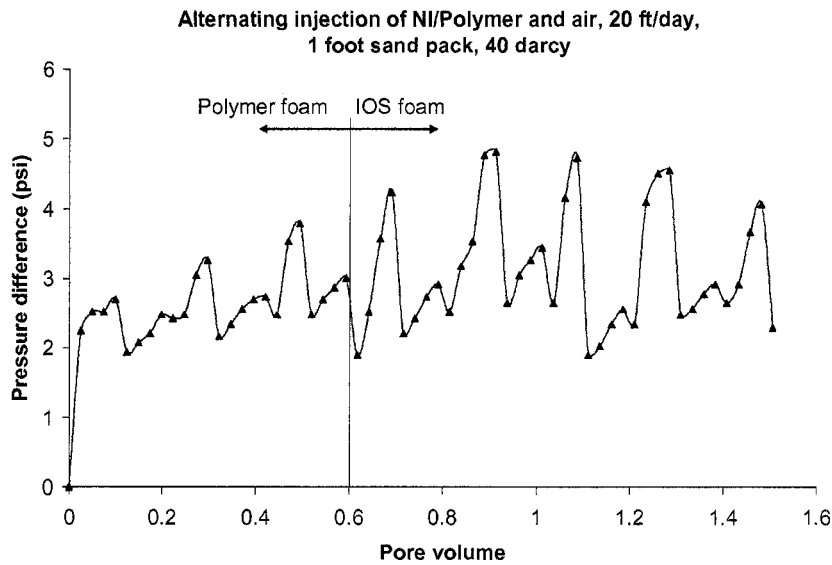


Fig. 6.21 Pressure history for polymer/foam flooding in 40 darcy sand pack

Finally 94% of the residual crude oil was recovered by polymer/foam flooding. Most of the crude oil was recovered between 1 and 1.6 PV. The pressure differences for this NI/polymer foam for the first 0.6 PV and the IOS foam drive after 0.6 PV are close, which means that the apparent viscosities of NI/polymer foam and IOS foam are close. In a foam displacing water experiment, the NI/polymer foam apparent viscosity is 44 cp and the IOS foam apparent viscosity is 81 cp. But in this displacing oil process, the IOS foam will contact some N67-7PO in the NI/polymer foam and perhaps a little crude oil left after the surfactant flooding, which may decrease the strength of the IOS foam. During the experiment, the

air (not bubble) breaks through around 0.9 PV. The reason for early air breakthrough may be some air get into oil bank and even some distance ahead of oil bank.

6.4.2 200 darcy sand pack

In a 200 darcy sand pack, we performed a similar foam displacing oil experiment using the same procedure as in 40 darcy sand pack. The pictures for the displacement process, the effluents' pictures, the accumulated recovery efficiency and the pressure history are shown in Fig 6.22 to Fig 6.25.

The residual oil saturation after water flooding is 30% from measurement. Around 96% of the residual crude was recovered. The oil breakthrough at about 0.8 PV, which is earlier than 1.0 PV in 40 darcy sand pack. The reason is that the mobility ratio between the foam and the oil bank is smaller in 200 darcy sand pack than in 40 darcy sand pack. The NI/polymer foam apparent viscosity in 200 darcy sand pack is 215 cp at 20 ft/day in the foam displacing brine experiment described in section 5.2. The IOS foam in 200 darcy sand pack has the similar strength to the NI/polymer foam because the measured pressure difference was nearly

the same (Fig. 6.25). The air breaks through the sand at around 0.7 PV which is earlier than in 40 darcy sand pack. The reason may be that the air gets into the oil bank and some distance ahead of oil bank. Because oil bank breaks through earlier in 200 darcy sand pack than in 40 darcy sand pack, the air also breaks through earlier.

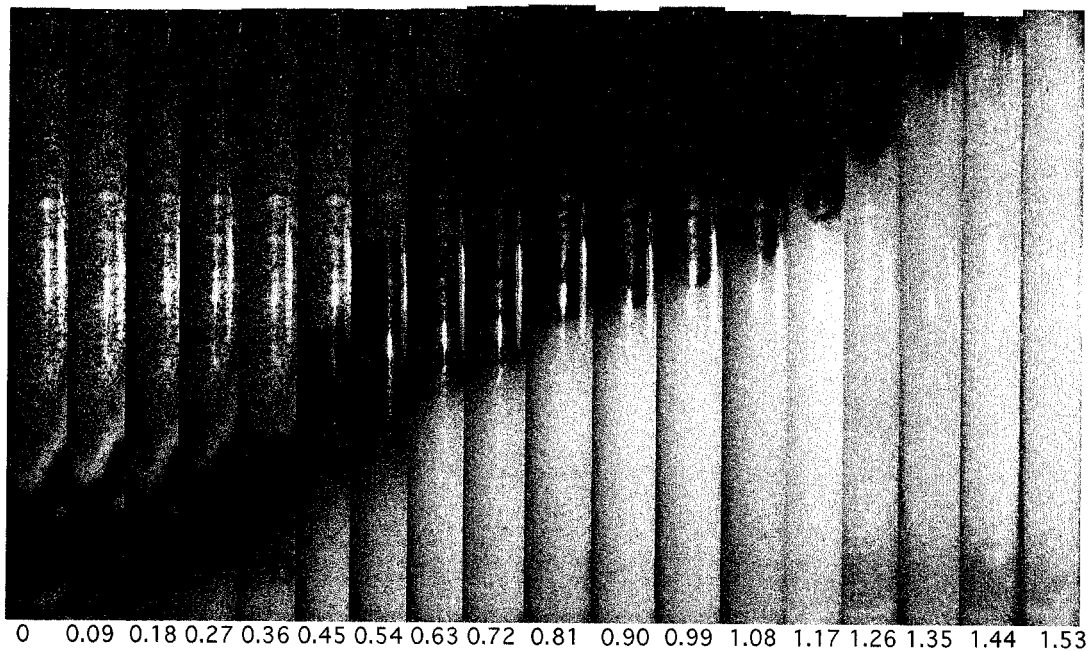


Fig. 6.22 Pictures for the displacement of residual crude oil by polymer/foam in 200 darcy sand pack (Unit: PV)

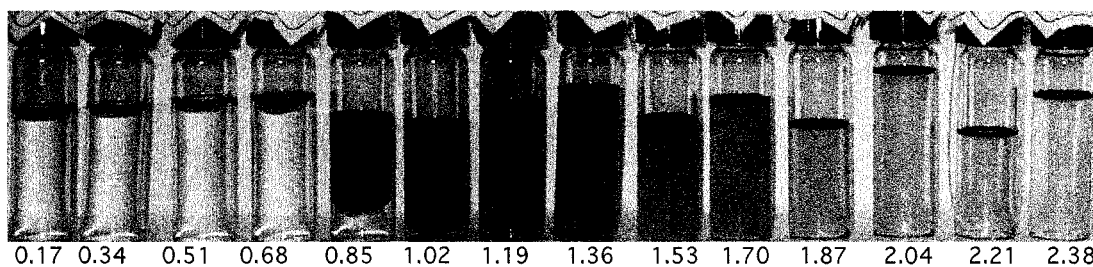


Fig. 6.23 Pictures for effluents for polymer/foam flooding in 200 darcy sand pack (Unit: PV)

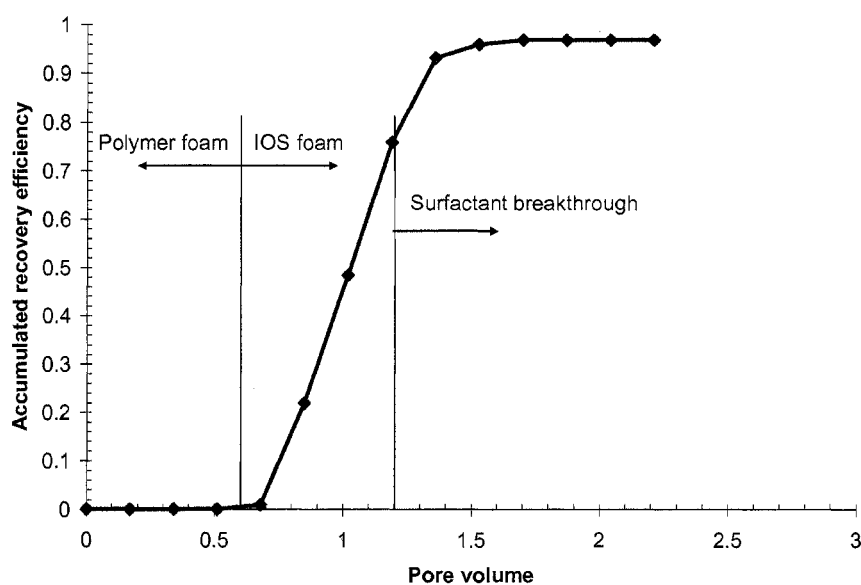


Fig. 6.24 Recovery efficiency for polymer/foam flooding in 200 darcy sand pack

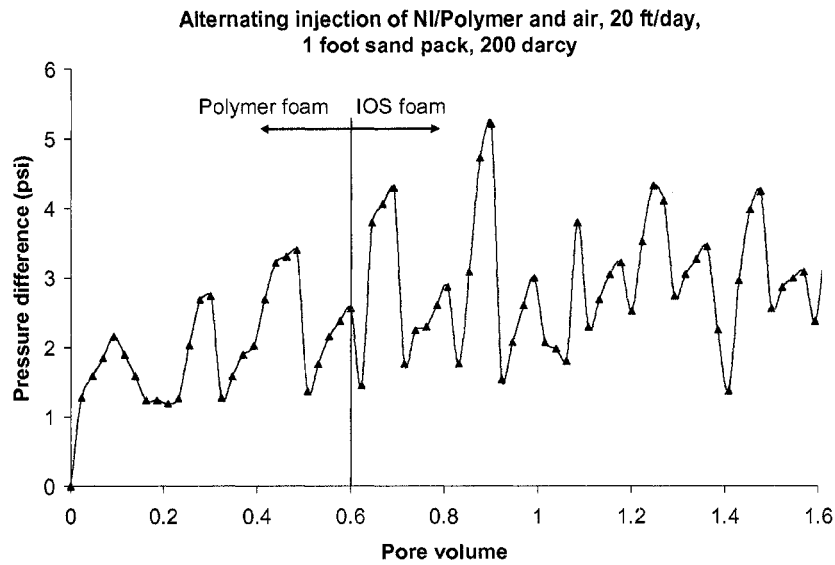


Fig. 6.25 Pressure history for polymer/foam flooding in 200 darcy sand pack

6.4.3 Comparison between the foam flooding in 40 darcy and 200 darcy sand packs

Fig. 6.26 shows the total apparent viscosity during the foam flooding in the 40 darcy and 200 darcy sand packs. The apparent viscosity in 200 darcy sand pack is about 4~5 times the apparent viscosity in 40 darcy sand pack. The schematic description of the different regions during ASPF is shown in Fig. 6.27. The apparent viscosity for IOS foam at 20 ft/day is 81 cp for the 40 darcy region and 284 cp for the 200 darcy region from foam displacing brine experiment. But from the foam displacing residual

crude oil experiment in one dimensional sand pack (Fig. 6.26), the apparent viscosity of the IOS foam wasn't as strong as expected from measurement in IOS foam displacing brine experiment. The reason may be that the N67-7PO in the polymer/surfactant slug and a little crude oil left behind surfactant slug make the IOS foam weaker. From the oil displacement experiment, the apparent viscosity of the IOS foam is close to the apparent viscosity of the NI/polymer foam because the pressure difference didn't change much before and after the polymer foam was displaced out of the sand pack.

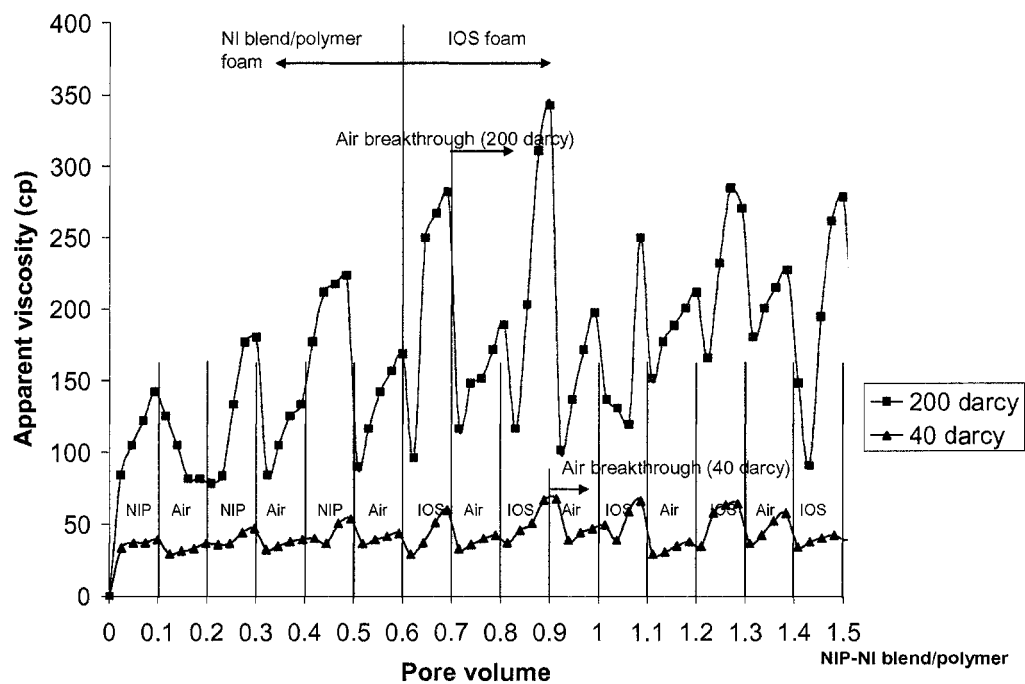


Fig. 6.26 Apparent viscosity during the foam displacing oil for both 40 darcy and 200 darcy sand packs

The relative mobility of the foam is obtained by the pressure difference after the foam has filled the sand pack from equation (6.1).

$$M_{foam} = \left(\frac{k}{u} \frac{\Delta p_{foam}}{L} \right)^{-1} \quad (6.1)$$

Where M_{foam} is the relative mobility of the foam in the sand pack, u is the superficial velocity, k is the permeability of the sand pack, Δp_{foam} is the pressure difference after the foam has filled the sand pack, and L is the length of the sand pack.

The relative mobility of the water zone which has the residual oil saturation is calculated from the pressure difference during water flooding as in equation (6.2). The relative mobility of water with residual oil in 40 darcy region is 0.05 cp^{-1} and 0.025 cp^{-1} in 200 darcy region.

$$M_w = \left(\frac{k}{u} \frac{\Delta p_w}{L} \right)^{-1} \quad (6.2)$$

Where M_w is the relative mobility of the water in the sand pack with water flood residual oil, and Δp_w is the pressure difference at the steady state of the water flooding.

The length of the oil bank is from measurement of the oil bank front and material balance, that is, the oil content in the oil bank should be equal to the residual oil content of the swept and being swept zones as in equation (6.3).

$$L_{ob} = \frac{(L_{foam1} + L_{foam2})S_{ro}}{S_{ob} - S_{ro}} \quad (6.3)$$

$$L = L_w + L_{ob} + L_{foam1} + L_{foam2} \quad (6.4)$$

Where S_{ro} is the water flood residual oil saturation, S_{ob} is the oil saturation in the oil bank, L_w is the length of the water with residual oil region, L_{ob} is the length of the oil bank, L_{foam1} is the length of the NI/polymer foam region and L_{foam2} is the IOS foam region. Because the relative mobility of NI/polymer foam and IOS foam are equal, the length of

the NI/polymer foam region and the length of the IOS foam region can be combined into a foam region as in equation (6.5).

$$L_{foam} = L_{foam1} + L_{foam2} \quad (6.5)$$

The total relative mobility of the sand pack can be obtained from equation (6.6), where Δp is the pressure difference across the sand pack. The relative mobility of oil bank is obtained from equation (6.7). The relative mobility of the oil bank is found to be 0.022 cp⁻¹ in the 40 darcy region and 0.012 cp⁻¹ in the 200 darcy region.

$$M = \left(\frac{k}{u} \frac{\Delta p}{L} \right)^{-1} \quad (6.6)$$

$$\frac{L_{ob}}{M_{ob}} = \frac{L}{M} - \frac{L_w}{M_w} - \frac{L_{foam}}{M_{foam}} \quad (6.7)$$

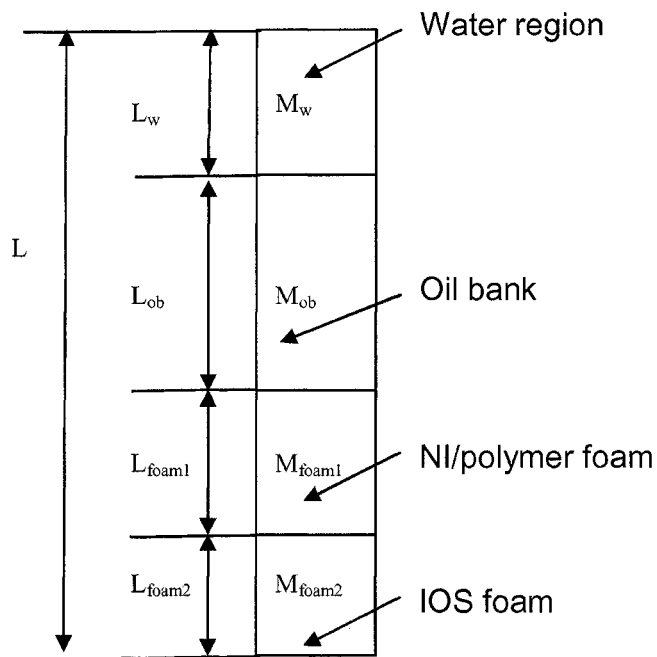


Fig. 6.27 Schematic description of the different regions during the ASPF process in sand pack

From the above discussion, the relative mobilities of water and oil bank in 200 darcy sand pack are about half of those in 40 darcy sand pack and the foam relative mobility in 40 darcy sand pack is $1/5$ of that in 200 darcy sand pack. The reason for the relative mobility difference of water and oil bank in the 40 darcy and 200 darcy sand packs may be the residual oil saturation is different in the two experiments. The relative mobility ratio in 200 sand pack is about 2~3 times lower in 40 darcy sand pack. This may explain why the oil bank breaks through earlier in 200

darcy sand pack. The results for the apparent viscosity and relative mobility in the sand in the two experiments are summarized in Table 6.1.

Permeability	S_{ro}	M_w (cp ⁻¹)	M_{ob} (cp ⁻¹)	M_{foam} (cp ⁻¹)	μ_{foam} (cp)
40 darcy	25%	0.05	0.022	0.023	47
200 darcy	30%	0.025	0.012	0.0047	215

Table 6.1 Summary of the relative mobility and apparent viscosity for the two ASPF experiments in 40 darcy and 200 darcy sand packs respectively

6.5 Calculations for ASPF in heterogeneous system

The main advantage of the foam displacing oil process is in heterogeneous system. Foam has higher apparent viscosity in the high permeability region than in the low permeability region, which may divert the fluid into the low permeability region. Consider a reservoir with 100 feet width, 100 feet thickness and 2000 feet length. The pressure of the reservoir is 1000 psia and its temperature is 80 F like the condition in Yates Field, West Texas. The reservoir has two layers with different permeability – 200 darcy and 40 darcy. The porosity is 35%. The length L

of the reservoir is 2000 feet and the thickness of layer 1 h_1 is 20 feet with 200 darcy permeability and the thickness of layer 2 h_2 is 80 feet with 40 darcy permeability as in Fig. 6.28. The designed process to recover the residual oil in the reservoir is:

1. Alternate injecting NI blend/polymer and air at 20 ft/day in 0.1 PV increment for total 0.6 PV. NI blend includes 0.2% N67-7PO and IOS at 4:1 ratio, 0.5% polymer, 2% NaCl and 1% Na_2CO_3 .
2. Alternate injecting IOS and air in 0.1 PV increment to get IOS foam as drive. IOS solution includes 0.2% IOS at 2% NaCl and 1% Na_2CO_3 .

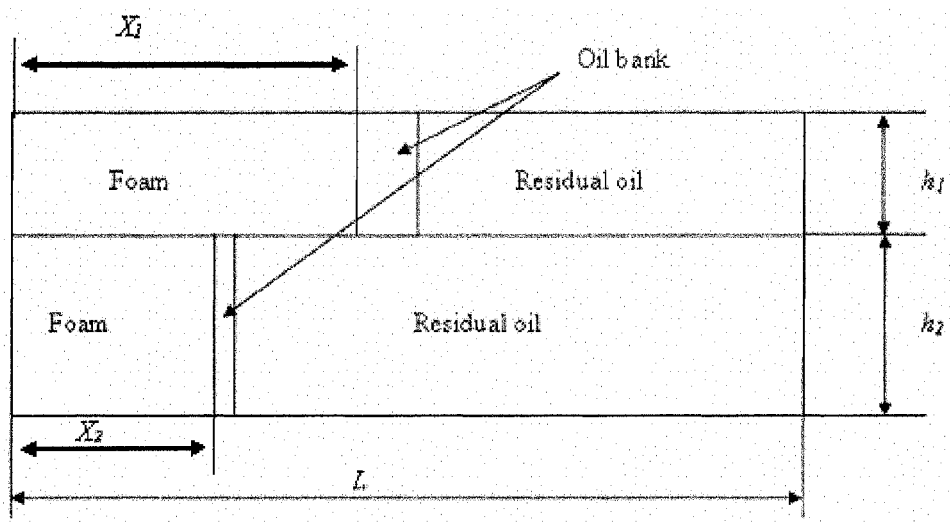


Fig. 6.28 Schematic of a reservoir with 2 layers at different permeability

From the result of experiment in section 6.3, the apparent viscosity of the crude oil is 19 cp. When the residual oil saturation is 25%, the relative mobility of the residual oil region is 0.05 cp⁻¹ and the relative mobility of the oil bank is 0.022 cp⁻¹. The foam apparent viscosity is 215 cp in the 200 darcy layer and 46 cp in the 40 darcy layer.

The calculation can be made with the assumptions:

1. Piston-like displacement;
2. The same pressure difference in each layer;
3. No crossflow;
4. All the oil has been recovered in the region after the oil bank.
5. The foam apparent viscosity of IOS foam is the same as the NI/polymer foam;
6. Foam apparent viscosity is dependent on permeability.

The foam front position can be calculated from Darcy's law.

$$\frac{dx_l}{dt} = -k_l \lambda_{r,l} \frac{\Delta p}{L} \quad l = 1, 2 \quad (6.8)$$

Four regions exist in the sand pack during ASPF flooding as in Fig. 6.29. They are: water flood residual oil, oil bank, NI blend/polymer foam, IOS foam. The relative mobility in each layer can be obtained from Darcy's law in equation (6.8).

$$\overline{\lambda_{rl}} = \left[\frac{x_{foam1l}}{\lambda_{foam1l}} + \frac{x_{foam2l}}{\lambda_{foam2l}} + \frac{x_{obl}}{\lambda_{obl}} + \frac{x_{rol}}{\lambda_{rol}} \right]^{-1} \quad l = 1, 2 \quad (6.9)$$

Where $x_{foam1}, x_{foam2}, x_{ob}, x_{ro}$ are the lengths of IOS foam, NI blend/polymer foam, oil bank and water flood residual oil phases respectively and $\lambda_{foam1}, \lambda_{foam2}, \lambda_{ob}, \lambda_{ro}$ are the relative motilities for these phases.

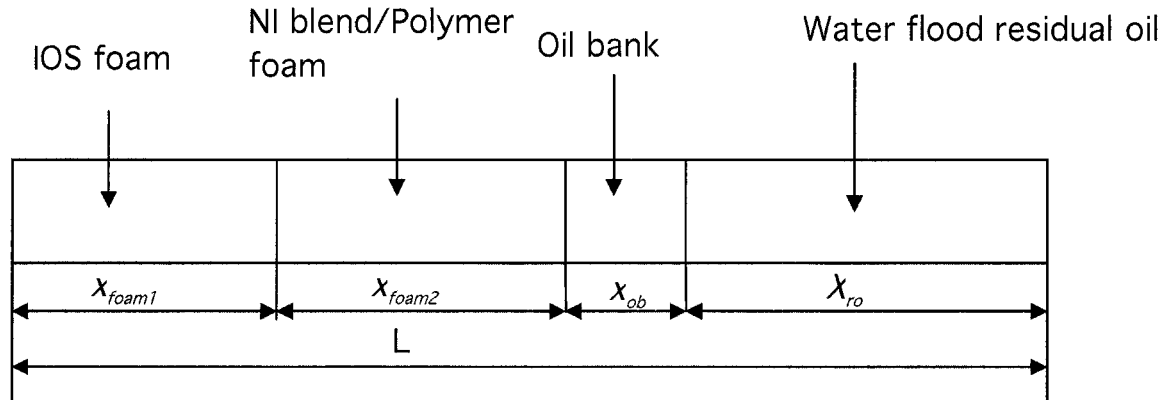


Fig. 6.29 schematic illustration of ASPF flooding

In this particular case, the relative mobility of IOS foam λ_{foam1l} is equal to that of the NI blend/polymer foam λ_{foam2l} . Because all the oil after the oil bank has been recovered, the oil bank length x_{ob} can be related to the length of the length of foam $(x_{foam1l} + x_{foam2l})$ by the material balance.

$$x_{obl} = \frac{(x_{foam1l} + x_{foam2l})S_{rol}}{(S_{obl} - S_{rol})} \quad l = 1, 2 \quad (6.10)$$

where S_{rol} is the water flood residual oil saturation and S_{obl} is the oil saturation in oil bank.

Taking the ratio of the velocities in the two layers will eliminate time and pressure drop since both layers experience the same Δp . Then in two layers with different permeability,

$$\frac{dx_1}{dx_2} = \frac{k_1}{k_2} \frac{\overline{\lambda_{r1}}}{\overline{\lambda_{r2}}} \quad (6.11)$$

where x_1 and x_2 are the dimensionless front positions of foam in high permeability and low permeability layers, k_1 and k_2 are the permeabilities

of the two layers, $\overline{\lambda_{r1}}$ and $\overline{\lambda_{r2}}$ are the relative mobilities in the different layers.

Using numerical methods, we can find the front positions of foam in layer 1 and layer 2 at different pore volumes.

$$x_1(i) = \Delta x \cdot i \quad (6.12)$$

$$x_2(i+1) = x_2(i) + \Delta x \frac{k_2}{k_1} \frac{\overline{\lambda_{r2}}}{\overline{\lambda_{r1}}} \quad (6.13)$$

where Δx is the dimensionless step length in layer 1 which is set to be 0.01 and i is the time indexing. x_1 can be over 1 and it is the hypothetical front of the foam out of the layer 1 to track the volume of fluid injected. When $x_1 > 1$, $\overline{\lambda_{r1}}$ is based on the fluids preset for $x_1 \leq 1$.

The sweep efficiency is obtained as:

$$\text{Sweep efficiency} = \frac{(x_1 h_1 + x_2 h_2)}{h_1 + h_2} \quad \text{when } x_1 < 1 \quad (6.14)$$

$$\text{And Sweep efficiency} = \frac{(h_1 + x_2 h_2)}{h_1 + h_2} \quad \text{when } x_1 \geq 1 \quad (6.15)$$

The result is shown in Fig. 6.30 by the calculation with the above assumptions. It shows that less than 1.06 total pore volume of foam is needed to sweep the heterogeneous system while 1.36 pore volume of polymer is needed to get the same sweep with ASP process. The foam breaks through layer 1 around 0.85 total pore volume and the polymer breaks through around 0.45 total pore volume. The ASP process calculation is similar to that for ASPF process except that the foam regions are replaced by surfactant slug and polymer drive regions, which are both assumed to have an apparent viscosity of 46 cp. The most important difference is that the polymer has the same apparent viscosity in different layers.

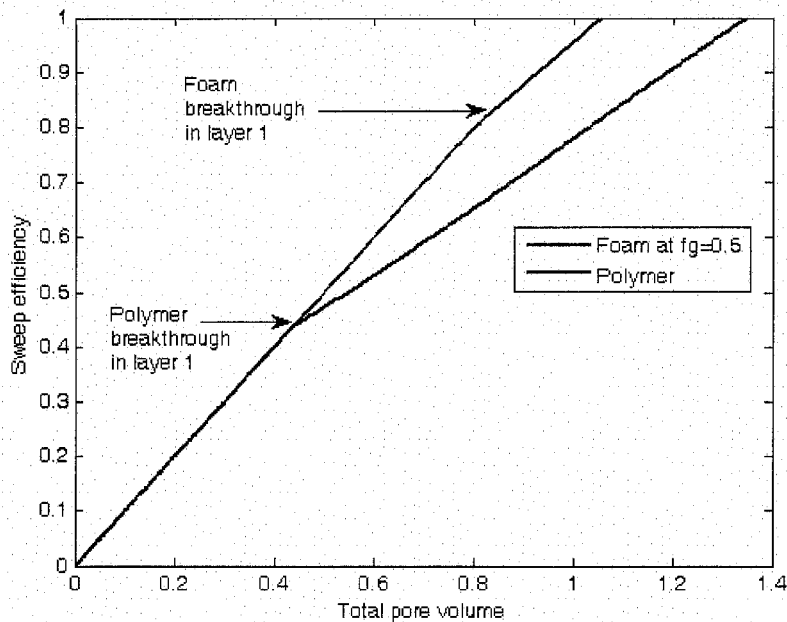


Fig. 6.30 Sweep efficiency of foam or polymer sweep in a heterogeneous system with 5:1 permeability ratio and 1:4 thickness ratio

Because the foam is injected at gas fractional flow of 0.5, 0.53 PV of liquid injection is needed, which includes 0.3 PV polymer-surfactant solution at 0.5% polymer and 0.2% NI blend, and 0.23 PV 0.2% IOS solution. For a conventional ASP process, 1.36 PV of liquid is needed which includes 0.3 PV polymer-surfactant solution at 0.5% polymer and 0.2% NI blend, and 1.23 PV of polymer solution at 0.5% concentration.

In each process, a total 0.3 PV NI blend was injected in the heterogeneous system. By tracking the foam front of the IOS foam in ASPF or the polymer drive front in ASP, there was 0.08 PV of NI blend/polymer solution flowing into layer1 and 0.22 PV into layer 2 in ASPF while there was 0.17 PV of NI blend/polymer solution flowing into the higher permeability layer and 0.13 PV into the lower permeability layer 2 with ASP. The foam diverted more surfactant solution from high permeability layer to low permeability layer. 73% of NI blend solution flows into layer 2 which contains 80% of the residual oil by ASPF process while only 43% of NI blend solution gets into layer 2 by ASP process. The diversion effect by ASPF process is important because enough surfactant must be injected in real reservoir to overcome the loss by the adsorption of surfactant. This example here with permeability ratio 5 is not as severe as may be encountered in other formations, where thief zone (high permeability region) could be an order of magnitude or more greater than mean permeability. Then the ASPF process could be even more beneficial.

Tables 6.1 and Table 6.2 list assumptions and results of calculations illustrating the difference between revenue and chemical expenses for ASPF and ASP processes in this reservoir. The cost of natural gas takes

the largest part in the whole cost of ASPF and the chemical cost is less than 10% of oil price. The price of natural gas is the current market price. If the process is applied in a reservoir where natural gas co-exists with crude oil, the cost can be greatly decreased. In other words, the profit for the ASPF process can be higher than indicated. Although it seems that the revenue minus expenses per bbl by ASPF or ASP process is only about 16% saving, the advantage of ASPF is that more surfactant solution is diverted into the low permeability layer to get the residual oil there because in ASP process a larger surfactant slug is needed process to overcome adsorption losses or accept lower recovery in lower permeability layers. ASPF process should be more attractive for a reservoir where there is no nearby pipeline to transport produced gas but there is a way to transport oil produced by EOR.

	Natural gas	N67-7PO	IOS	Polymer	Crude oil
Unit price	\$7.28 /MCF	\$3.00 /pound	\$1.00 /pound	\$1.00 /pound	\$35.00 /bbl
Amount	234,130 MCF	211,860 pounds	92,806 pounds	662,080 pounds	1,251,600 bbl
Revenue or expense	\$1,704,500	\$635,580	\$92,806	\$662,080	\$43,805,000
Revenue minus expense	\$40,710,034	Revenue minus expense per bbl crude oil	\$32.53/bbl	Expense per bbl crude oil	\$2.47/bbl

Table 6.1 Revenue and expense calculation for ASPF process

	N67-7PO	IOS	Polymer		Crude oil
Unit price	\$3.00 /pound	\$1.00 /pound	\$1.00 /pound		\$35.00 /bbl
Amount	211,860 pounds	42,372 pounds	2,983,300 pounds		1,251,600 bbl
Revenue or expense	\$635,580	\$42,372	\$2,983,300		\$43,805,000
Revenue minus expense	\$40,143,748	Revenue minus expense per bbl crude oil	\$32.07/bbl	Expense per bbl crude oil	\$2.93/bbl

Table 6.2 Revenue and expense calculation for ASP process

CONCLUSIONS AND RECOMMENDATIONS

7.1 Conclusions

In this thesis, we studied foam flow in homogeneous fractures and found the mechanisms that can affect foam apparent viscosity in fractures. The foam diversion effect in heterogeneous fractures can be explained and predicted from the mechanisms. Foam application in reservoirs without fractures was also investigated and foam was found to be promising to work in alkaline/surfactant processes to replace polymer as mobility control agent.

7.1.1 Foam flow in homogeneous fracture

For foam as individual bubbles, which have a diameter larger than the fracture aperture, the apparent viscosity is the sum of two contributions: that resulting from liquid between bubbles and that resulting from the resistance to deforming the interface when a bubble passes through a fracture. The surface tension gradient contribution does not appear to be significant in our experiments.

At conditions of sufficiently low Reynolds numbers and bubble sizes where no coalescence occurs in homogeneous fracture, for the foam flow through a smooth, uniform fracture, the foam texture (a measure of the bubble volume) is a key parameter in determining n_L , the number of lamellae per unit length, which is the main factor affecting the foam viscosity in smooth uniform fractures when the (undeformed) bubble diameter exceeds fracture aperture. Changes which increase n_L , e.g., higher gas fractional flow f_g and larger ratios of aperture thickness to bubble size, cause apparent viscosity to increase. The aperture thickness effect is the basis for producing a more uniform sweep by the use of foam.

For bulk foam at low to medium gas fractional flow, Pal's equation can well predict the apparent viscosity of bulk foam in fractures, i.e., when bubble diameter is somewhat less than fracture aperture. From Pal's equation, gas fractional flow f_g is the main factor to affect the apparent viscosity for bulk foam.

7.1.2 Foam diversion in heterogeneous fractures

We investigated different factors' effects on sweep efficiency by foam in smooth heterogeneous fractures and applied our theory to this situation assuming the same f_g in each portion of the fracture and minimal crossflow. Foam apparent viscosity in each portion of a heterogeneous fracture can be calculated using the theoretical result for a homogeneous fracture.

Foam can greatly improve the sweep efficiency in a heterogeneous fracture system if bubble size is the same in all fractures. The amount of surfactant solution required is reduced substantially both by foam's ability to divert flow into smaller fractures and by the need for less liquid to fill a given volume of fractures. Gas fractional flow, aperture ratio and bubble size can greatly affect the sweep efficiency.

Agreement of theoretical predictions and experimental results was shown in previous chapters and confirms validity of the theory's assumptions of equal f_g , minimal crossflow and constant bubble size.

Dykstra-Parson's model was applied in predicting the sweep efficiency by foam in heterogeneous fracture system with log-normal distributed apertures. The sweep efficiency was found to be greatly affected by the apparent viscosity ratio in different layers. If the foam apparent viscosity in the thicker layer is larger than that in the thinner layer, foam can improve the sweep efficiency. But if the foam apparent viscosity is lower in the larger aperture layer, e.g., when the bubble size is at a fixed ratio to aperture in each layer or in many cases when bulk foam exists in the large aperture layers, contrary diversion may happen and the sweep efficiency is decreased.

7.1.3 Surfactant evaluation

Two different surfactant blends were evaluated and NI blend was found to be the better candidate in alkaline/surfactant EOR processes because it can get ultra-low interfacial tension at its optimal salinity which is closer to the formation salinity than TC blend. But from the foaming ability test, NI blend is much weaker than TC blend. From our investigation, it was found that IOS by itself is a strong foamer while N67-7PO is a weak foamer. The reason may be that N67-7PO is quite hydrophobic, especially at optimal salinity. From the test of foam stability with the presence of

residual oil, NI blend can get almost the same strength with or without residual oil while IOS foam is slightly weaker with residual oil than without residual oil. But that doesn't mean the foam by NI blend is more stable with the presence of residual oil. The reason is that NI blend can displace almost all the residual oil during the experiment. And IOS can get much stronger foam than NI blend even with the presence of residual oil. To try to simplify the alkaline surfactant EOR process, from our surfactant evaluation, NI blend is a good choice for displacing oil with optimal salinity close to formation brine salinity and IOS is a good candidate as foamer.

7.1.4 Foam in alkaline/surfactant/ polymer/foam EOR process

In the conventional alkaline/surfactant/polymer (ASP) EOR process, polymer was used as mobility control agent both in the displacement phase together with alkaline and surfactant and in the subsequent drive phase. To save the consumption of expensive polymer, we tried to use foam to replace polymer as mobility control agent in the drive phase. We got a successful experiment by using alkaline-surfactant-polymer-foam to displace residual crude oil in a one-dimensional sand pack. That demonstrates the potential of using foam in ASP EOR process to save the amount of polymer.

The biggest advantage of foam as mobility control agent over polymer is that foam can have higher apparent viscosity in the higher permeability regions and divert the alkaline/surfactant solution from high to low permeability regions. This feature is especially beneficial to heterogeneous reservoirs where foam can sweep a larger portion of the reservoir with less surfactant. Because NI blend itself is a good surfactant blend for displacing oil but not a good foamer, N67-7PO is used together with polymer to get low enough mobility ratio. It was found that the foam with NI blend and polymer in 200 darcy sand pack is 4~5 times stronger than in 40 darcy sand pack. Moreover, the ASPF process can recover almost all the residual oil in less than 1.0 PV of injected liquid in either 40 darcy or 200 darcy sand pack, which shows the possibility of using foam as mobility control agent in the heterogeneous reservoir to recover residual crude oil.

7.2 Recommendations for future work

7.2.1 Foam flow in fractures

From previous description, it is found in our surfactant system that the foam apparent viscosity in fractures results from two contributions – liquid between bubbles and bubble deformation. But from Hirasaki and

Lawson [1985], the foam apparent viscosity in capillary tubes is from three contributions – liquid slugs, bubble deformation and surface tension gradient. The reason that we didn't observe the surface tension gradient in fractures may be that in our surfactant system the surfactant concentration is much above the CMC and the salinity is higher than in the surfactant system used in capillary tube experiments, which may cause the surfactant to be adsorbed and desorbed more rapidly. To investigate if the contribution from surface tension gradient can appear in fractures, new surfactant system with zero salinity should be tested in fractures.

Both in our work in fractures and the work by Hirasaki and Lawson [1985], there is a common assumption that the fractures or capillary tubes are smooth. But when the foam is used in reservoir, the fractures may have different roughness. When the roughness is large enough, the foam bubbles may deform or even break into smaller bubbles which may increase the apparent viscosity of foam. This should be investigated to find the relationship of the roughness of the fractures to the apparent viscosity of foam.

7.2.2 Surfactant

In the foam aided alkaline surfactant EOR process, the surfactant has two functions – to get ultra-low interfacial tension and to stabilize foam. We tested two different surfactant blends in our research – TC blend and NI blend. TC blend can generate strong foam but it will get phase separation at low salinity. NI blend can well displace oil but N67-7PO in NI blend makes the foam bubbles unstable. Although we can use NI blend to displace oil and then use IOS to generate foam as drive, the change of surfactants will make the process more complicated. If a surfactant or surfactant blend can be found that can both displace oil well at the suitable salinity and generate strong foam, the process will be greatly improved and then foam can be more widely used in EOR process.

7.2.3 ASPF process

The alkaline-surfactant-polymer-foam process works well in 40 darcy and 200 darcy sand packs. It is recommended to develop the process in lower permeability matrix, especially in reservoir cores. And the experiments by ASPF process in two dimensional heterogeneous sand pack are recommended to study the diversion effect by foam in heterogeneous

system and find the foam apparent viscosity change from one-dimensional to two-dimensional system in ASPF.

REFERENCES

A.H. Falls, G.J. Hirasaki, T.W. Patzek, D.A. Gauglitz, D.D. Miller, and T. Ratulowski, "Development of a Mechanistic Foam Simulator: The Population Balance and Generation by Snap-Off", *SPERE* 3, 884 (1998)

A.H. Falls, J.J. Musters, and J. Ratulowski, "The Apparent Viscosity of Foams in Homogeneous Bead Packs", *SPE Reservoir Engineering*, May 1989, 155-164

A.R. Kavscek and C.J. Radke, Fundamentals of Foam Transport in Porous Media, in: L.L. Schramm (Ed.), *Foams: Fundamentals and Applications in the Petroleum Industry*, American Chemical Society, Washington D.C., 1994, pp. 115-164.

A.R. Kavscek, and C.J. Radke, "Pressure-driven Capillary Snap-off of Gas Bubbles at Low Wetting-liquid Content", *Colloids and Surfaces A: Physicochem. Eng. Aspects* 212 (2003) 99-108

A.R. Kavscek, and C.J. Radke, "A Comprehensive Description of Transient Foam Flow in Porous Media", Prepared for D.O.E./NIPER Symposium on Field Application of Foams for Oil Production, 1993

A.R. Kavscek, and C.J. Radke, "Gas Bubble Snap-Off under Pressure-Driven flow in Constricted Noncircular Capillaries", *Colloids and Surfaces, A: Physicochemical and Engineering Aspects* 117 (1996) 55-76

A.R. Kavscek, and H.J. Bertin, "Estimation of Foam Mobility in Heterogeneous Porous Media", Submitted to 2002 SPE/DOE Improved Oil Recovery Symposium, 2002

A.R. Kavscek, D.C. Tretheway, P. Persoff and C.J. Radke, Foam Flow through a Transparent Rough-Walled Rock Fracture, Journal of Petroleum Science and Engineering, 13 (1995), 75-86.

C. Wang, B. Wang, X. Cao, and H. Li, "Application and Design of Alkaline-Surfactant-Polymer System to Close Well Spacing Pilot Gudong Oilfield", SPE 38231, 1997

C.J. Radke, and T.C. Ransohoff, "Mechanisms of Foam Generation in Glass Bead Packs", SPE 15441, prepared for presentation at the 61st ATCE at New Orleans, LA (October 5-8, 1986)

C.K. Mamun, J.G. Rong, S.I. Kam, H.M. Lijestrland, and W.R. Rossen, "Extending Foam Technology from Improved Oil Recovery to Enviromental Remediation", SPE 77557, prepared for presentation at the SPE ATCE at San Antonio, TX (29 September-2 October 2002)

C.R. Wilson, An Investigation of Laminar Flow in Fractured Porous Rocks, Ph.D. Thesis, University of California, Berkeley, 1970.

D. Exerowa, and P.M. Kruglyakov, "Foam and Foam Films, Theory, Experiment, Application", Elsevier, 1998

D. Weaire, and S. Hutzler, "The Physics of Foams", Oxford University Press, 1999

D. Tanzil, G.J. Hirasaki, and C.A. Miller, "Mobility of Foam in Heterogeneous Media: Flow Parallel and Perpendicular to Stratification", SPE 78601, presented at the 2000 SPE ATCE at Dallas (1-4 October, 2000)

D. Tanzil,, "Foam Generation and Propagation in Heterogeneous Porous Media", Thesis for Ph.D., 2001

D. Wang, Z. Zhang, C. Cheng, J. Yang, S. Gao, and L. Li, "Pilot Tests of Alkaline/Surfactant/Polymer Flooding in Daqing Oil Field", SPE Reservoir Engineering, Nov 1997

E.S. Basheva, S. Stoyanov, N.D. Denkov, K. Kasuga, N. Satoh, and K. Tsujii, "Foam Boosting by Amphiphilic Molecules in the Presence of Silicone Oil", Langmuir 2001, 17, 969-979

E.S. Basheva, S. Stoyanov, N.D. Denkov, K. Kasuga, N. Satoh, and K. Tsujii,, "Role of Bertaine as Foam Booster in the Presence of Silicone Oil Drops", Langmuir 2000, 16, 1000-1013

F.M. Llave, F.T.-H. Chung, R.W. Louvier, and D.A. Hudgins, Foams as Mobility Control Agents for Oil Recovery by Gas Displacement, Society of Petroleum Engineers/Department of Engineering, 20245, Prepared for Presentation at the SPE/DOE Seventh Symposium on EOR at Tulsa, OK (April 22-25, 1990).

F.M. Llave, F.T-H. Chung, R.W. Louvier, and Hudgins D.A., "Foams as Mobility Control Agents for Oil Recovery by Gas Displacement", SPE/DOE 20245, prepared for presentation at the SPE/DOE Seventh Symposium on EOR at Tulsa, OK (April 22-25, 1990)

F.P. Bretherton, The Motion of Long Bubbles in Tubes, *Journal of Fluid Mechanics*, 10 (1961), 166-188.

G. Singh, G.J. Hirasaki, and C.A. Miller, "Dynamics of Foam Films in Constricted Pores", *AIChE Journal*, Dec 1997, Vol. 43, No. 12, 3241-3252

G.G. Bernard, and L.W. Holm, "Effect of Foam on Permeability of Porous Media to Gas", *SPE Journal*, September 1964, 267-274

G.J. Hirasaki and J.B. Lawson, Mechanisms of Foam Flow in Porous Media: Apparent Viscosity in Smooth Capillaries, *Society of Petroleum Engineers Journal*, 25 (2), 1985, 176-190.

G.J. Hirasaki, D.L. Zhang, Surface Chemistry of Oil Recovery From Fractured, Oil-Wet, Carbonate Formations, *Society of Petroleum Engineers Journal*, 9(2), 2004, 151-162.

G.J. Hirasaki, R.E. Jackson, M. Jin, J.B. Lawson, J. Londergan, H. Meinardus, C.A. Miller, G.A. Pope, R. Szafranski, and D. Tanzil, Field Demonstration of the Surfactant/Foam Process for Remediation of a Heterogeneous Aquifer Contaminated with DNAPL, in: S. Fiorenza, C. A. Miller, C. L. Oubre, and C. H. Ward (Eds.), *NAPL Removal: Surfactants, Foams, and Microemulsions*, Lewis Publishers, 2000.

H. Yaghoobi, J.S. Tsau, and J.P. Heller, Improving CO₂ Floods in Heterogeneous Media, *Society of Petroleum Engineers*, 35403, Prepared for SPE/DOE Improved Oil Recovery Symposium at Tulsa, OK (April 21-24, 1996).

H.J. Bertin, "Foam Diversion Modeling Using a Bubble-Population Correlation", SPE 59366, presented at the 2000 SPE/DOE Improved Oil Recovery Symposium at Tulsa, OK (3-5 April 2000)

H.J. Bertin, O.G. Apaydin, L.M. Castanier, and A.R. Kavscek, "Foam Flow in Heterogeneous Porous Media: Effect of Crossflow", SPE 39678, prepared for presentation at the 1998 SPE/DOE Improved Oil Recovery Symposium at Tulsa, OK (19-22 April 1998)

H.J. Bertin, O.G. Apaydin, L.M. Castanier, and A.R. Kavscek, Foam Flow in Heterogeneous Porous Media: Effect of Cross Flow, Society of Petroleum Engineers Journal, 4 (2), 1999, 75-82.

H.M. Princen, Rheology of Foams and Highly Concentrated Emulsions, I. Elastic Properties and Yield Stress of a Cylindrical Model System, Journal of Colloid Interface Science (1983) 91, No. 1 160-175.

H-L Chen, M-J. Ke, T-K Chuang, and R.W. Flumerfelt, "Experimental Studies of Capillary Pressure Effects of Foams in Porous Media", SPE 20069, prepared for presentation at the 60th California Regional Meeting at Ventura, CA (April 4-6, 1990)

I.M. Krieger, Rheology of Monodisperse Latices, Advances in Colloid and interface Science, 1972, 3, 111-136.

J. E. Hanssen, , "Foam as a Gas-blocking Agent in Petroleum Reservoirs I: Empirical Observations and Parametric Study", Journal of Petroleum Science and Engineering, 10 (1993) 117-133

J.B. Lawson, and G.J. Hirasaki, "Foam for Control of Injection Profiles", Report prepared for the 1984 Reservoir Engineering/Research conference, 1984

J.B. Lawson, J. Reisberg, Alternate Slugs of Gas and Dilute Surfactant for Mobility Control during Chemical Flooding, Society of Petroleum Engineers, 8839, Presented at SPE/DOE Enhanced Oil Recovery Symposium, Tulsa, OK (Apr 20-23, 1980).

J.E. Gale, Comparison of coupled fracture deformation and fluid models with direct measurements of fracture pore structure and stress-flow properties. In: I.W. Farmer, J.J.K. Daemen, C.S. Desai, C.E. Glass and S.P. Neuman, (Eds.), Rock Mechanics: Proceedings of the 28th US Symposium. Tucson, Arizona. Rotterdam, Balkema, Rotterdam (1987), 1213-1222.

J.E. Hassen, L.M. Surguchev, and I. Svorstol, "SAG Injection in a North Sea Stratified Reservoir: Flow Experiment and Simulation", SPE 28847, presented at the European Petroleum Conference at London, UK (25-27 October 1994)

J.F. Casteel and N.F. Djabbarah, Sweep Improvement in CO₂ Flooding by Use of Foaming Agents, Society of Petroleum Engineers Reservoir Engineering, Nov 1988, 1186-1192.

J.P. Heller, and M.S. Kuntamukkula, "Critical Review of the Foam Rheology Literature", Ind. Eng. Chem. Res. 1987, 26, 318-325

K.R. Kibodeaux, S.C. Zeilinger, and W.R. Rossen, "Sensitivity Study of Foam Diversion Processes for Matrix Acidization", SPE 28550, presented at the 69th SPE ATCE at New Orleans, LA (September 26-28, 1994)

L. Cheng, A. B. Reme, D. Shan, D. A. Coombe, and W. R. Rossen,, Simulating Foam Processes at High and Low Foam Qualities, Society of Petroleum Engineers, 59287, Presented at the SPE/DOE Improved Oil Recovery Symposium at Tulsa, OK (Apr 3-5, 2000).

L. Cheng, A. B. Reme, D. Shan, D.A. Coombe, and W.R. Rossen, "Simulating Foam processes at High and Low Foam Qualities", SPE 59287, prepared for presentation at the 2000 SPE/DOE Improved Oil Recovery Symposium held in Tulsa, OH (3-5 April 2000)

L.L. Schramm, "Foams, Fundamentals and Applications in the Petroleum Industry", American Chemical Society, 1994.

L.W. Lake, Enhanced Oil Recovery, Prentice Hall, New Jersey, 1989, 201-205.

M. Dalland, and J. E. Hanssen, "Enhanced Foams for Efficient Gas Influx Control", SPE 37217, presented at the 1997 SPE International Symposium at Houston, TX

M. Palar, R.J. Jasinski, and J.A. Robert , "A Experimental Study of Foam Flow through Berea Sandstone with Applications to Foam Diversion in Matrix Acidizing", SPE 29678, prepared for presentation at the Western Regional Meeting at Bakersfield, CA (8-10 march 1995)

M. Zerhboub, K. Ben-Naceur, E. Touboul and R. Thomas, Matrix Acidizing: A Novel Approach to Foam Diversion, Society of Petroleum Engineers Production & Facilities, 9(2), 1994, 121-126.

M.J. Mooney, The Viscosity of a Concentrated Suspension of Spherical Particles, Journal of Colloid Science, 1951, 6, 162-170.

P.A. Gauglitz, F. Friedmann, S.I. Kam, and W.R. Rossen, "Foam Generation in Porous Media", SPE 75177, prepared for presentation at the SPE/DOE thirteenth Symposium on EOR at Tulsa, OK (13-17 April 2002)

P.R. Garret, "Defoaming, Theory and Industrial Applications", Marcel Dekker Inc., 1993

Q.P. Nguyen, P.K. Currie, and P.K.J. Zitha, , "Effect of Capillary Cross-Flow on Foam-Induced Diversion in Layered Formations", SPE 82270, presented at the SPE European Formation Damage conference at Hague, Netherlands (13-14 May, 2003)

Q.P. Nguyen, P.K. Currie, and P.K.J. Zitha, Effect of Capillary Cross-Flow on Foam-Induced Diversion in Layered Formations, Society of Petroleum Engineers, 82270, Presented at the SPE European Formation Damage Conference at Hague, Netherlands (May 13-14, 2003).

R. Gillette, "Characterizing the Viscosity of Foam Used in a Semiconductor Wafer Cleaning System", Summer 2001 Intern Report

R. Pal, Rheology of Polymer-thickened Emulsions, Journal of Rheology, 36(7), 1992

R.A. Nelson, "Geologic Analysis of Naturally Fractured Reservoirs", Gulf Professional Publishing, 2001

R.A. Nelson, Geologic Analysis of Naturally Fractured Reservoirs, second ed., Gulf Professional Publishing, 2001.

R.J. Akers, , "Foams", Academic Press, 1975

R.K. Prud'homme, and S.A. Khan, "Foams, Theory, Measurements, and Applications", Marcel Dekker Inc., 1995

R.L. Detwiler, H. Rajaram, and R.J. Glass, "Nonaqueous-Phase-Liquid Solution in Variable-Aperture fractures: Development of a Depth-Averaged Computational Model with Comparison to a Physical Experiment", Water Resources Research, Vol. 37, No. 12, Pages 3115-3129, December 2001

R.O. Baker, A. Telesford, S. Wong, V. Li, G. Smith, and H. Schoendorfer, An Integrated Fracture Characterization of a Heavy Oil Naturally Fractured carbonate Reservoir, paper no. 2001-13, Prepared for Presentation at the Petroleum Society's Canadian International Petroleum Conference held in Calgary, AB, Canada (June 12-14, 2001).

S. Jayanti, L.N. Britton, V. Dwarakanath, G.A. Pope, "Laboratory Evaluation of Custom Designed Surfactants to Remediate NAPL Source Zones", Paper, 2002

S. Siddiqui, S. Talabani, S.T. Saleh, and M.R. Islam, A Laboratory investigation of Foam Flow in Low Permeability Berea Sandstone Cores, Society of Petroleum Engineers, 37416, Prepared for Presentation at the 1997 SPE Production Operations Symposium at Oklahoma City, OK (March 9-11, 1997).

S.I. Kam, and W.R. Rossen, , "A Model for Foam Generation in Homogeneous Media", SPE77698, presented at the SPE ATCE at San Antonio, TX (29 September - 2 October 2002)

T. Baker, H.K. Celius , T. Lie, H.A. Martinsen , L. Rasmussen, and F. Vassenden, "Foam for Gas Mobility Control in the Snorre Field: the FAWAG Project", SPE 56478, presnted at the 1999 SPE ATCE at Houston, TX (3-6 October 1999)

T.J. Myers, and C.J. Radke, "Transient Foam Displacement in the Presence of Residual Oil: Experiment and Simulation Using a Population-Balance Model", Ind. Eng. Chem. Res. 2000, 39, 2725-2741

Tanzil, D., Hirasaki, G.J. and Miller, C.A., "Conditions for Foam Generation in Homogeneous Porous Media", SPE 75176, presented at SPE/DOE Thirteenth Symposium on EOR at Tulsa, OK (13-17 April 2002)

W.R. Rossen and M.W. Wang., Modeling Foams for acid Diversion, Society of Petroleum Engineers, 24179, Society of Petroleum Engineers Journal, 6(4), 1999, 92-100.

W.R. Rossen, "Snap-off in Constricted Tubes and Porous Media", Collids and Surfaces, A: Physicochemical and Engineering Aspects 166 (2000) 101-107

W.T., Osterloh and M. J. Jante Jr., Effects of Gas and Liquid Velocity on Steady State Foam Flow at High Temperature, Society of Petroleum Engineers, 24179, Prepared for Presentation at the 1992 SPE/DOE Symposium on Enhanced Oil Recovery at Tulsa, OK (April 22-25, 1992).

Wang Demin, Cheng Jiecheng, Yang Zhenyu, Li Qun, Wu Wenxiang, Yu Huiyu, Successful Field Test of the First Ultra-Low Interfacial Tension Foam flood, Society of Petroleum Engineers, 72147, Presented at the SPE Asia Pacific Improved Oil Recovery Conference, Kuala Lumpur, Malaysia (Oct 8-9, 2001)

Z.I. Khatib, G.J. Hirasaki, and A.H. Falls, , "Effects of Capillary Pressure on Coalescence and Phase Mobilities in Foams Flowing through Porous Media", SPE 15442, presented at the 51st ATCE of SPE at New Orleans, LA (Oct 5-8, 1986)

APPENDICES

APPENDIX A. DERIVATION FOR THE EQUIVALENT LAMELLAE PER UNIT LENGTH n_L

Assuming that bubbles are distributed uniformly, the total number of bubbles N_{bubble} in a rectangular area having length L and width W is:

$$N_{bubble} = (n_L L) \times (n_L W) = LW n_L^2 \quad (A.1)$$

Then the total volume occupied by gas is:

$$v_{gas} = N_{bubble} \left(\frac{4}{3} \right) \pi r_B^3 = \left(\frac{4}{3} \right) \pi r_B^3 LW n_L^2 \quad (A.2)$$

However, the total volume occupied by gas is also given by:

$$v_{gas} = LW b f_g \quad (A.3)$$

where b is the fracture thickness.

Combine the above two equations to obtain the number of equivalent lamellae per unit length:

$$n_L = \left[3f_g b / (4\pi r_B^3) \right]^{1/2} \quad (\text{A.4})$$

APPENDIX B. CALCULATION FOR THE SWEEP EFFICIENCY IN 2 LAYER HETEROGENEOUS FRACTURES

Based on the assumptions listed at the beginning of section 2.3, the calculation for the sweep efficiency in 2 layer heterogeneous fractures was derived as below.

The foam front position in each region may be determined from Darcy's law

$$dx_l / dt = v_l = -k_l \lambda_{rel} \Delta p / L, \quad l=1, 2 \quad (B.1)$$

where v_l is the velocity in region l , and λ_{rel} is the relative mobility in region l defined by

$$\lambda_{rel} = [x_l / \lambda_{app,l} + (1 - x_l) / \lambda^0]^{-1} = [\mu_{app,l} x_l + \mu^0 (1 - x_l)]^{-1} \quad \text{for } x_l < 1 \quad (B.2)$$

$$\text{or } \lambda_{rel} = \lambda_{app,l} = \mu_{app,l}^{-1} \quad \text{for } x_l > 1$$

where $\lambda_{app,l}$ is the relative mobility of foam, λ^0 is the relative mobility of water, $\mu_{app,l}$ is the apparent viscosity of foam in region l and μ^0 is the water viscosity .

Taking the ratio of the velocities in the two regions will eliminate time and the pressure drop since both regions experience the same Δp . Thus before breakthrough ($x_l < 1$), we have

$$dx_1 / dx_2 = (k_1 / k_2)(\mu_{app,2} / \mu_{app,1})[x_2 + (1 - x_2)M_2] / [x_1 + (1 - x_1)M_1] \quad (B.3)$$

where M_1, M_2 are the mobility ratios, e.g. $M_l = \lambda_{app,l} / \lambda^0 = \mu^0 / \mu_{app,l}$, k_1, k_2 are the permeabilities, $k_l = b_l^2 / 12$ in fractures where b_l is the aperture. Moreover,

$$\int_0^{x_1} k_2 \mu_{app,1} [x_1 + (1 - x_1)M_1] dx_1 = \int_0^{x_2} k_1 \mu_{app,2} [x_2 + (1 - x_2)M_2] dx_2 \quad (B.4)$$

$$(1 - M_1)x_1^2 / 2 + M_1x_1 = (k_1 \mu_{app,2}) / (k_2 \mu_{app,1}) [(1 - M_2)x_2^2 / 2 + M_2x_2] \quad (B.5)$$

When the foam front reaches the outlet of the thicker region ($x_1 = 1.0$), the dimensionless front position at the thinner region is

$$x_2 = \{ [M_2^2 + (1 - M_2)(1 + M_1)(k_2 \mu_{app,1}) / (k_1 \mu_{app,2})]^{1/2} - M_2 \} / (1 - M_2) \quad (B.6)$$

Then the dimensionless time in the injected liquid pore volume needed for the sweep of thicker region is

$$\text{Dimensionless time} = (x_2 b_2 + b_1)(1 - f_g) / (b_1 + b_2) \quad (B.7)$$

As the thinner region continues to be swept, the hypothetical dimensionless front position z_1 in the thicker region (outside the fracture) can be obtained from

$$dz_1 / dx_2 = (k_1 / k_2)(\mu_{app,2} / \mu_{app,1})[x_2 + (1 - x_2)M_2] \quad (B.8)$$

That is, the product $(z_1 - 1)lbw$ is the volume of foam produced from fracture 1 after foam breakthrough.

$$\int_1^{z_1} dz_1 = \int_{x_2^0}^{x_2} (k_1 / k_2)(\mu_{app,2} / \mu_{app,1})[x_2 + (1 - x_2)M_2] dx_2 \quad (B.9)$$

$$z_1 = 1 + (k_1 / k_2)(\mu_{app,2} / \mu_{app,1})[(1 - M_2)(x_2^2 - (x_2^0)^2) / 2 + M_2(x_2 - x_2^0)] \quad (B.10)$$

Setting $x_2 = 1.0$, and

$x_2^0 = \{[M_2^2 + (1 - M_2)(1 + M_1)(k_2 \mu_{app,1}) / (k_1 \mu_{app,2})]^{1/2} - M_2\} / (1 - M_2)$, one finds

$$z_1 = 1 + k_1 \mu_{app,2} / (k_2 \mu_{app,1})[(1 + M_2) / 2 - (1 + M_1)k_2 \mu_{app,1} / (2k_1 \mu_{app,2})] \quad (B.11)$$

And the dimensionless time or the injected liquid pore volume needed to sweep the thinner region is

$$\text{Dimensionless time} = (z_1 b_1 + b_2)(1 - f_g) / (b_2 + b_1) \quad (B.12)$$

APPENDIX C. CALCULATION FOR THE EXAMPLES IN DYKSTRA-PARSONS' PAPER

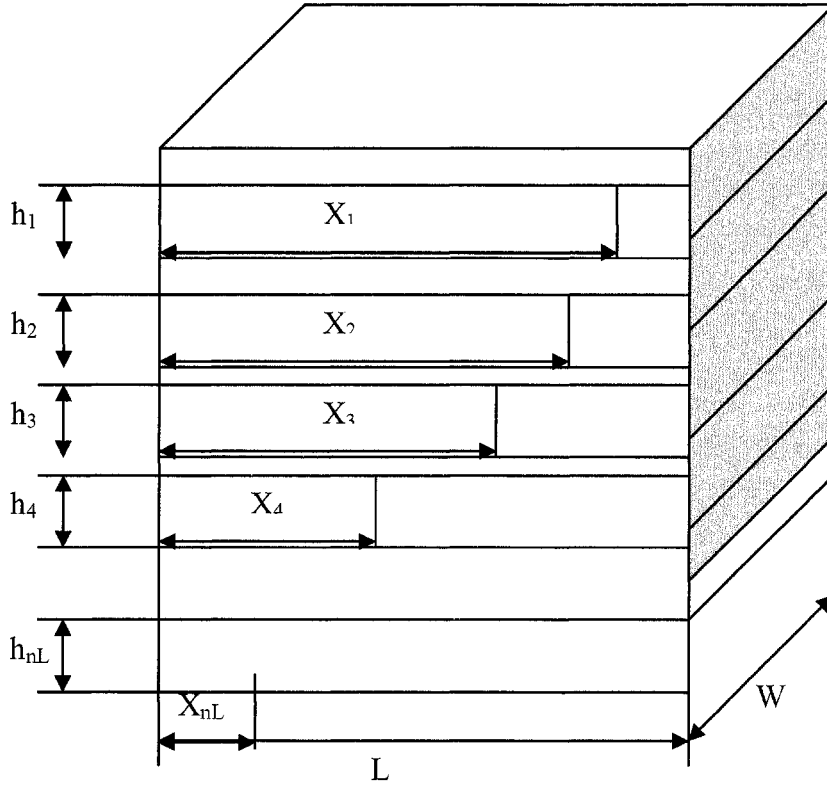


Figure C1. Schematic illustration of heterogeneous reservoirs

As in figure C1, h_i is the layer thickness, W is the width of each layer and L is the length of these layers. Here we assume each layer has the same length and width while the thickness is different. x is the front of the displacing fluid. The other assumptions are:

1. No crossflow.

2. Pressure difference across each layer in the direction of flow is the same.

The number of break-through layer at some water oil ratio WOR was obtained by

$$WOR = \frac{\sum_{i=1}^n Q_i}{\sum_{i=n+1}^{n_L} Q_i} \quad (C.1)$$

Where n_L is the total number of layers and n is the number of layers water breaks through. Q_i is the flow rate in layer i .

$$Q_i = -\frac{k_i}{\mu_i} \frac{\Delta p}{L} h_i w \quad (C.2)$$

$$\mu_i = x_i \mu_{1i} + (1 - x_i) \mu_{2i} \quad (C.3)$$

where x is the dimensionless front position between the displacing and displaced fluid.

For the pressure difference over the entire length of the layer $\frac{\Delta p}{L}$ is the same for each layer, the equation to get WOR can be obtained.

$$WOR = \frac{\sum_{i=1}^n \frac{k_i h_i}{\mu_{1i}}}{\sum_{i=n+1}^{n_f} \frac{k_i h_i}{[x_i \mu_{1i} + (1-x_i) \mu_{2i}]}} \quad (C.4)$$

where μ_1 is the apparent viscosity of water and μ_2 is the apparent viscosity of oil, x is the dimensionless front position of water. The equation for x is derived as below:

$$\frac{dx_i}{dt} = -\frac{k_i}{\mu_i} \frac{\Delta p}{L} \frac{1}{\Phi \Delta S_w} = -\frac{k_i}{[x_i \mu_{1i} + (1-x_i) \mu_{2i}]} \frac{\Delta p}{L} \frac{1}{\Phi \Delta S_w} = -\frac{k_i / \mu_{1i}}{x_i + (1-x_i) m_i} \frac{\Delta p}{L} \frac{1}{\Phi \Delta S_w} \quad (C.5)$$

Where Φ is the porosity and ΔS_w is the water saturation difference between the water and oil zone. Now we assume Φ and ΔS_w keep the same in each layer. m_i is the mobility ratio in layer i and m_i is obtained by

$$m_i = \frac{\mu_{2i}}{\mu_{1i}} \quad (\text{C.6})$$

Before layer k breakthrough,

$$\frac{dx_k}{dx_i} = \frac{k_k}{k_i} \frac{\mu_{1i}}{\mu_{1k}} \frac{x_i + (1-x_i)m_i}{x_k + (1-x_k)m_k} \quad (\text{C.7})$$

$$\int_0^{x_k} k_i \mu_{1k} [x_k + (1-x_k)m_k] dx_k = \int_0^{x_i} k_k \mu_{1i} [x_i + (1-x_i)m_i] dx_i \quad (\text{C.8})$$

$$\frac{(1-m_k)}{2} x_k^2 + m_k x_k = \frac{k_k \mu_{1i}}{k_i \mu_{1k}} \left[\frac{(1-m_i)}{2} x_i^2 + m_i x_i \right] \quad (\text{C.9})$$

By setting $x_k = 1.0$

$$x_i = \frac{\left\{ m_i^2 + \frac{(1-m_i)(1+m_k)}{\left(\frac{k_k \mu_{1i}}{k_i \mu_{1k}} \right)} \right\}^{1/2} - m_i}{1-m_i} \quad (\text{C.10})$$

x_i in this equation is the water front for “slow layer” (not breakthrough).

If the thickness of a heterogeneous system is arranged from large layer

to small layer, the water front in all the layers with the layer number larger than k can be obtained from equation (C.10).

After layer k breakthrough, we can use the similar method to find the hypothetical front for “fast layer” (already breakthrough)

$$\frac{dx_k}{dx_i} = \frac{k_k}{k_i} \frac{\mu_{1i}}{\mu_{1k}} [x_i + (1 - x_i)m_i] \quad (C.11)$$

$$\int_1^{x_k} dx_k = \int_{x_i^0}^{x_i} \frac{k_k}{k_i} \frac{\mu_{1i}}{\mu_{1k}} [x_i + (1 - x_i)m_i] dx_i \quad (C.12)$$

$$x_k = 1 + \frac{k_k}{k_i} \frac{\mu_{1i}}{\mu_{1k}} \left[\frac{(1 - m_i)}{2} (x_i^2 - (x_i^0)^2) + m_i (x_i - x_i^0) \right] \quad (C.13)$$

$$\text{by setting } x_i = 1.0 \text{ and } x_i^0 = \frac{\left\{ m_i^2 + \frac{(1 - m_i)(1 + m_k)}{\left(\frac{k_k \mu_{1i}}{k_i \mu_{1k}} \right)} \right\}^{1/2} - m_i}{1 - m_i}$$

$$x_k = 1 + \frac{k_k}{k_i} \frac{\mu_{1i}}{\mu_{1k}} \left[\frac{(1 + m_i)}{2} - \frac{(1 + m_k)}{2 \left(\frac{k_k \mu_{1i}}{k_i \mu_{1k}} \right)} \right] \quad (C.14)$$

At specific WOR, the number n can be found by the way of linear interpolation. Then the water front in already breakthrough layer and not breakthrough layer can be obtained from the equations (C.14) and (C.10). After finding the water front, the sweep efficiency and dimensionless time at that WOR can be calculated. The sweep efficiency can be shown as the percentage of the whole volume that has been covered by displacing fluid. The dimensionless time is shown as how much pore volume of displacing fluid is injected.

$$\text{Sweep efficiency} = \frac{\sum_{i=1}^n h_i + \sum_{i=n+1}^{n_L} x_i h_i}{\sum_{i=1}^{n_L} h_i} \quad (\text{C.15})$$

$$\text{Dimensionless time} = \frac{\sum_{i=1}^{n_L} x_i h_i}{\sum_{i=1}^{n_L} h_i} \quad (\text{C.16})$$

In Dykstra-Parsons' paper, there are 8 examples for calculation of sweep efficiency (coverage) for water flooding in oil fields at different

permeability variation V and mobility ratio m . At the assumption of the 50 layers in the examples is at equal thickness h_i , we got similar results from the simulation to those results in Dykstra-Parsons' paper which is shown in Fig. C2. The water/oil sweep has a constant mobility ratio and constant viscosity of water and oil viscosity in each layer. The other assumption is the layers have log-normal distributed permeability.

Heterogeneity

The simulation was on the assumption that the permeability is in a lognormal distribution. The lognormal permeability distribution can be described by the function

$$C = \frac{1}{2} \left[1 + \operatorname{erf} \left(\frac{\tau}{\sqrt{2}} \right) \right] \quad (\text{C.17})$$

$$\text{where } \tau = \frac{\ln(\frac{k}{\bar{k}})}{\sqrt{V}}$$

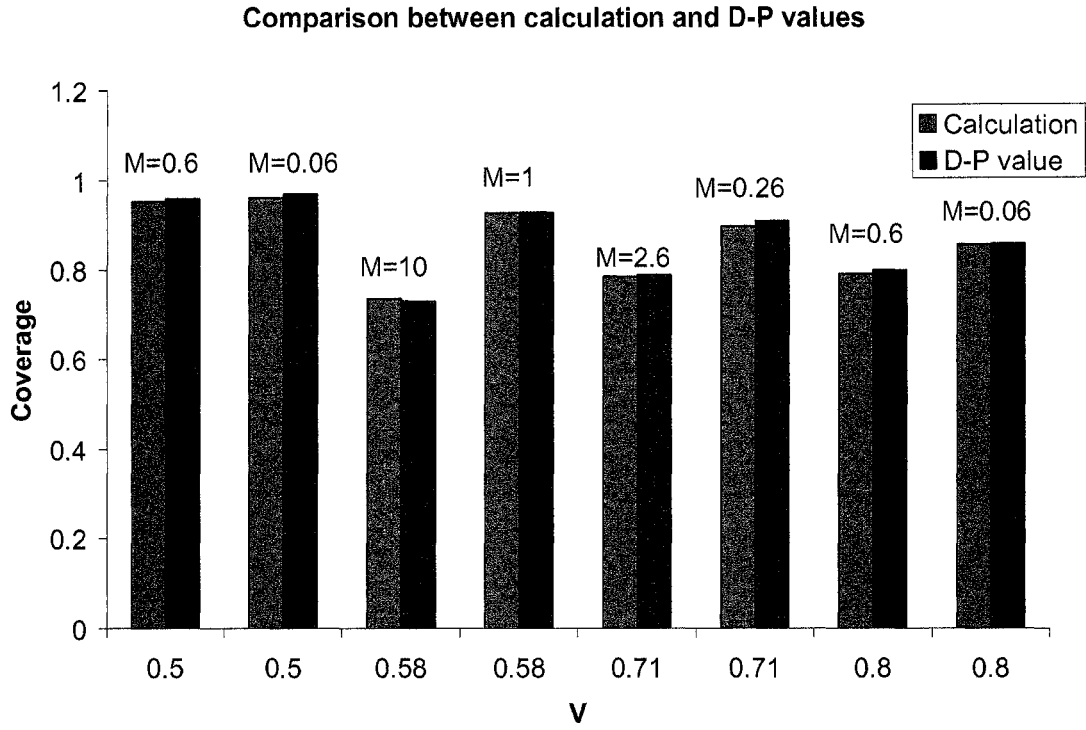


Fig. C.2 Comparison of simulation results with Dykstra Parson's value

The function $C(k)$ is the fraction of the samples that have permeability less than k , i.e., cumulative probability function. The parameter \bar{k} is the median permeability or log-mean permeability. The parameter ν is the variance of the distribution. We may divide the cumulative probability 100% by the layers number and get the different values of C . If the log-mean value \bar{k} and variance ν are known, different values of k can be obtained.

Dykstra and Parsons defined a permeability variation V . The relationship between V and ν is

$$\nu = [\ln(1 - V)]^2 \quad (\text{C.18})$$